CHEMICAL SYSTEMS FOR ELECTROCHEMICAL MECHANICAL PLANARIZATION OF COPPER AND TANTALUM FILMS

by

Ashok Kumar Muthukumaran

A Dissertation Submitted to the Faculty of the

DEPARTMENT OF MATERIALS SCIENCE AND ENGINEERING

In Partial Fulfillment of the Requirements
For the Degree of

DOCTOR OF PHILOSOPHY

In the Graduate College

THE UNIVERSITY OF ARIZONA

2 0 0 8

THE UNIVERSITY OF ARIZONA
GRADUATE COLLEGE

As members of the Dissertation Committee, we certify that we have read the dissertation prepared by **Ashok Kumar Muthukumaran**

entitled **Chemical Systems for Electrochemical Mechanical Planarization of Copper and Tantalum Films**

and recommend that it be accepted as fulfilling the dissertation requirement for the Degree of **Doctor of Philosophy**

_____ Date: 02/19/08
Srini Raghavan

_____ Date: 02/19/08
Pierre Lucas

_____ Date: 02/19/08
Harold G. Parks

Final approval and acceptance of this dissertation is contingent upon the candidate's submission of the final copies of the dissertation to the Graduate College.

I hereby certify that I have read this dissertation prepared under my direction and recommend that it be accepted as fulfilling the dissertation requirement.

_____ Date: 02/19/08
Dissertation Director: Srini Raghavan

STATEMENT BY AUTHOR

This dissertation has been submitted in partial fulfillment of requirements for an advanced degree at the University of Arizona and is deposited in the University Library to be made available to borrowers under rules of the Library.

Brief quotations from this dissertation are allowable without special permission, provided that accurate acknowledgment of source is made. Requests for permission for extended quotation from or reproduction of this manuscript in whole or in part may be granted by the head of the major department or the Dean of the Graduate College when in his or her judgment the proposed use of the material is in the interests of scholarship. In all other instances, however, permission must be obtained from the author.

SIGNED: Ashok Kumar Muthukumaran

ACKNOWLEDGEMENTS

First and foremost, I would like to sincerely thank my advisor, Prof. Srini Raghavan for his guidance and support in the completion of this dissertation. I want to convey my deepest appreciation to Prof. Raghavan for his advice and encouragement. Prof. Raghavan has been very kind, patient and has always given me opportunity to explore areas outside my research. Over the years, I have learned a lot from him for which I would always remain indebted to him.

I would also like to thank my committee members: Prof. Pierre Lucas and Prof. Harold G. Parks for being on my committee and taking time to read my dissertation. I want to acknowledge Mr. Lorenzo Lujan, staff engineer from Chemical & Environmental Engineering, for his support on designing the laboratory scale ECMP tool. Also, I thank Ms. Mary Kay Amistadi from soil, water and environmental science department for helping me with the ICP-MS analysis. As a friend and former fellow graduate student, I thank Dr. Subramanian Tamilmani and Dr. Viral Lowalekar. They taught me a lot during the early part of my graduate life and helped me throughout. I would like to thank and appreciate the help of Ms. Nandini Venkataraman in performing certain experiments and useful discussions. She helped me understand some of the complex electrochemical mechanism. I would like to thank all my current and past research colleagues and fellow graduate students who have made my graduate experience a memorable one. I must also acknowledge the financial support provided SRC/Sematech Engineering Research Center for Environmentally Benign Semiconductor Manufacturing.

I would like to thank all my friends for their support and encouragement throughout my entire life. Finally, and most importantly, I want to convey my love and gratitude to my parents, Mr. R. Muthukumaran and Mrs. M. Venmal, my sister, uncles, aunts, nephews, cousins, grandparents and all relatives, for their unconditional love, affection and support, without which this would not have been possible.

TABLE OF CONTENTS

TABLE OF CONTENTS - *Continued*

TABLE OF CONTENTS - *Continued*

LIST OF ILLUSTRATIONS

LIST OF ILLUSTRATIONS – *Continued*

LIST OF ILLUSTRATIONS – *Continued*

LIST OF ILLUSTRATIONS – *Continued*

LIST OF ILLUSTRATIONS – *Continued*

LIST OF ILLUSTRATIONS – *Continued*

LIST OF ILLUSTRATIONS – *Continued*

LIST OF TABLES

LIST OF TABLES - *Continued*

ABSTRACT

Electro-Chemical Mechanical Planarization (ECMP) is a new and highly promising technology just reaching industrial application; investigation of chemistries, consumables, and tool/control approaches are needed to overcome technological limitations. Development of chemical formulations for ECMP presents several challenges. Unlike conventional CMP, formulations for ECMP may not need an oxidant. Organic additives, especially inhibitors used to control planarity (i.e. to protect recessed regions), need to be stable under applied anodic potential. To have a high current efficiency, the applied current should not induce decomposition of the formulations. In addition, to enable clearing of the copper film, the interactions between multiple exposed materials (barrier material as well as copper) must be considered. Development of a full sequence ECMP process would require the removal of the barrier layer as well. Chemical systems that exhibit a 1:1 selectivity between the barrier layer and copper would be ideal for the barrier removal step of ECMP. The main goal of this research is to investigate the chemistries suitable for ECMP of copper and tantalum films.

Copper was electroplated onto the gold electrode of quartz crystals, and its dissolution/passivation behavior in hydroxylamine solutions was studied at different applied potential values. The dissolution rate of copper is pH dependent and exhibits a maximum in the vicinity of pH 6. Copper dissolution increases with respect to overpotential (η) and dissolution rates as high as 6000 Å/min have been obtained at overpotential of 750mV. While both benzotriazole (BTA) and salicylhydroxamic acid

(SHA) serve as good inhibitors at lower overpotentials, their effectiveness decreases at higher overpotentials.

A fundamental study was undertaken to evaluate the usefulness of a sulfonic acid based chemical system for the removal of tantalum under ECMP conditions. Tantalum as well as copper samples were polished at low pressures (~0.5 psi) under galvanostatic conditions in dihydroxy benzene sulfonic acid (DBSA) solutions maintained at different pH values. At a current density of 0.5 mA/cm^2 and a pH of 10, tantalum removal rate of 200 Å/min with a 1:1 selectivity to copper was obtained in 0.3M DBSA solutions containing 1.2M H_2O_2. The presence of a small amount (~ 0.1%) of colloidal silica particles was required to obtain good removal rates. A comparison of DBSA and methane sulfonic acid (MSA) based chemical system was studied for the removal of tantalum. The performance of DBSA is better than that of MSA. Additionally, DBSA solution has been used for tantalum nitride removal under ECMP conditions. However, DBSA is not as effective for tantalum nitride as it is for tantalum. Polishing of the patterned test structure in optimized solution containing 0.01M BTA results in complete removal of barrier layer and surface planarity is achieved.

CHAPTER 1: INTRODUCTION

1.1. Introduction

For more than four decades, device scaling has been a primary means by which the semiconductor industry has achieved unprecedented gains in productivity and performance. The development of integrated circuits (IC) has evolved from few thousand transistors per chip in 1970 to nearly 1 billion transistors per chip in 2007 [1.1]. The metal oxide semiconductor field effect transistor (MOSFET) is the most widely used semiconductor device and is at the heart of every digital circuit.

The exponential progress of MOS technology is best illustrated by the evolution of the number of MOS transistors integrated in a single memory chip or single microprocessor, as a function of a calendar year. Figure 1.1 shows that the number of transistors doubles every 18 months. This exponential growth of integration density with time is known as Moore's Law [1.2]. The integration density of memory circuits is about 5 to 10 times higher than that of logic circuits such as microprocessors because of the more repetitive layout of arrays in memory chips. The increase in integration density is essentially due to the reduction of transistor size [1.3]. Figure 1.2 shows the decrease in nominal feature size from a few microns in the 1970s to 65 nm in 2007. This continuous scaling trend in IC development has increased the complexity of fabrication technologies and requires the introduction of new materials. To reflect further growth of the complexity, the term ULSI, which stands for "Ultra-Large Scale Integration," was proposed for chips of complexity of more than 1 billion of transistors.

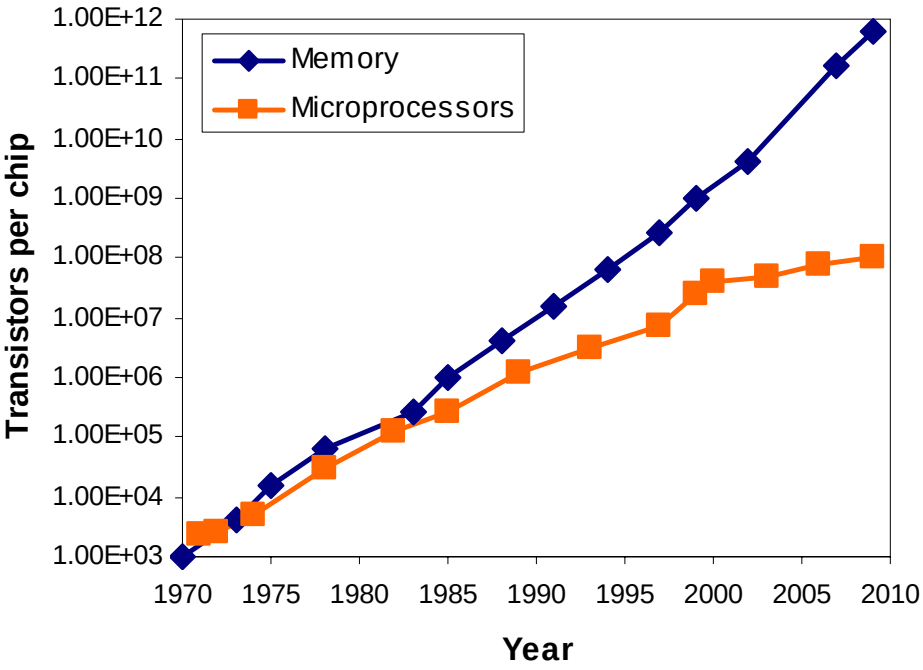

Figure 1.1: Trend in microprocessors and memory devices [1.1]

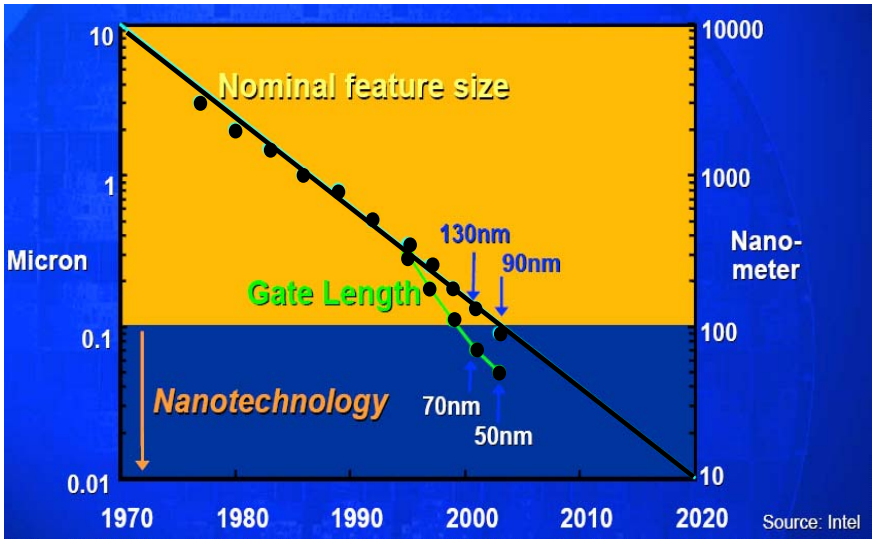

Figure 1.2: Decrease in nominal feature size since 1970 [1.1].

Multilevel metallization has become the key process in fabricating ULSI devices [1.4]. Interconnects serve as local and global wiring, which connect circuit elements and distribute power. Earlier, aluminum (resistivity ~ 2.5 μΩ.cm) was used as the interconnect metal in devices with large feature size. Due to the need for faster devices, metals with lower resistance than aluminum are required to reduce the interconnect time delay. Copper (resistivity ~ 1.67 μΩ.cm) has become the metal of choice for fabricating submicron devices. Not only has copper the ability to reduce the resistance-capacitance product (RC) delay due to its lower resistivity, but also increase the circuit reliability because of its higher electromigration resistance [1.5]. Additionally, low-k (dielectric) materials are replacing the conventionally used silicon dioxide (dielectric constant, k ~ 4) in order to reduce the RC delay. The 2007 International Technology Roadmap for Semiconductors (ITRS) predicts that devices with a 32 nm (DRAM ½ pitch) technology node for both microprocessor and memory chips with copper metallization will be used in the year 2013 (Table 1.1 and Table 1.2) [1.6]. The metal aspect ratio is steadily increasing and the effective dielectric constant is decreasing. Additionally, 13 and 4 metal layers may be required for the microprocessor and memory devices, respectively.

1.2. Copper/Low- k Dielectric Materials

Figure 1.3 shows a schematic representation of an interconnect structure. For such a system the time delay, τ, is approximately equal to 0.89 R(C+ C') where R is the line resistance of the wire, C is the capacitance between adjacent wires on the same level of metal, and C' is the capacitance between the wiring levels [1.7]. From this expression, it is clear that by lowering the dielectric constant and/or decreasing the resistivity of the interconnect metal, RC time delays are reduced, allowing faster chip performance. If the

device dimensions are large, the overall speed will be dominated by the time constants associated with the transistor and not by the interconnect structure. However, when the device dimensions shrink, this is not the case.

Figure 1.4 shows the (a) gate delay (b) interconnect delay and (c) total delay time as a function of minimum feature size [1.8]. The gate delay decreases with the device feature size. However, the interconnect delay for Al/SiO_2 and copper/low-k structures increases due to the increased resistance of smaller dimension wiring, and increased capacitance due to more closely packed lines and thinner insulators. As the minimum feature size decreases, the overall circuit delay is dominated by the interconnect delay. As shown in the figure, the replacement of copper along with low-k material significantly reduces time delay compared to that with aluminum lines and SiO_2. This has led to the introduction of low-k materials in copper damascene structures. Other significant advantages of using low-k materials include reduced power consumption and cross talk noise. Table 1.3 lists some of the low-k materials along with their dielectric constants [1.7].

The ITRS interconnect technology requirements for the current and future nodes are tabulated in Table 1.4 [1.6]. A number of qualitative observations made earlier are apparent in this table. Note the decreasing metal resistivity requirement which cannot be met by aluminum, and the decreasing dielectric constant required for intermetal dielectrics, which cannot be met by SiO_2. Clearly, new materials will have to be introduced to meet these objectives. Copper interconnects and low-k dielectrics are the likely answer to these requirements.

Year of Production	*2005*	*2006*	*2007*	*2008*	*2009*	*2010*	*2011*	*2012*	*2013*
DRAM ½ Pitch (nm) (contacted)	*80*	*70*	*65*	*57*	*50*	*45*	*40*	*36*	*32*
MPU/ASIC Metal 1 ½ Pitch (nm)(contacted)	*90*	*78*	*68*	*59*	*52*	*45*	*40*	*36*	*32*
MPU Physical Gate Length (nm)	*32*	*28*	*25*	*22*	*20*	*18*	*16*	*14*	*13*
Number of metal levels	11	11	11	12	12	12	12	12	13
Number of optional levels – ground planes/capacitors	4	4	4	4	4	4	4	4	4
Total interconnect length (m/cm^2) – Metal 1 and five intermediate levels, active wiring only [1]	1019	1212	1439	1712	2000	2222	2500	2857	3125
FITs/m length/cm^2 × 10^{-3} excluding global levels [2]	4.9	4.1	3.5	2.9	2.5	2.3	2	1.8	1.6
J_{max} (A/cm^2) – intermediate wire (at 105°C)	8.91E+05	1.37E+06	2.08E+06	3.08E+06	3.88E+06	5.15E+06	6.18E+06	6.46E+06	8.08E+06
Metal 1 wiring pitch (nm)	180	156	136	118	104	90	80	72	64
Metal 1 A/R (for Cu)	1.7	1.7	1.7	1.8	1.8	1.8	1.8	1.8	1.9

Table 1.1: Microprocessor interconnect technology requirements predicted in 2007 ITRS [1.6].

Year of Production	*2005*	*2006*	*2007*	*2008*	*2009*	*2010*	*2011*	*2012*	*2013*
DRAM ½ Pitch (nm) (contacted)	*80*	*70*	*65*	*57*	*50*	*45*	*40*	*36*	*32*
MPU/ASIC Metal 1 ½ Pitch (nm)(contacted)	*90*	*78*	*68*	*59*	*52*	*45*	*40*	*36*	*32*
MPU Physical Gate Length (nm)	*32*	*28*	*25*	*22*	*20*	*18*	*16*	*14*	*13*
Number of metal layers	4	4	4	4	4	4	4	4	4
Contact A/R – stacked capacitor	15	16	16	17	17	>20	>20	>20	>20
Metal 1 wiring pitch (nm) *	160	140	130	114	100	90	80	72	64
Specific contact resistance (Ω-cm^2) for n$^+$ Si	2.50E-08	2.30E-08	2.00E-08	1.70E-08	1.40E-08	1.20E-08	9.80E-09	8.20E-09	6.90E-09
Specific contact resistance (Ω-cm^2) for p$^+$ Si	4.50E-08	3.80E-08	3.20E-08	2.70E-08	2.20E-08	1.80E-08	1.50E-08	1.30E-08	1.10E-08
Specific via resistance (Ω-cm^2)	7.00E-10	6.00E-10	5.00E-10	4.00E-10	3.50E-10	2.90E-10	2.50E-10	2.10E-10	1.70E-10
Conductor effective resistivity (μΩ-cm) assumes no scattering for Cu	3.3	3.3	2.2	2.2	2.2	2.2	2.2	2.2	2.2
Interlevel metal insulator – effective dielectric constant (κ)	3.6–4.1	3.6–4.1	3.6–4.1	3.1–3.4	3.1–3.4	3.1-3.4	2.7–3.0	2.7–3.0	2.7–3.0

**Refer to Executive Summary Figure 4 for definition of Metal 1 pitch*

Manufacturable solutions exist, and are being optimized
Manufacturable solutions are known
Interim solutions are known
Manufacturable solutions are NOT known

Table 1.2: DRAM interconnect technology requirements predicted in 2007 ITRS [1.6].

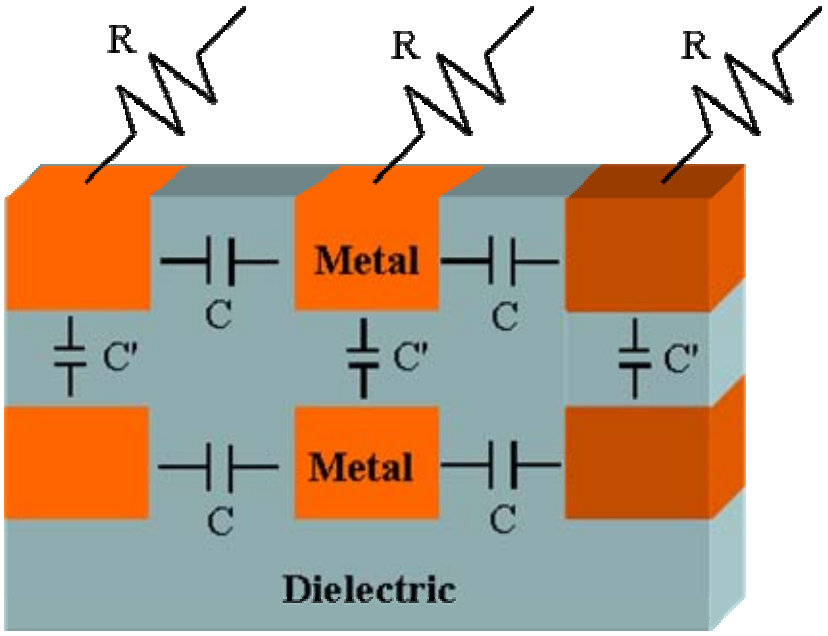

Figure 1.3: Schematic representation of an interconnect structure [1.7].

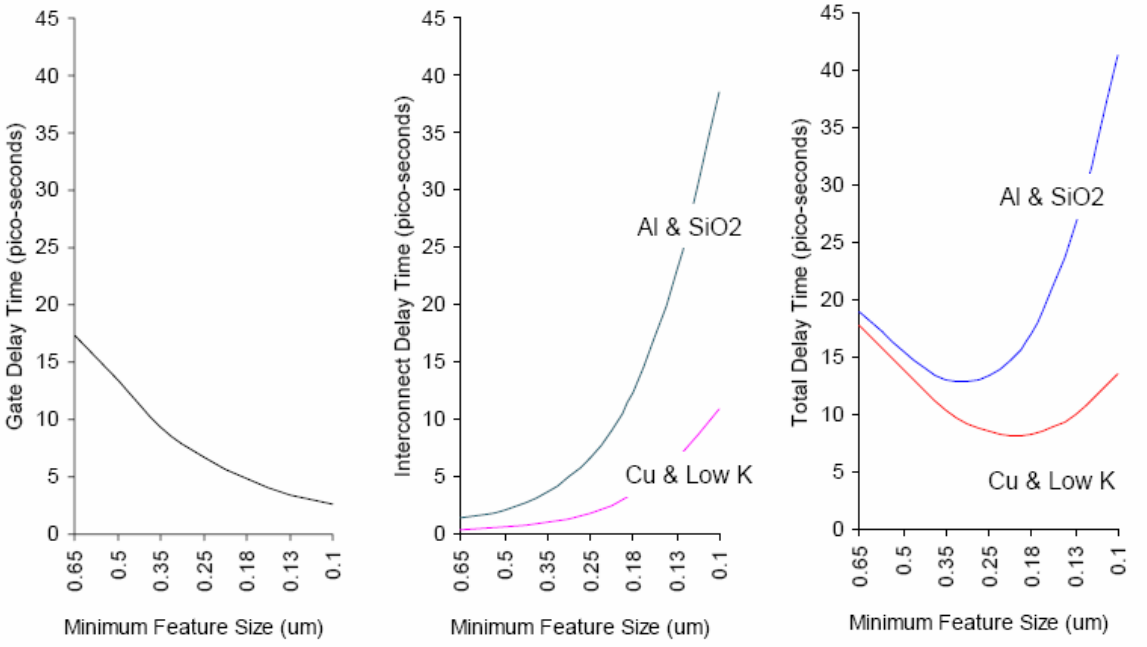

Figure 1.4: Variation of time delay as a function of device generation [1.8].

	Material		Dielectric constant (k)
Inorganic Dielectrics	SiO_2		4.0
	FSG		3.4 – 3.8
	HSQ (Hydrogensilses-quioxane)		2.8 – 3.0
	Porous Silica		1.8 – 2.4
Organic Dielectrics	SiLK		2.6
	Porous SiLK		2.2
	SiOC		2.7 – 2.9
	Porous SiOC		2.2 – 2.5
	MSQ (methylsilses-quioxane)		2.7 – 2.9
	Porous MSQ		1.8 – 2.5
	Organic Polymer	Polyimide	3.0 – 3.5
		Parylane	2.2 – 3.0
		Teflon	2.0 – 2.5
	Amorphous Carbon (F-doped)		< 2.5
	CDO (carbon doped oxide)		~ 2.6

Table 1.3: List of candidate low-k materials [1.7].

Year of Production	*2005*	*2006*	*2007*	*2008*	*2009*	*2010*	*2011*	*2012*	*2013*
DRAM ½ Pitch (nm) (contacted)	*80*	*70*	*65*	*57*	*50*	*45*	*40*	*36*	*32*
MPU/ASIC Metal 1 ½ Pitch (nm)(contacted)	*90*	*78*	*68*	*59*	*52*	*45*	*40*	*36*	*32*
MPU Physical Gate Length (nm)	*32*	*28*	*25*	*22*	*20*	*18*	*16*	*14*	*13*
Line length (μm) where 25% of switching voltage is induced on victim minimum global wire by crosstalk [4]	170	147	137	130	128	124	120	115	97
Cu thinning of maximum width global wiring due to dishing and erosion (nm), 10% × height, 80% areal density	220	220	230	230	240	240	240	250	250
Cu thinning global wiring due to dishing (nm), 100 μm wide feature	24	21	19	17	15	14	13	13	10
Conductor effective resistivity (μΩ–cm) Cu wiring, assumes no scattering	2.2	2.2	2.2	2.2	2.2	2.2	2.2	2.2	2.2
Interlevel metal insulator – effective dielectric constant (κ)	3.1–3.4	3.1–3.4	2.7–3.0	2.7–3.0	2.5–2.8	2.5–2.8	2.5–2.8	2.1–2.4	2.1–2.4
Interlevel metal insulator (minimum expected) – bulk dielectric constant (κ)	≤ 2.7	≤ 2.7	≤ 2.4	≤ 2.4	≤ 2.2	≤ 2.2	≤ 2.2	≤ 2.0	≤ 2.0

**Refer to Executive Summary Figure 4 for definition of metal 1 pitch*

Manufacturable solutions exist, and are being optimized
Manufacturable solutions are known
Interim solutions are known
Manufacturable solutions are NOT known

Table 1.4: MPU interconnect technology requirements predicted by ITRS [1.6].

1.3. Integration Challenges for Copper/Low-k Interconnects

Some of the important properties of low-k dielectrics and SiO_2 are listed in Table 1.5 [1.7]. The mechanical properties of low-k materials are about an order of magnitude less compared to SiO_2. For example, the modulus of SiO_2 and low-k dielectric material is 3.5 and ~0.3 GPa, respectively. The introduction of porosity can reduce the dielectric constant; however, it also reduces the hardness and modulus of these materials. This directly affects CMP because the downforce and rotation rates must be lowered to avoid mechanical damage and scratching [1.9, 1.10].

Conventional CMP processing for Cu/SiO_2 structures uses high downforce pressure (~8 psi). With the introduction of low-k materials, the CMP process has to be carried out at low downforce pressure (2-5 psi). Also, it requires the development of new CMP consumables such as slurries and pads. Another issue is layer-to-layer adhesion. Figure 1.5 shows the delamination in ultra low-k film [1.11]. As the mechanical strength of the low-k materials is drastically reduced, film delamination can occur due to high mechanical stress developed at the edges of the wafer during CMP.

1.4. High-k and Metal Gate

For more than 30 years, SiO_2 has been a preferred material for gate dielectric in MOS based structures. The conventional gate oxide (SiO_2) poses problems as device features are scaled down, because as the thickness of the silicon dioxide approaches less than 1.5 nm, leakage current can increase. Managing that leakage is crucial for reliable high-speed operation, and is becoming an increasingly important factor in chip design. Additionally, the dopants may penetrate through the ultra-thin SiO_2 layer, causing direct

tunneling in the ultra-thin oxide film. When dopants penetrate into the channel of a MOSFET device, it breaks down during operation. Therefore, the quality of the dielectric and performance of the device become poor [1.12]. The ideal solution to reduce the gate leakage current would be simply replacing the SiO_2 layer with a different dielectric material. Intel has made a significant breakthrough in solving the chip power problem, identifying a new "high-k" material called hafnium to replace the transistor's silicon dioxide gate dielectric, and new metals to replace the polysilicon gate electrode of NMOS and PMOS transistors. These new materials, along with the right process recipe, reduce gate leakage more than 100-fold, while delivering record transistor performance [1.13].

Aluminum metallization processes begin with a blanket layer deposition of aluminum followed by patterning and etching; the trenches are then filled with silicon dioxide. This process is called subtractive metallization. Most advanced chips are now being constructed with copper interconnects, since copper has lower resistivity than aluminum at advanced technology nodes. The use of reactive ion etching (RIE) to pattern copper is impractical, because volatile copper compounds form only at elevated temperatures [1.14].The damascene process provides a solution to the problems arising from the lack of a directional metal etch capability. In this approach, dielectric is patterned by RIE, followed by barrier and copper deposition. The barrier layer becomes necessary when using copper as an interconnect material to prevent the rapid diffusion of the copper into the dielectric. The copper deposition leaves a topography based on the dielectric pattern. The final step uses chemical mechanical planarization (CMP) to polish the excess metal away and provides local and global planarization. Figure 1.6 (a) and (b) show the comparison of a cross sectional view of a MOSFET device showing three layers

of unplanarized metal interconnect structure and planarized surface without topography buildup, respectively [1.15].

CMP is the only viable technique for achieving required global planarity for advanced ULSI devices with feature size of 130 nm and below. In a CMP process, a wafer coated with metal and/or dielectric films is held in a rotating carrier and pressed against a polymeric pad while slurry is delivered to the pad. The principal objectives of a CMP process are to remove films at a desired rate while planarizing the surface. Removal rate and planarization depend on a number of factors such as down force (pressure) on the wafer, relative velocity between the pad and the wafer and chemistry of a slurry system. Planarization of copper films by CMP is now a well established process, and is used in the formation of interconnect structures. Conventional CMP processes that are currently in use suffer from certain limitations that are making it difficult to extend to the fabrication of sub-65 nm devices that use ultra low-k dielectrics. These limitations include high dishing/erosion and film delamination/peeling due to high pressure [1.10]. Since removal rate in CMP is usually a function of pressure, resorting to low pressure processes may be a solution; however, this may come at the expense of removal rates. To overcome this drawback, variants of CMP are being actively investigated. Electrochemical mechanical planarization (ECMP) is a process in which the removal rate is directly controlled by an applied current. In this method, a metallic film, typically copper, is polarized anodically by an applied voltage, while a pad makes mechanical contact with the film at very low applied pressure (< 0.3 psi) [1.16- 1.18]. ECMP allows modification of the polish recipe based on the thickness profile of the incoming wafer. The applied current can be varied at different radial ‘zones’ on the wafer, thereby

allowing control of removal rate to desired values [1.19]. Due to enhancement of electrochemical factors, the particulate content of the slurry can be significantly reduced, or in some cases eliminated [1.20].

The chemical system used for ECMP typically contains ingredients to dissolve and complex the metal, and a corrosion inhibitor, which is required to protect low lying areas by forming a passive film while higher areas are selectively removed through pad contact. The passive film must have excellent chemical stability but poor mechanical stability, so that it can be removed easily by the application of a very small downforce [1.10]. Benzotriazole (BTA, $C_6H_5N_3$), a commonly used copper corrosion inhibitor, is often used in ECMP formulations [1.21-1.24].

During the last few years, the ECMP technique has been actively explored for bulk copper removal in the fabrication of Cu-low k structures. However, the development and implementation of a full-sequence ECMP process, which includes the removal of the barrier layer as well, is in its infancy. Tantalum CMP is done using silica slurries with a high solid content (~10% weight) at alkaline pH values. It has been reported that the removal of tantalum is predominantly a ‘mechanical’ process which involves the removal of the native oxide formed on the surface [1.25]. ECMP formulations, as mentioned earlier, are designed to be more chemically active with very small or no solid content. Tantalum, being a refractory metal, is not attacked by many chemical systems and hence poses challenges to the development of ECMP formulations.

Property	Low-k	SiO_2
Density (g/cm^3)	1.03	2.2
Dielectric Constant	~ 1.9 – 2.5	4.0
Modulus (GPa)	~ 3 – 9	55 – 70
Hardness (GPa)	~ 0.3 – 0.8	3.5
Coefficient of Thermal Expansion (ppm/K)	~ 10 - 17	0.6

Table 1.5: Comparison of properties of low-k materials and oxide [1.7]

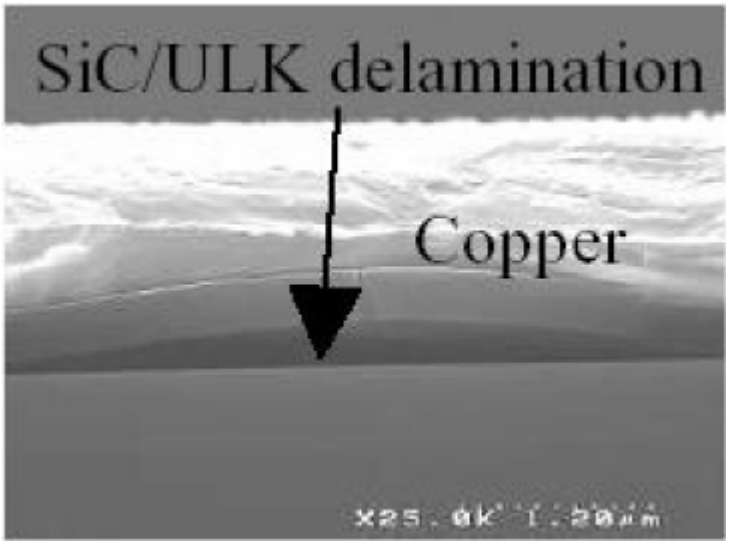

Figure 1.5: Delamination of ultra low k film [1.11].

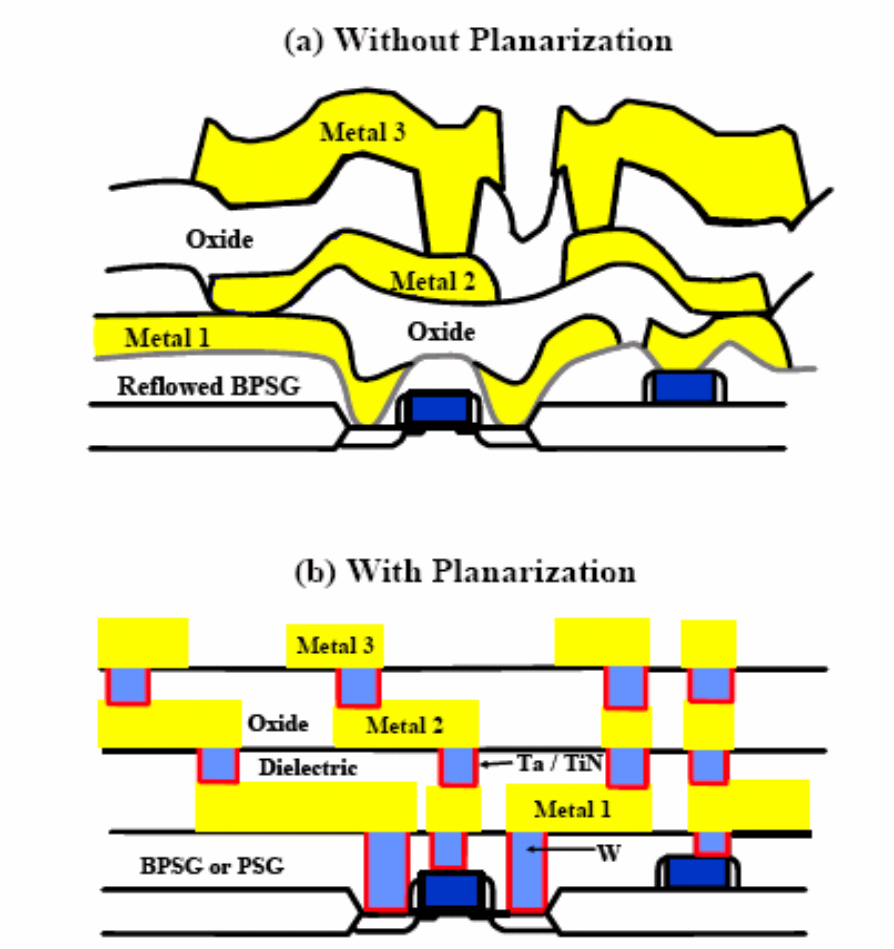

Figure 1.6: Cross sectional view of MOSFET device with 3 metal layers interconnects: a) surface topography without any planarization, b) planarized surface without topography buildup [1.15].

1.5. Research Objectives

The main goal of this research is to develop chemical systems suitable for ECMP of copper and tantalum through electrochemical investigations. Specific objectives are as follows:

1. Investigate the use of hydroxylamine based chemical system for ECMP of copper.
2. Characterize the effect of applied anodic potential on the dissolution behavior of electrodeposited copper films in hydroxylamine solutions.
3. Compare the effectiveness of salicylhydroxamic acid (SHA) with that of commonly used benzotriazole (BTA) as a suitable inhibitor for copper ECMP.
4. Evaluate the usefulness of 2, 5 dihydroxy benzene sulfonic acid (DBSA) for the electrochemical mechanical removal of tantalum films.
5. Explore conditions that would provide a 1:1 selectivity between tantalum and copper.
6. Comparison of DBSA and methane sulfonic acid (MSA) based chemical systems for tantalum removal.
7. Evaluate DBSA solution for the removal of tantalum nitride.
8. Study on patterned test structure using DBSA based chemical system.

CHAPTER 2: BACKGROUND

2.1. Chemical Mechanical Planarization

Chemical mechanical planarization or polishing (CMP) is a process by which local and global planarization can be achieved through the combined action of chemical and mechanical forces. It is used to planarize and prepare the surface for the following lithographic step, avoiding depth focus problems. It has become a key technology in ultra large-scale integrated (ULSI) device manufacturing to fabricate sub-micrometer metal and dielectric structures. CMP is most widely used in the back end of line integrated circuit (IC) manufacturing. The back end line process steps involve a multilayer deposition of metal and dielectric materials to form interconnections between an active device and the outside world. Currently, it is the most cost-effective technique for removing excess electrodeposited copper and reducing topography by planarizing copper.

Figure 2.1 shows the schematic of the copper damascene process. The first step is the fill process, which includes a diffusion barrier (tantalum) layer of thickness ~ 25 nm, a copper seed layer, and electrochemical deposition of copper for the bulk fill. The filling of the trenches leaves a severe topography on the metal surface. Most copper CMP processes involve a two step polishing method, each optimized for a different part of the stack [2.1]. The first step in copper CMP is to remove 80-90% of bulk copper. This is usually achieved by a slurry chemistry that has a high copper dissolution rate of 3000 to 5000 Å/min. At the end of first stage polishing, a very thin flat layer of copper remains, without exposing the barrier layer. Second stage polishing involves the removal of remaining copper and the barrier metal (tantalum). Ideally, the selectivity between

tantalum and copper should be 1:1. The removal rate in this phase is typically around 300 Å/min. At the end of second stage polishing, the dielectric material is slightly overpolished. This helps correct underlying topography problems left over from previous CMP steps, and also removes dielectric faceting that often occurs during the dielectric etch/resist strip/PVD clean sequence used in damascene processing. Heavy faceting, which knocks off the top corners of the dielectric, brings copper lines dangerously close together, inviting cross-capacitance coupling or even shorts [2.2]. A final CMP step buffs, cleans and passivates the wafer, which prevents corrosion.

After CMP, the surface topography is evaluated for local and global planarity. Figure 2.2 shows the topography developed as a result of metal deposition on a dielectric feature of step height D_1 [2.3]. The height of the metal over dielectric and trench is M_1 and M_2, respectively. If the step height is D_2 and R is the planarization length which is the distance from the edge of the step to the next level of topography, then the planarization angle θ is given by:

$$\theta = \tan^{-1}\left(\frac{D_2}{R}\right)$$

The planarization angle, θ, varies with patterned density. At high pattern density, R will decrease in relation to D_2 thereby causing θ to be high. In areas of low pattern density, θ will be low. The goal of CMP is to reduce topographical variation and obtain global planarity, $\theta < 0.5^{o}$. In order to reduce D_2, the reduction of M_1 must be greater than M_2. This is called step-height reduction (SHR).

$$SHR = 1 - \frac{D_2\,(post - planarization)}{D_2\,(pre - planarization)}$$

The degrees of planarity are shown in Table 2.1. Local planarization is defined as the process in which the step coverage distance is in the range of < 100 μm. Similarly, the process in which the planarization length is in the range of millimeters is termed global planarization.

Planarity	**R (μm)**	**θ**
Surface Smoothing	0.1 – 2.0	$> 30^o$
Local Planarization	2 – 100	$30^o – 0.5^o$
Global Planarization	> 1000	$< 0.5^o$

Ideal planarity, $\theta = 0^o$

Table 2.1: Degree of planarity [2.3].

Success in copper CMP processes is judged not only by the final planarity of the surface, but also by the amount of copper loss, uniformity across the wafer, defects, particles, residues, oxide loss, corrosion and, of course, the over-all cost of the process. During the CMP of patterned copper samples, two phenomena, copper dishing and inter layer dielectric (ILD) erosion as shown in Figure 2.3, led to deviations from the ideal case [2.2]. Dishing is the loss in thickness of the inlaid material and is usually a result of mechanical action. Copper is a comparatively soft material compared to the dielectric, so it is more easily removed in open areas through a combination of pad flexing and abrasive gouging. Another pattern-dependent problem that also reduces planarity is called erosion, where some oxide is removed in localized areas. A desirable goal is to have dishing of < 200 Å on a 100 μm feature and erosion of < 100 Å on a 90% dense feature, but that is often far from what is normally achieved in production [2.2].

Dishing and erosion are often seen as the most critical and insidious problems affecting planarity and sheet resistance which can change the circuit characteristics. Steigerwald et al [2.4] polished patterned copper wafer in ammonia based slurry containing 2.5 % wt. alumina as the abrasives at a pressure of 2.3 psi. Figure 2.4 (a) and (b) shows copper dishing and SiO_2 erosion for linewidth of 2 to 200 μm and patterned densities of 20 to 80%. It is clear that dishing is a strong function of linewidth. For example, the dishing has increased from 50 to 500 nm for a linewidth of 2 to 200 μm, respectively. However, erosion is a strong function of pattern density and not of linewidth. The SiO_2 erosion has increased from 50 to 250 nm for a patterned density of 20% to 80%, respectively.

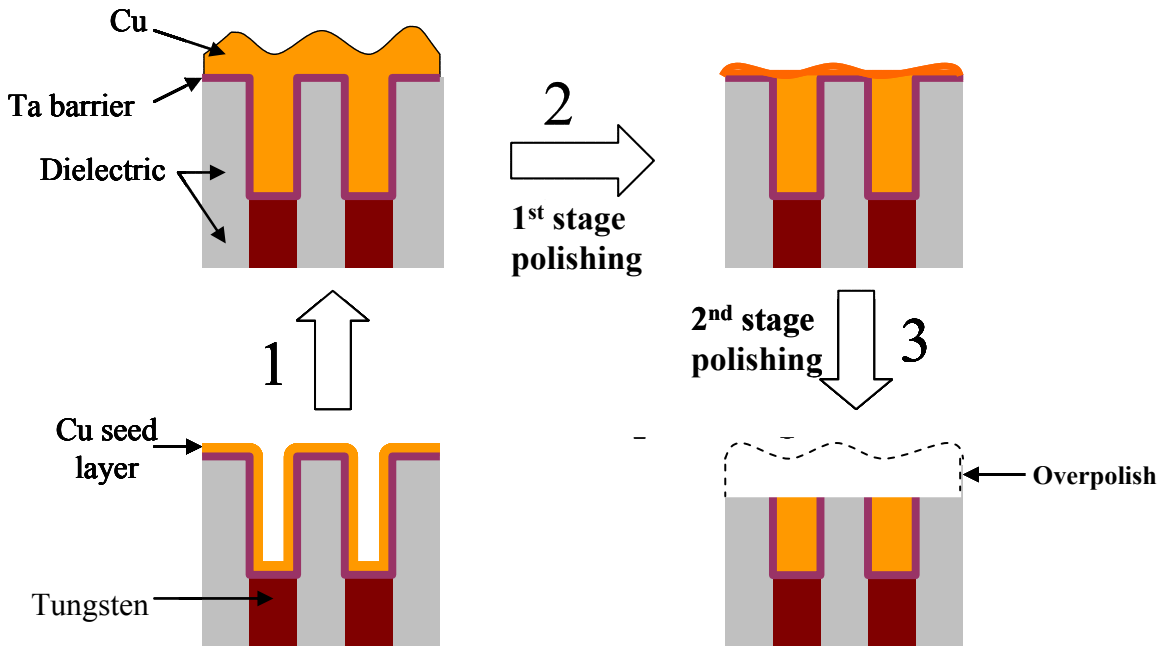

Figure 2.1: Schematic of the copper damascene process (1) Electrodeposition of copper to fill the trenches. (2) Bulk copper removal. (3) Tantalum removal and overpolish.

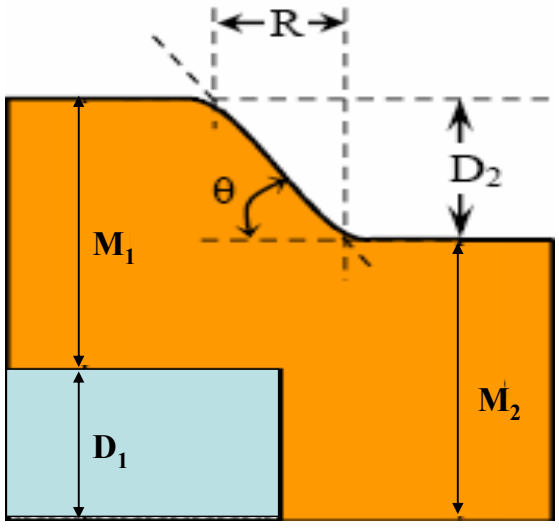

Figure 2.2: Quantitative measurement of planarity [2.3]

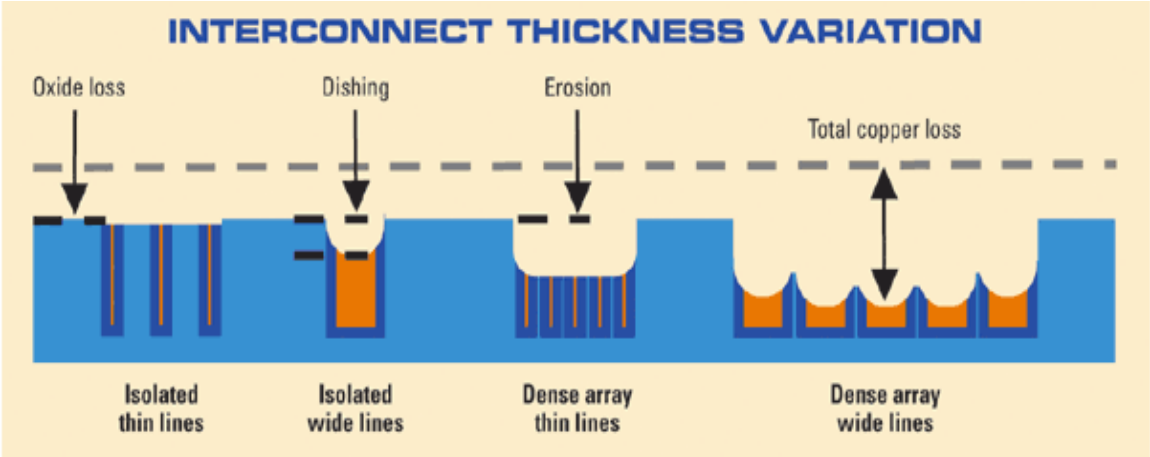

Figure 2.3: Schematic representation showing the effect of interconnect thickness on dishing, erosion, oxide and copper loss [2.2].

(a) (b)

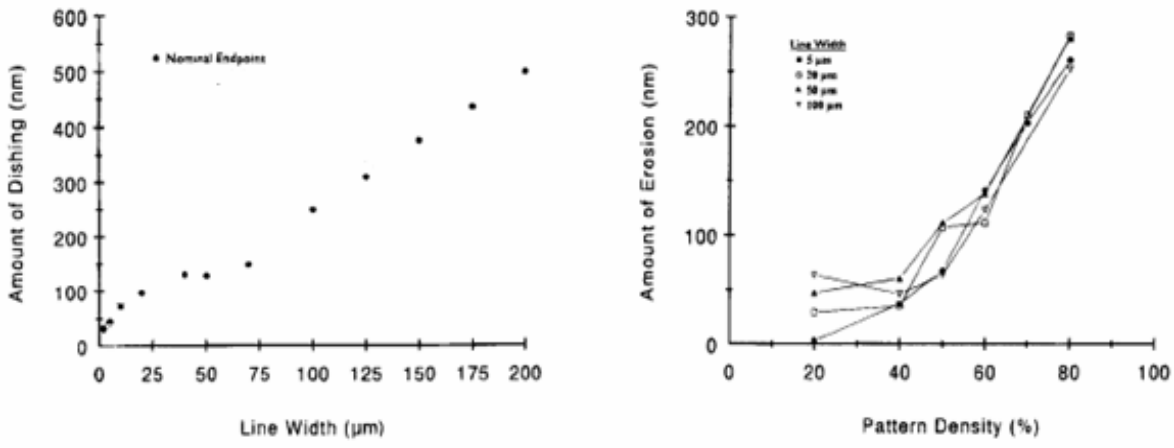

Figure 2.4: (a) Dishing as a function of linewidth (b) SiO_2 erosion vs. % patterned density for different linewidth [2.4].

2.1.1. CMP Tools

A typical CMP tool consists of a rotating platen that is covered by a polishing pad, and a wafer that is mounted face down within a carrier wafer. The retaining ring keeps the wafer in the correct horizontal position. Both the polishing platen and the carrier wafer rotate using a separate drive system, hence the name rotary tool. A schematic representation of the rotary CMP tool showing (a) side view and (b) top view is shown in Figure 2.5. During CMP, pressure is applied by down force on the carrier and the slurry is supplied from above on the platen, as shown in Figure 2.5. The magnitude of offset between the axis of rotation of carrier and the platen determines the relative velocity between the pad and the wafer. The relative velocity is a very important factor which influences the removal rate of the material. The two main disadvantages of the rotary tool are the large variation in relative velocity across the wafer, and its inefficient slurry distribution. Less than 20% of the dispensed slurry is actually used for planarization. The rest of the slurry runs off the pad and into the waste stream.

The CMP tool is obviously a very complex piece of equipment with various mechanical and electrical control systems. Depending on the complexity and generation of the tool, the number of platens can vary from one to three. Figure 2.6 shows the Applied Reflexion 300mm LK CMP tool using a 4-head/3-platen architecture which provides high performance planarization for copper damascene, shallow trench isolation (STI), oxide, polysilicon, and tungsten applications [2.5]. Platen 1 is used to remove 80-90 % of bulk copper, leaving a thin copper film without exposing the underlying Ta/TaN diffusion barrier. This is followed by a fine polish step to remove the remaining copper film on platen 2. The wafer is then transferred to platen 3. At this point, since tantalum

has quite different polishing properties than copper, it's often desirable to switch to different polishing slurry and perhaps a different polishing pad. After the barrier is removed, a final CMP step buffs, cleans and passivates the wafer, which prevents corrosion. To further reduce contamination and increase device yield, the Reflexion LK have megasonic cleaning and full-immersion Marangoni vapor drying technology to eliminates watermark defects on low-k surfaces and reduces ultra-small particle contamination on patterned and unpatterned wafer surfaces. The Applied Reflexion LK CMP system also implements a full suite of endpoint methods, in-line metrology and advanced process control capabilities that ensure excellent within-wafer and wafer-to-wafer process control and repeatability for all planarization applications. Its patented window-in-pad technology enables accurate real-time polish control of every wafer without compromising throughput. The new FullVision in-situ endpoint system uses broadband spectroscopy to minimize wafer scrap caused by drifts in consumable sets and incoming wafer variations.

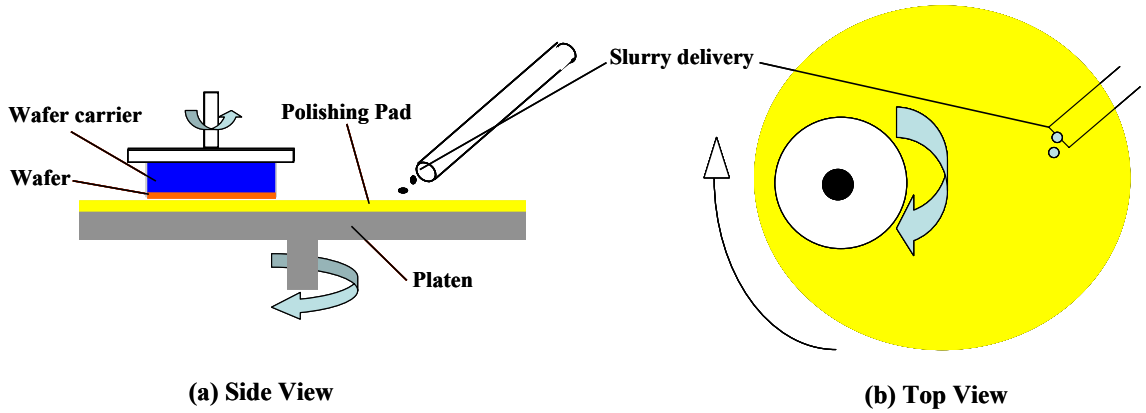

Figure 2.5: Schematic representation of the rotary CMP tool showing (a) side view and (b) top view.

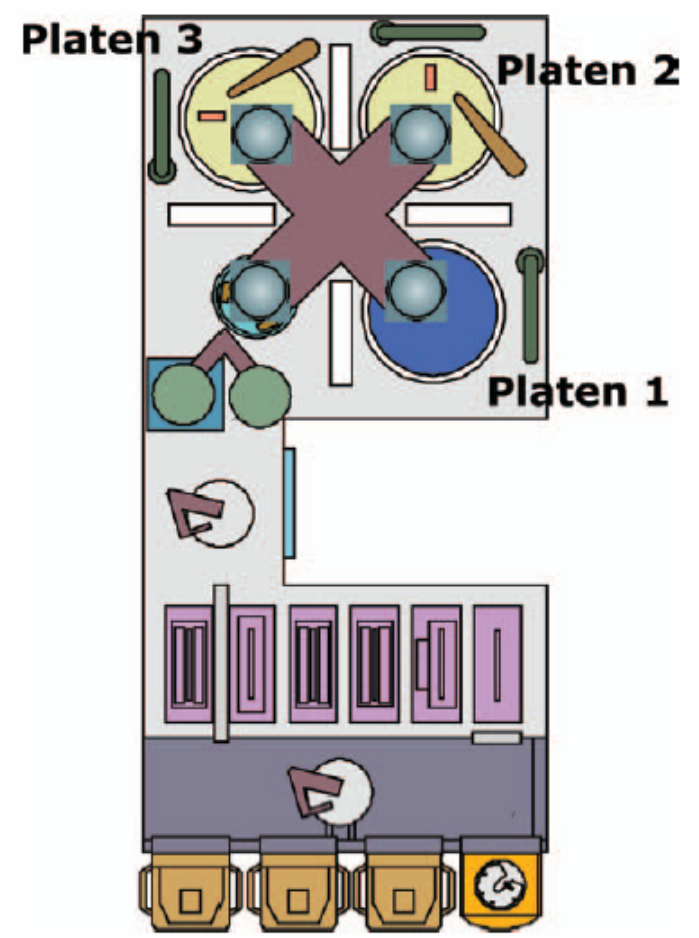

Figure 2.6: Schematic configuration of Reflection 300 mm LK CMP tool [2.5].

2.1.2. CMP Consumables

2.1.2.1 Polishing Pads

One of the most important components of the CMP system is the polishing pad. The main function of a CMP pad is to provide mechanical action and deliver slurry to the wafer surface to be planarized. Also, the pad aids in the removal of byproducts (slurry containing dissolved material being polished) and unused slurry away from the wafer. The most commonly used CMP pads are made of polyurethane [2.6]. Polyurethanes are typically composed of atleast three components (i) Long chain polyol, (ii) Diisocyanate and (iii) Chain extender. Polyurethanes combine good mechanical properties with excellent chemical stability and their properties can be precisely controlled. Furthermore, with polyurethane technology it is possible to fabricate a wide range of pad microstructures including foams, impregnated felts and solid pads, and to use a variety of manufacturing processes including casting, molding, extrusion and sintering. The pad may be categorized into four types differentiated by their microstructure [2.6]. The types are as follows:

Type 1: Polymer impregnated felts

Type 2: Poromerics (synthetic leather)

Type 3: Filled polymer sheets

Type 4: Unfilled textured polymer sheets

Table 2.2 summarizes the key features, properties, commercial trade names and typical applications for the different pad types. Apart from the hardness, size, and shape, groove pattern and asperities of the pad are also important. While perforated, XY and K-grooved pads are most commonly used, many groove designs are commercially available.

The pad is typically characterized by its specific gravity, hardness and compressibility [2.7, 2.8]. These properties can be tailored to meet the specific requirements during the casting and polymerization process. Table 2.3 lists several important properties of four polishing pads.

Pad	Specific gravity	Compressibility	Hardness
IC-1000	0.6	5%	55 (Shore D)
IC-60	0.7	N/A	52 (Shore D)
Suba IV	0.3	16%	55 (Shore A)
Suba 500	0.34	12%	65 (Shore A)

Table 2.3: Properties of the polishing pads [2.8].

Specific gravity indicates the pad porosity; the lower the specific gravity, the higher the porosity. Porosity is important because the pores aid in slurry transport and the pore walls aid in the removal of reaction products from the polish site. Hardness and compressibility have been found empirically to affect planarity [2.9]. The harder and more non-compressible the pad, the less it will bend and conform to the wafer surface to removal material at the low lying regions. On the other hand, if the pad is too hard, it may cause defects such as scratching. If the pad is too soft, it will conform to the topography, and global planarity cannot be achieved. Typically, pad configuration consists of a stack of a soft pad under a hard pad, with the hard pad making contact with the wafer [2.10]. For example, a stack of IC 1010 (hard pad) and Suba IV (soft pad) is currently the system of choice used by many manufacturers. The final buffing processes use very soft pads

such as Suba IV and Politex to polish the wafer to smooth out any scratches and reduce the amount of particulate contaminants left on the surface.

The novel design of pads has made it possible to retain the slurry on the platen without much wastage and efficiently transfer it to the wafer. During CMP, the abrasive particles in the slurry are caught in between the asperities of the pad, causing the wafer to hydroplane, and reducing the removal rate. This problem is typically eliminated by pad conditioning. Various pad conditioning methods are used to stabilize the removal rate. The pad is continuously conditioned at frequent intervals with a disc embedded with diamond particles. The pad conditioning restores asperities on the polishing pad surface and eliminates glazing or build up of the polishing by-products. The fixed abrasive pad (FAP) has emerged as a potential replacement for traditional slurry based CMP. The pad surface has abrasive particles evenly dispersed in a composite binder. The abrasive particles are bonded to the polycarbonate layer on the pad. Fixed abrasive pads with truncated pyramids, cylinders, and various other shapes are available. The main advantage of using FAP is the elimination of the use of abrasive particles in the slurry. The absence of particulates in the system drastically reduces the defects on polished wafers. The literature indicates that the use of FAP in polishing shallow trench isolation (STI) structures leads to high removal rates with good uniformity and less dishing [2.11].

	Type 1	Type 2	Type 3	Type 4
Structure	Felted fibers impregnated with polymeric binder	Porous film coated on a supporting substrate	Microporous polymer sheet	Non-porous polymer sheet with surface macrotexture
Microstructure	Continuous channels between fibers	Vertically oriented, open pores	Closed cell foam	None
Slurry loading capacity	Medium	High	Low	Minimal
Pad Examples	Pellon™, Suba™	Politex™, Surfin™, UR100™, WWP3000™	IC1000™, IC1010™, IC1400™, FX9™, MH™	OXP3000™, IC2000™
Compressibility	Medium	High	Low	Very Low
Stiffness	Medium	Low	High	Very High
Hardness	Medium	Low	High	Very High
Typical Applications	Si stock polish, Tungsten CMP	Si final polish, Tungsten CMP, post-CMP buff	Si stock, ILD CMP, STI, metal damascene CMP	ILD CMP, STI, metal dual damascene
Key US Patents	4,728,552 4,927,432	3,100,721 3,763,054 4,841,680 6,099,954	5,578,362 5,900,164	5,489,233 6,022,268

Note: Suba™, Politex™, UR100™, WWP3000™, IC1000™, IC1010™, IC1400™, MH™, OXP3000™, and IC2000™ are trade-names of Rodel Inc., Pellon™ and FX9™ of Freudenburg, and Surfin™ of Fujimi.

Table 2.2: List of the major types of pads and their properties [2.6].

2.1.2.2. Slurry

Slurry provides a combination of chemical and mechanical effects during polishing. It also acts as a dissipating medium to reduce the frictional forces developed at the pad/wafer interface. CMP slurry consists of abrasives, solution and additives such as inhibitors. The abrasive component provides mechanical action. It impacts and abrades the chemically treated surface exposing fresh surface for further attack. Silica (SiO_2) and cerium oxide (CeO_2) particles are the most commonly used abrasives [2.12-2.14]. The main role of chemical ingredients in slurry is to interact with the surface to be polished.

CMP is used in several process modules (STI, ILD, tungsten and copper) and each module requires different abrasives, chemicals and process properties to be effective. For example, oxide CMP slurries use a high concentration of silica particles (~ 10% weight) at alkaline pH values, as the removal is mostly mechanical in nature. The particle size varies from 50 - 150 nm [2.14, 2.15]. On the other hand, slurries for copper CMP typically contain a lesser amount of abrasives (~ 3% weight) at acidic pH values, as the removal rate is limited by the concentration of oxidizer and complexing agents [2.16, 2.17]. Commonly used oxidizers are hydrogen peroxide (H_2O_2), hydroxylamine (NH_2OH), potassium ferricyanide ($K_3Fe(CN)_6$), potassium iodate (KIO_3) and ferric nitrate ($Fe(NO_3)_3$). The complexing agents are added to ensure the solubility of the metal in solution. A key component of the slurry is a corrosion inhibitor, which is required to protect low lying areas by forming a passive film while higher areas are selectively removed by pad contact. Additionally, the inhibitors must be able to protect the film from further oxidation and corrosion before cleaning. A good example is benzotriazole (BTA, $C_6H_5N_3$), in copper CMP formulations. The chemical structure of BTA is shown in

Figure 2.7 (a). BTA ($C_6H_5N_3$) has one replaceable H atom attached to the N atom in the triazole group. The interaction of BTA with copper has been studied extensively [2.17-2.21]. The formation of insoluble Cu-BTA film is known to be responsible for the corrosion inhibiting properties of BTA. Under certain conditions, the formation of a thick, multilayered coating has been confirmed [2.22, 2.23]. Hydroxamic acids, which are synthesized by the reaction of an ester with hydroxylamine in alkaline solutions, are known to chelate cupric ions very strongly. Depending on the type and length of the organic chain, the stability constant of the chelates could be in the range of 10^8-10^{14} [2.24]. The use of salicylhydroxamic acid (SHA, $C_7H_7NO_3$), a compound containing two acidic groups, the phenolic OH and the hydroxamic acid, as an inhibitor for copper has been reported in the literature [2.25]. The chemical structure of SHA is shown in Figure 2.7 (b).

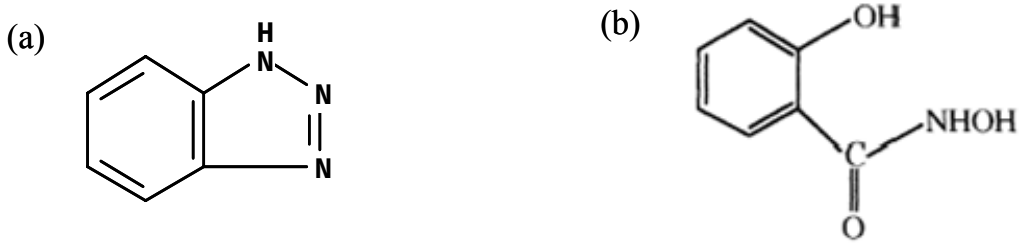

Figure 2.7: Chemical structure of (a) BTA and (b) SHA.

2.1.3. CMP Mechanism

The earliest polishing model based on mechanical parameters such as relative velocity and load was proposed by Preston [2.26]. The Preston equation states:

$$RR = K_P \, P \, R_V$$

where R_V is the linear velocity of the pad relative to the sample, P is the applied pressure (load per unit area) and K_P is the Preston coefficient. According to the Preston equation, the removal rate is directly proportional to both the velocity of the pad and the pressure. The proportionality constant K_P encompasses a number of parameters such as the elastic constants of the pad, wafer surface and abrasive material, frictional behavior, viscosity of the slurry, actual area of contact between pad and wafer etc. Several new models have been developed considering the concepts such as Young's modulus, film and pad hardness, and localized pressures, slurry flow, surface morphology and patterning [2.27-2.29]. Brown and Cook found that K_P had an inverse relationship with the modulus of polished glass material [2.30-2.32]. A detailed analysis and review of various models can be found in literature [2.33, 2.34].

2.1.4. Chemical Systems for Copper CMP

2.1.4.1. Hydrogen Peroxide - Glycine Based Chemical System

Hydrogen peroxide acts as an oxidizing agent by accepting one or two electrons as shown in following equations [2.35].

$$H_2O_2 + 2H^+ + 2e^- \rightarrow 2H_2O$$

$$H_2O_2 + H^+ + e^- \rightarrow {}^*OH + H_2O$$

The hydroxyl radicals (*OH) have a higher oxidizing power than the hydrogen peroxide itself. It has been reported in the literature that hydroxyl radical generation has been observed during copper CMP [2.36]. Hariraputhiran et al. [2.37] investigated the copper dissolution/polish rate in peroxide-glycine based chemistries. Figure 2.8 shows the dissolution rate as a function of rotation speed in 5% H_2O_2 containing 1% glycine solution. The dissolution rate increases up to 800 rpm and then plateaus out. Since the lifetime of hydroxyl radicals is in microseconds, the diffusion of radicals from the bulk to the surface interface is highly unlikely. Thus the dissolution rate is dominated by the amount of *OH radicals at the interface. The *OH generation is catalyzed by Cu (II) - $(glycine)_2$ chelate, which determines the dissolution rates.

Figure 2.9 shows the polishing rate as a function of glycine concentration in 5% H_2O_2, in the presence and absence of 3 % alumina particles [2.37]. As is clear from Figure 2.9, the polish rate increases with glycine concentration in both cases. However, the removal rate of copper is almost twice in the presence of abrasive at 2 % glycine. The dissolved/abraded copper from surface generates a high concentration of copper ions which complexes with glycine to catalyze *OH generation.

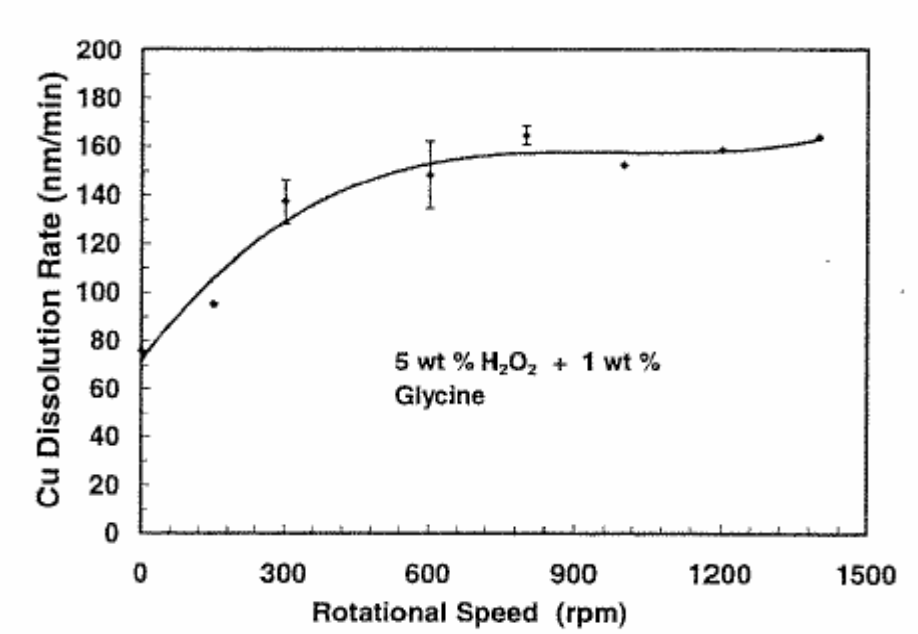

Figure 2.8: Dissolution rate of copper as a function of rotation speed [2.37].

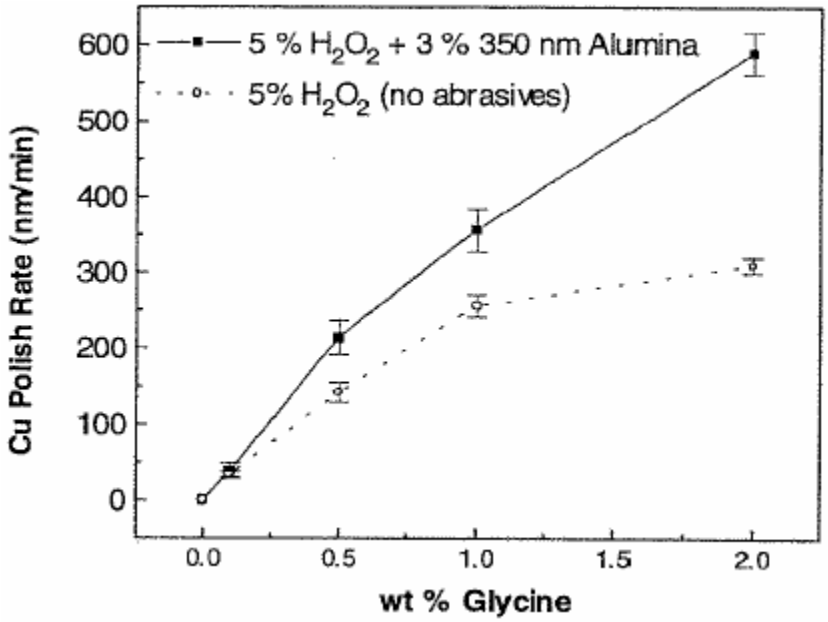

Figure 2.9: Polishing rate of copper as a function of glycine concentration in peroxide based slurry [2.37].

2.1.4.2. Ferricyanide and Nitric Acid Based Chemical System

To investigate the chemical and mechanical components of copper CMP, Steigerwald et al. used ferricyanide and nitric acid based chemical system containing alumina particles [2.38]. Figure 2.10 shows the polish rate of copper as a function of (a) potassium ferricyanide concentration at a pressure of 2 and 4.6 psi and (b) nitric acid concentration at a pressure of 2 psi. As shown in Figure 2.10 (a), at low ferricyanide concentration (≤ 1 wt%), the polish rate is linearly dependent on the ferricyanide concentration. Copper removal rate of ~ 3 μm/min was observed at a pressure of 2 psi for 1 wt % $K_3Fe(CN)_6$. However, at higher ferricyanide concentrations (> 1 wt %), the polish rate is independent of concentration. Also, while the change in applied pressure does not affect the polish rate at low ferricyanide concentrations, it does increase the polish rate at high concentrations.

Figure 2.10 (b) shows the removal rate of copper as a function nitric acid concentration in slurry containing 5 wt % alumina particles [2.38]. At 2.5% nitric acid concentration, copper removal rate of the order of 2 μm/min was observed. Above 2.5 vol % HNO_3, the polish rate is independent of concentration. Based on the existence of the two polishing regimes, Steigerwald et al. hypothesized that removal of copper during CMP is controlled by a two step process: (1) mechanical abrasion of the copper surface followed by (2) chemical dissolution of the abraded material. At high concentrations, the polish rate is limited by step (1) and therefore independent of oxidant concentration. The concentration of oxidant is high enough that the slurry fully dissolves all of the material abraded from the surface. Consequently, at high oxidant concentration, increasing the concentration does not increase the polish rate.

(a)

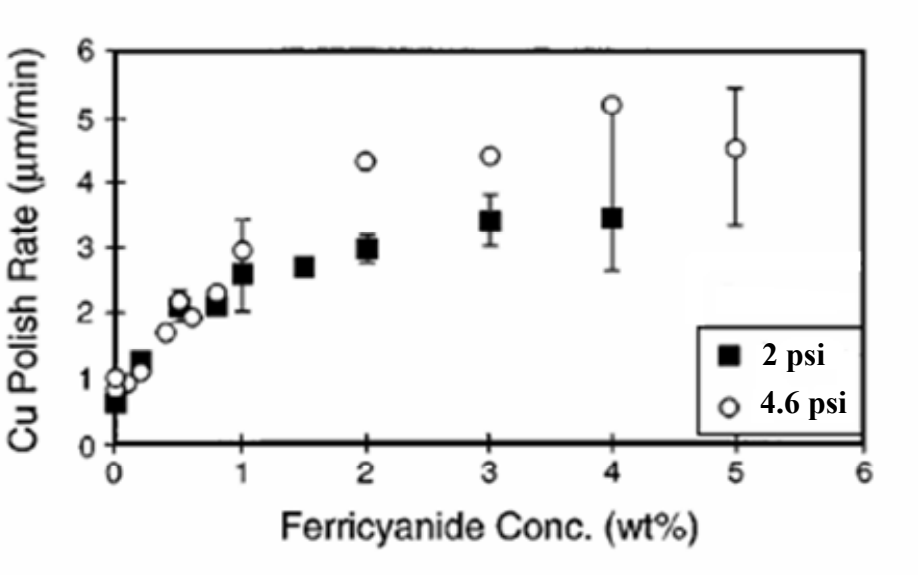

(b)

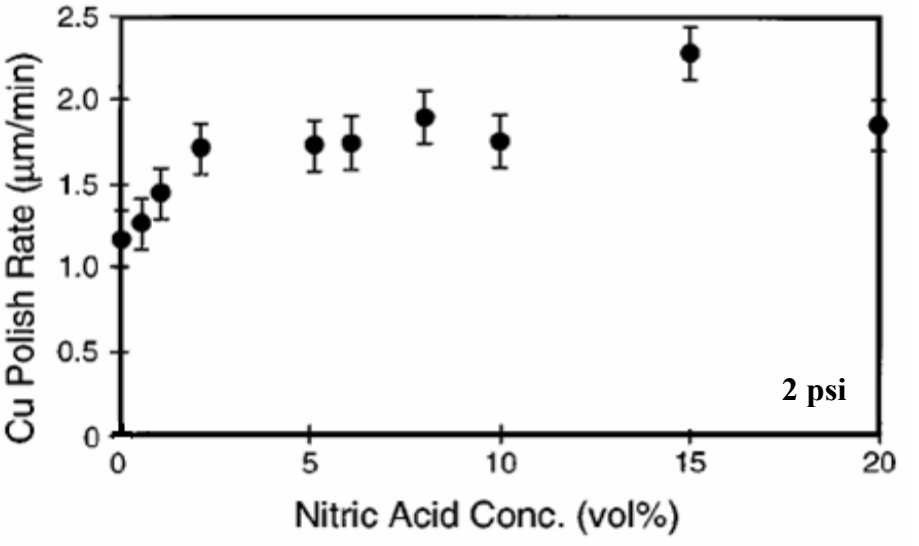

Figure 2.10: Copper polish rate as a function of (a) potassium ferricyanide concentration and (b) nitric acid concentration in slurry containing 5% alumina particles [2.38].

2.1.4.3. Hydroxylamine Based Chemical System

Hydroxylamine solution containing silica particles is used in copper CMP [2.39-2.44]. Hydroxylamine (NH_2OH) tends to function as an oxidizing agent at acidic pH values and as a reducing agent at higher pH values [2.45]. It is a weak base and is characterized by a pKa of 5.8 [2.46]. Copper dissolution rates in 0.5M hydroxylamine solution at different pH values are shown in Figure 2.11 [2.47]. The dissolution exhibits a maximum value in the vicinity of pH 6. The figure 2.11 also shows the speciation of hydroxylamine as a function of pH. It is interesting that the maximum dissolution rate occurs at a pH value very near the pKa of hydroxylamine. A free radical based dissolution mechanism of copper in hydroxylamine has been proposed by Carter and Small [2.48]. Using an electron spin resonance (ESR) technique, they found that when sulfuric acid was used for pH adjustments, $(HSO_3)_2NO^*$ free radicals were generated. They proposed that the free radical caused oxidation of copper via a catalytic mechanism. The oxidant becomes available in controlled amounts as it is being consumed during the metal removal step.

Tamilmani et al. [2.36] investigated the removal rates of copper in the presence and absence of abrasion in 0.5M hydroxylamine solution containing 4% SiO_2 particles (pH 6, with and without inhibitors). As shown in Figure 2.12, in the absence of any inhibitor (BTA or SHA) the static etch rate was very high ~ 850 Å/min, and the polish rate was 1200 Å/min. However, in the presence of 0.01M BTA or SHA, the static etch rate was almost zero and the polish rates were 170 and 400 Å/min respectively. This shows that the high areas can be removed by polishing while the low areas are completely protected, but the removal rates are low. At low concentrations of 0.005 M

BTA or SHA, the polish rates increased to ~ 1100 Å/min with a small increase in static etching (20 Å/min and 60 Å/min with 0.005M BTA and SHA, respectively). They proposed that the dissolution of copper takes place in three steps: 1) formation of nitrite from hydroxylamine through disproportionation 2) oxidation of copper by nitrite and 3) complexation of copper ions.

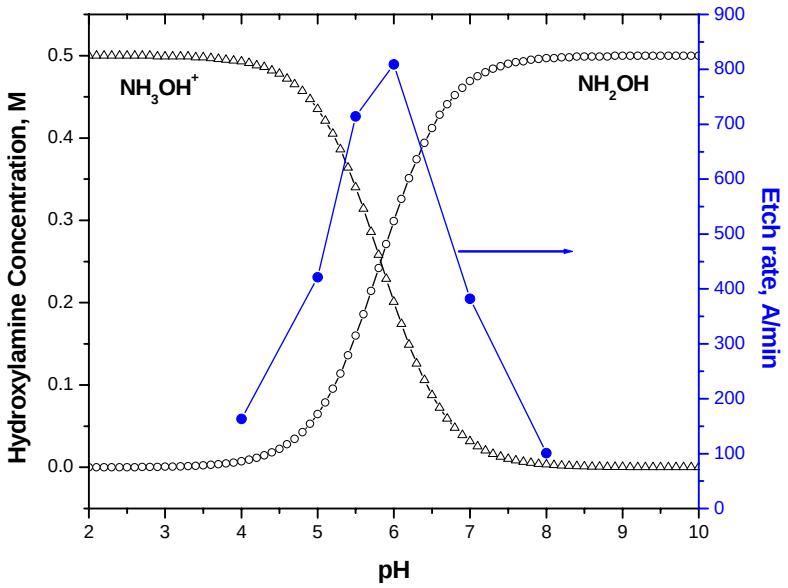

Figure 2.11: Dissolution rate of copper films in 0.5M hydroxylamine and the speciation of hydroxylamine as a function of pH [2.47].

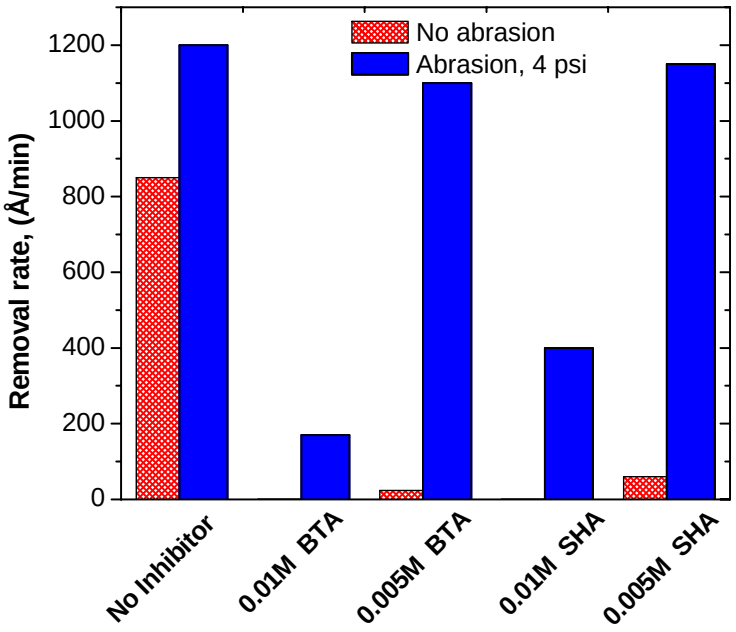

Figure 2.12: Removal rates of copper in the presence and absence of abrasion in 0.5M hydroxylamine solution containing 4% SiO_2 particles (pH 6, with and without inhibitors) [2.36].

2.1.5. Chemical Systems for Tantalum CMP

2.1.5.1. Alumina and Fumed Silica Based Chemical System

Jindal et al. studied the polishing of tantalum in DI water and peroxide based chemical system with and without abrasives at different pH values [2.49]. The polishing experiments were performed at a pressure of 6.3 psi. Figure 2.13 (a) shows the tantalum removal rates in DI water containing with and without abrasives at different pH values. As shown in Figure 2.13 (a), the polish rates without any abrasives are almost zero at all pH values studied, indicating the absence of direct dissolution and also suggesting that the abrasion between the pad and the passive film is insufficient for material removal. At pH less than 4, the removal rate of tantalum in the presence of alumina particles is very less ~ 15 nm/min, while the silica particles remove tantalum at a higher rate of 60 nm/min. The results indicate that tantalum removal in DI water is predominantly a process of removal of the pentoxide film at all the pH values. Alumina particles remove this layer by mechanical abrasion while silica removes it through its so-called ‘‘chemical tooth’’ action, as was established by Iler et al. [2.50-2.51]. A coordinate linkage is formed between tantalum and the ~SiOH groups, as shown in figure below. During polishing, the movement of silica particles away from the linkage site leads to the rupture of bonds, which in turn contributes to the removal of tantalum.

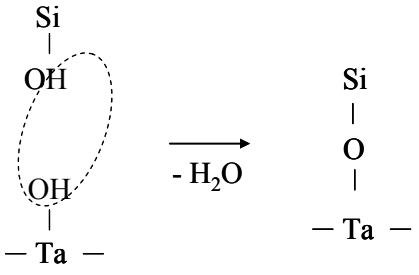

Figure 2.13 (b) shows the tantalum removal rates as a function of pH in 5 wt % peroxide solution in the presence and absence of silica and alumina particles [2.49]. Tantalum polish rates are very low, less than 5 nm/min in the absence of silica or alumina abrasives at all pH values. However, in the presence of alumina particles, the polish rate increases from pH 2 to 4, remains constant from pH 4 to 8, and then increases rapidly with pH, reaching ~ 240 nm/min at pH 12. The polish rates with silica particles were lower in the alkaline region but higher at pH $\leq$ 3. The tantalum removal in 5 wt % peroxide based slurry indicates the formation of different type of film on the surface. The exact structure and composition of the film has not been established. However, at pH values above 8, the oxide film becomes much softer, as determined by the hardness test. At such pH values, dissolution of the modified film assisted by mechanical abrasion is the dominant mechanism of tantalum removal [2.49].

(a)

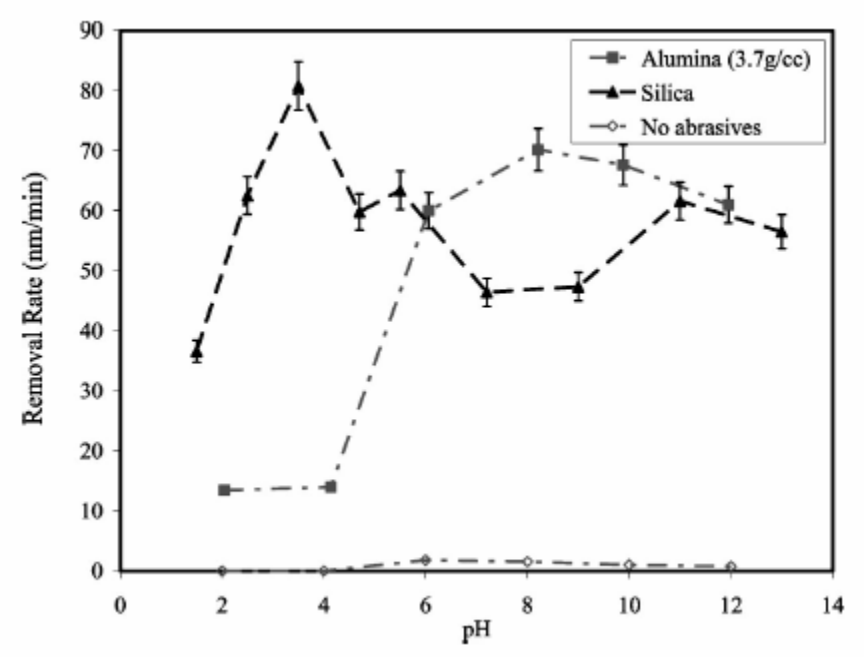

(b)

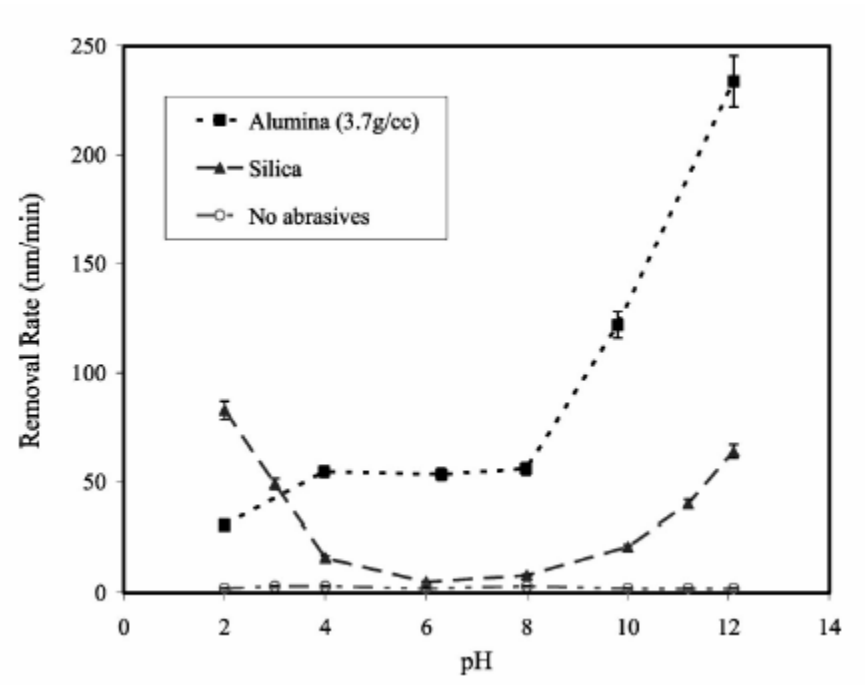

Figure 2.13: Tantalum removal rates as a function of pH in (a) DI water (b) 5 wt % peroxide solution, in the presence and absence of silica and alumina particles [2.49].

Hariraputhiran et al. studied the polishing of tantalum in fumed silica and alumina based slurry at a downforce pressure of 6.3 psi [2.52]. Table 2.4 lists the tantalum removal rate obtained using alumina particles dispersed in different oxidizing solutions [2.52]. The tantalum removal rate of 67 nm/min was obtained with alumina particles dispersed in DI water. However, the removal rate decreased with the addition of oxidants in the solution. For example, the addition of 0.1M ammonium persulfate decreases the removal rate to 32 nm/min. The decrease in removal rate was attributed to the enhanced formation of thick passive oxide film, which is harder than tantalum and hence difficult to remove. Table 2.5 lists the removal rates in various oxidizing solutions with and without silica abrasives [2.52]. These solutions did not contain any additives or stabilizers other than the chemicals listed. In the absence of the abrasive particles, no measurable removal rates were obtained in all cases. The removal rates obtained using slurries containing silica abrasives dispersed in DI water varied in the range of 36 to 74 nm/min, depending on the nature of the abrasives and the solids content in the slurry.

Tamilmani explored hydroxylamine and peroxide based chemical systems for tantalum CMP [2.36]. Figure 2.14 shows the removal rate as a function of pH in 0.5M hydroxylamine solution and 1.2M peroxide at a downforce of 9 psi [2.36]. The removal rate of tantalum decreases with decreasing pH in hydroxylamine solution. The highest removal rate of ~ 200 Å/min was obtained in 0.5M hydroxylamine solution at pH 8. However, in peroxide solution, the removal rate is ~ 50 Å/min and independent of pH. Tamilmani proposed that the metastable oxide formed on the surface may control the dissolution behavior of tantalum.

Slurry composition	Ta polish rate (nm/min)
3 wt % alumina[a] in DI water	67 ± 13
3 wt % alumina[a] + 0.1 M $Fe(NO_3)_3$ in DI water	32 ± 7
3 wt % alumina[a] + 0.1 M ammonium persulfate in DI water	32 ± 7
3 wt % alumina[a] + 1 wt % glycine + 5 wt % H_2O_2 + 1 wt % $Cu(NO_3)_2$ in DI water	48 ± 3

[a] Particle density of 3.7 g/cm^3 and a mean aggregate size of ~340 nm.

Table 2.4: Tantalum removal rates in various alumina-based slurries [2.52].

Abrasive	Solids content (wt %)	Ta polish rates in the presence of various chemicals (nm/min)		
		DI water	5 wt % H_2O_2	0.005 M $Fe(NO_3)_3$
No abrasives	0	0	0	0
Cab-o-sil L-90	3	36 ± 1	11 ± 2	16
	6	64 ± 1	30 ± 2	32 ± 2
Cab-o-sil L-150	3	57 ± 5	23 ± 2	19 ± 1
	6	74 ± 7	61 ± 3	65 ± 10
Aerosil 130	3	73 ± 4	20 ± 2	16 ± 3
Aerosil 200	3	58 ± 4	16 ± 3	13 ± 3

Table 2.5: Tantalum removal rates in various silica-based slurries [2.52].

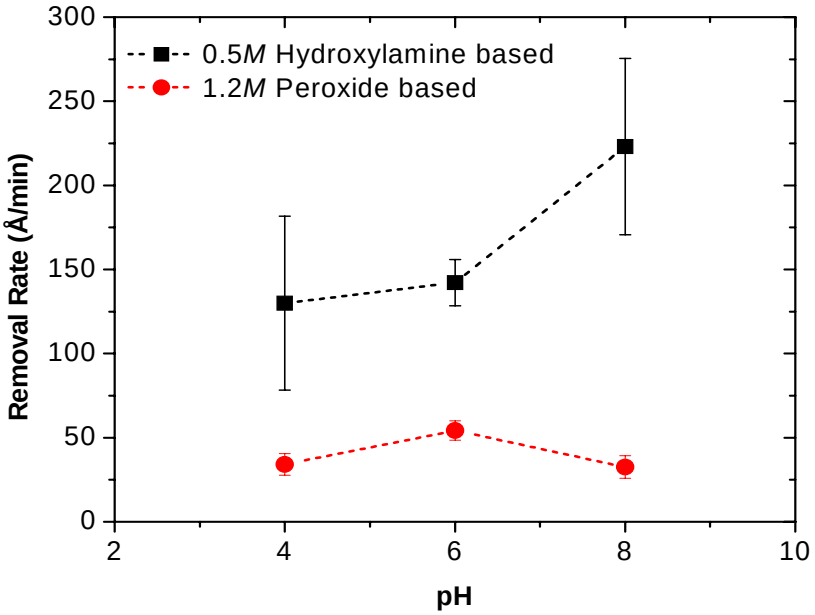

Figure 2.14: Removal rates of tantalum in 0.5M hydroxylamine and 1.2M hydrogen peroxide solution under abrasion using a fixed abrasive pad at 9 psi [2.36].

2.1.5.2. Colloidal Silica Based Chemical System

Tantalum undergoes oxidation in aqueous environments to form the native oxide (Ta_2O_5), which typically has a thickness of 20 Å. The pentoxide film is chemically inert due to its very limited aqueous solubility and solution reactivity. Zhang et al. studied the mechanism of tantalum removal in colloidal silica based slurries during polishing [2.53]. Figure 2.15 shows the tantalum removal rate in 1% peroxide solution containing 1% colloidal silica at two pH values at a pressure of 1.35 psi. The tantalum removal is linearly dependent as a function of polishing time at both pH. At pH 2, the tantalum removal is roughly 300 Å for one minute. However at pH 10, the tantalum removal is only ~ 50 Å for one minute. Under CMP conditions, tantalum which is covered with native oxide is removed but reformed as suboxide, Ta_xO_y as shown below. This suboxide has surface functional group depending on iso-electric point (IEP). The IEP of tantalum oxide is nearly 3.0. At pH 2, the oxide has more surface Ta-OH or $Ta\text{-}OH_2^+$ at pH 2 relative to $Ta\text{-}O^-$ groups compared with pH 10. Thus the interaction between the silica particles and the tantalum oxide was much greater at pH 2 than the pH 10. A schematic diagram showing the difference between surface functionalities at pH 2 and 10 is shown in Figure 2.16 [2.53].

The tantalum CMP mechanism is proposed to occur via a two step process. The first step is the oxidation of the tantalum surface to form an intermediate oxide. This oxide is then oxidized to form tantalum pentoxide as shown below. The second step is the removal of the surface oxide, thereby exposing a fresh tantalum surface for further reactions.

$$2Ta + 5H_2O_2 \rightarrow Ta_xO_y \rightarrow Ta_2O_5 + 5H_2O$$

The mechanical removal of the surface oxide is the rate limiting step in polishing conditions utilizing low downforces, low abrasive concentrations, and a soft pad. The removal of tantalum is predominantly a 'mechanical' process that involves the removal of the native oxide formed on the surface [2.53].

The effect of various oxidizing agents such as peroxide, persulfate and periodate on the removal rate of tantalum in 1% colloidal silica based slurry is shown in Table 2.6 [2.53]. The highest removal rate of tantalum has been reported at pH 2 and the oxidizer effectiveness for tantalum removal follows the trend persulfate > peroxide > periodate. At pH 2, tantalum removal rate of ~ 580 Å/min has been reported in persulfate solution. However, at pH 10, the removal rate is only 20 Å/min. The pH dependent changes in surface functionalities were responsible for observed polishing behavior.

	pH 2		pH 10	
	E^0 (V vs SHE)	Ta *RR* (Å/min)	E^0 (V vs SHE)	Ta *RR* (Å/min)
H_2O_2	1.66	330	1.18	54
$K_2S_2O_8$	2.00	580	1.53	20
KIO_3	1.05	150	0.58	16

Table 2.6: Removal rate of tantalum as a function of oxidizer type [2.53].

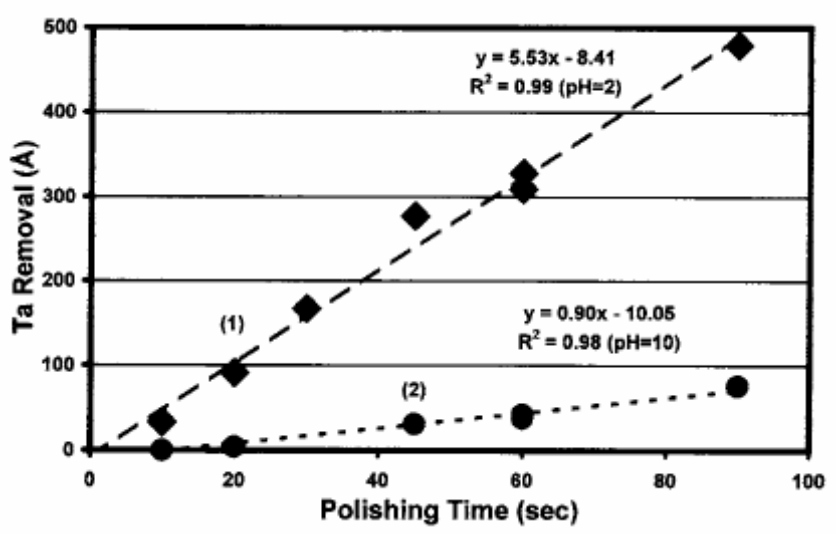

Figure 2.15: Tantalum removal rate as a function of time for pH 2 (curve 1) and pH 10 (curve 2) in colloidal silica-based slurry containing 1% H_2O_2 [2.53].

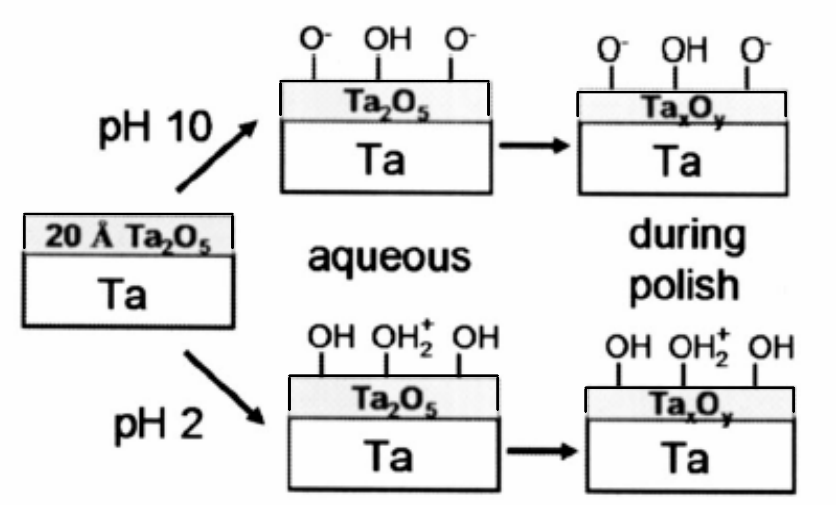

Figure 2.16: Schematic diagram showing the difference between surface functionalities at pH 2 and 10 [2.53]. Note that the intermediate state of the tantalum oxide is represented by Ta_xO_y with a slightly reduced thickness.

2.2. Motivations for Electro-chemical Mechanical Planarization (ECMP)

The conventional copper CMP process currently in use suffers from certain limitations that are making it difficult to extend the process to the fabrication of sub-65 nm devices that use ultra low-k dielectrics. These limitations include high dishing/erosion, use of high pressure (~ 2-5 psi) and film delamination/peeling, as mentioned earlier [2.54]. Since the removal rate in CMP is usually a function of pressure, resorting to low pressure processes may be a solution, although this may come at the expense of removal rates. To overcome this drawback, variants of CMP are being actively investigated.

A modification of the conventional CMP process known as Electro-Chemical Mechanical Planarization (ECMP) has emerged as a promising alternative. ECMP is a highly efficient process in which the removal rate is directly controlled by an applied current. In this method, a metallic film, typically copper, is polarized anodically by an applied voltage, while a pad makes mechanical contact with the film at very low applied pressure (< 0.3 psi) such that the copper film does not delaminate from the underlying low-k film [2.55-2.56]. Figure 2.17 shows the comparison of copper and barrier layer peeling in a conventional CMP and an ECMP process. As shown in the figure, no copper and barrier layer peeling was observed in ECMP process carried out at a very low pressure of 0.3 psi. However, in conventional CMP process, both copper and barrier layer peeling was observed at a pressure of 1.9 psi. The applied current can be varied at different radial ‘zones’ on the wafer, thereby allowing control of the removal rate to desired values [2.57]. Due to enhancement of electrochemical factors, the particulate content of the slurry can be significantly reduced, or in some cases eliminated [2.58]. The consumables cost for ECMP is around 30% less than that for conventional CMP [2.59]. It

has been reported in the literature that the ECMP technique is best suited for copper/low-k structures at the 65 nm device node and beyond [2.59].

Significant advantages of using the ECMP process include:

1. Better uniformity and more selective planarization, both locally and globally on the wafer;
2. Less dishing/erosion and reduced risk of film delamination/damage to low-k film due to very low downforce pressure. Also, low downforce polishing conditions increase the pad life;
3. Less defect density as a result of the reduction or elimination of solid content in electrolyte;
4. Precise electrochemical endpoint detection;
5. In addition to technology and throughput benefits, the replacement of expensive CMP slurry with a low cost electrolyte reduces the consumable costs and less waste generation.

2.3. ECMP Technology

Figure 2.18 shows a schematic representation of a bulk copper ECMP process. The copper film is polarized anodically by an applied current while a pad makes mechanical contact with the copper surface at a very low applied pressure. Copper is oxidized to Cu (II) ions with the release of two electrons,

$Cu \rightarrow Cu^{2+} + 2e^-$

Chemical formulations containing inhibitors protect low lying areas while higher areas are selectively removed, as shown in Figure 2.18. The passive film must have

excellent chemical stability but poor mechanical stability, so that it can be removed easily by the application of a very small downforce [2.60, 2.61]. A schematic representation of ECMP process steps are shown in Figure 2.19 [2.62]. Step 1 is the removal of bulk copper. Steps 2 and 3 are used to remove the remaining copper film and barrier film, respectively. Currently, copper ECMP has been explored for bulk copper removal only (step 1). The remaining steps are processed through conventional CMP.

Economikos et al. developed a copper ECMP process for 65nm and future generation device technology nodes in the fabrication of advanced interconnects [2.59, 2.62]. Figure 2.20 indicates that the applied charge controls the amount of copper dissolution. *Unfortunately, the literature does not provide any values for applied voltage or current used.* ECMP allows modification of the polish recipe based on the thickness profile of the incoming wafer. The applied current can be controlled by an independent electro-chemical zone system such that the charge at different portions of the wafer can be varied. They developed a mathematical model to determine the post polish profile, based on in-situ real time detected current. The thickness of incoming copper film on each wafer was automatically measured to accurately control the bulk copper removal and detect the endpoint. The copper removal rate of 6,000 Å/min was obtained at a pressure of 0.3 psi. Also, the remaining copper thickness was quite uniform regardless of the patterned structure (0.18 μm array, 0.25 μm array, 10 μm line and 50 μm bond pad), within a range of 200 Å or even less.

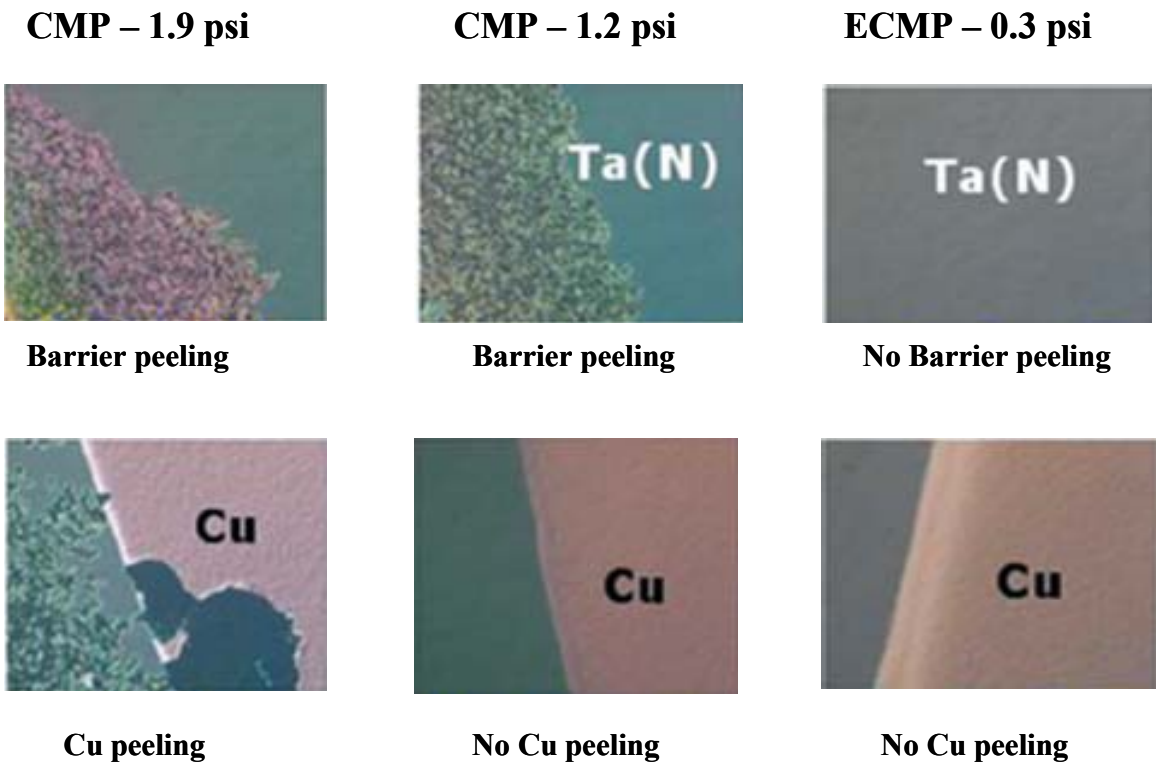

Figure 2.17: Comparison of copper and barrier layer peeling in a conventional CMP and an ECMP process [2.62].

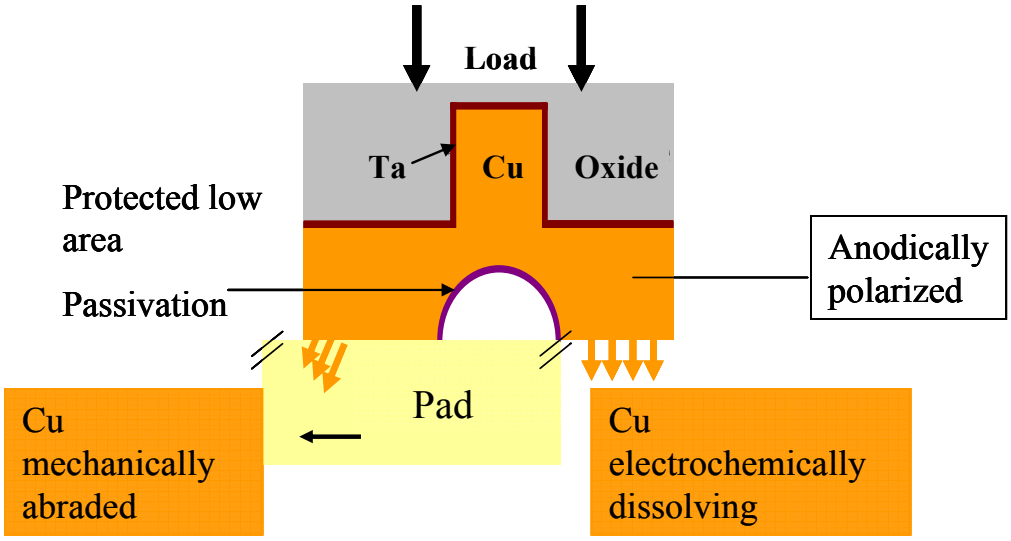

Figure 2.18: Schematic representation of bulk copper ECMP process.

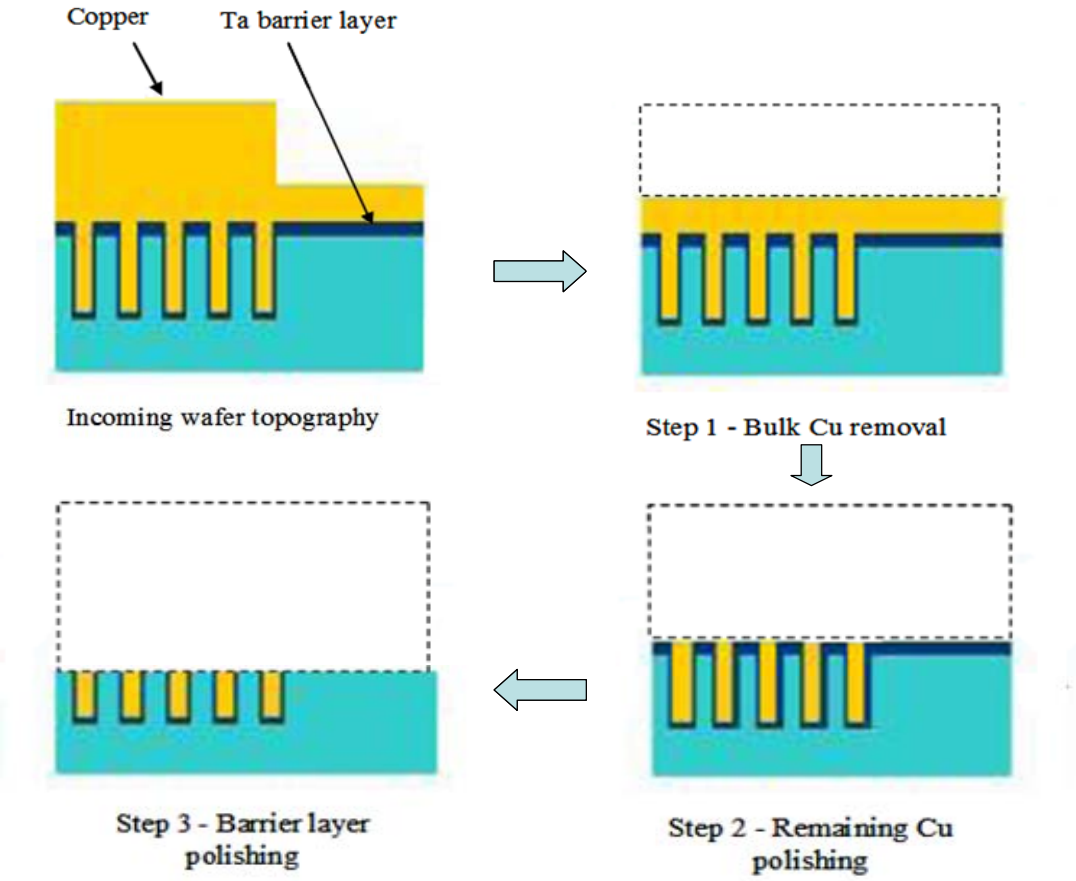

Figure 2.19: Schematic representation of ECMP process steps [2.62].

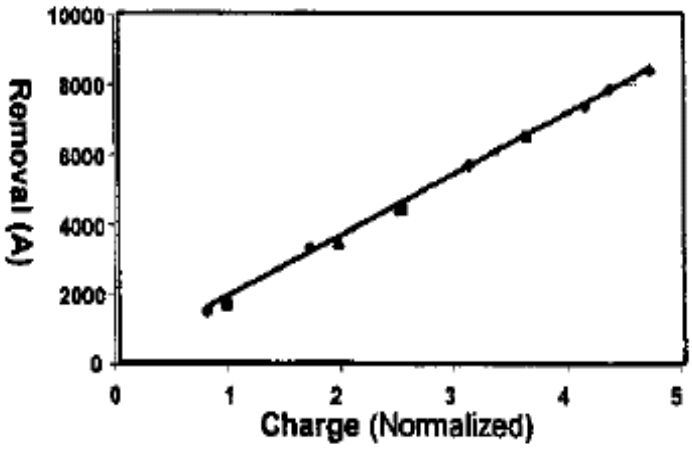

Figure 2.20: Relation between copper removal rate and applied charge [2.62].

2.3.1. ECMP Tool

A schematic representation of an ECMP tool is shown in Figure 2.21 [2.60]. The top part of the ECMP tool consists of copper wafer which acts as anode and a wafer carrier which is rotated by a motor. The electrolyte is delivered from the top. The bottom part consists of a conductive plate which acts as a cathode, and a perforated polishing pad to allow electrolyte to make ionic contact with the cathode surface. The bottom motor controls the rotation of the platen. As shown in the figure, the tool has been coupled with a power supply to apply an anodic bias to the wafer. A three-electrode setup has been used for all polishing experiments.

Recently, Applied Materials Inc., has made a major breakthrough in planarization technology with its revolutionary 300mm Reflexion LK ECMP tool. Figure 2.22 shows the Reflexion LK 300 mm ECMP tool showing single platen [2.5, 2.63]. The perforated polishing pad is attached to the bottom platen and the wafer is held by the carrier on top. The applied current can be varied at different radial 'zones' on the wafer thereby allowing control of removal rate to desired values. In-situ conditioning of the pad is provided by means of a diamond disc as shown in the figure. Based on the Reflexion LK CMP tool (as discusses in section 2.1.1), the Reflexion LK tool performs electrochemical mechanical planarization in copper/low-k applications at the 45-nm node and beyond. The tool has three platens architecture which provides high performance planarization for copper damascene structure. The first platen remove bulk copper at a high rate (~ 6000 Å/min) by electric charge with a very low pressure (less than 0.3 psi) that minimizes device pattern sensitivity associated with conventional CMP. This is followed by a fine polish step to remove the remaining thin copper film on platen 2, and finally a barrier

removal step on platen 3. Reflexion LK ECMP tool also features key process control capabilities, including its proprietary integrated iMap radial scan technology, which provides incoming film thickness profile information to accurately control bulk copper removal profile and endpoint detection. The Applied Reflexion LK ECMP tool includes the Desica cleaner, which integrates a full immersion vapor dryer for complete compatibility with low-k and ultra low-k films.

2.3.2. Pads/Electrodes for ECMP

During ECMP, anodic biasing of metallic film with respect to solution is typically done through conductive areas in the pad. The conductive area can be a piece of embedded metal or a conductive coating. The pad designed by Kondo et al. [2.64] consists of a surface carbon layer (anode), an intermediate insulating layer, and an underlying cathode sheet as shown in Figure 2.23. The insulating layer between the anode and the cathode acts as a cushion to improve within wafer non-uniformity. The soft carbon layer prevents damage to the copper surface. More than a hundred electro-cells, each about 5 mm thick, are fabricated inside the pad. The electrolyte is supplied through small holes in the platen. The electrolyte can also flow along the channel between the anode and cathode and drains outside to the edge of the pad. This design prevents Cu^{2+} ions from being electroplated onto the cathode surface. This also reduces the risk of delamination of copper film which often causes scratching on the wafer surface. An adhesive sheet was used to stick the carbon pad onto the CMP platen. This provided the flexibility of converting a CMP system into an ECMP system by replacing the conventional polyurethane pad with the carbon one. The power was supplied at the edge

of the pad. Ideally, the anode, which is exposed to ECMP electrolyte, must be inert with a wide potential window for water stability. This could improve current efficiency. One such electrode material is *boron doped diamond*.

An overview of the pad/electrode structure designed by Wada et al. [2.65] is shown in Figure 2.24. It consists of two parts: a processing electrode (cathode) used to remove the copper film, and a feeding electrode (anode) used to supply current. Both electrodes have an ion exchange film that serves as a catalyst, and they touch the copper film on the wafer. An electrolyte can be supplied to the interface of the copper film/ion exchanger, the ion exchanger, and the interface of the electrodes/ion exchanger. The current flows in a path from the anode, through the copper film and the electrolyte towards the cathode. The ion exchanger increases the ionic concentration of the electrolyte. Removal of copper film takes place underneath the processing electrode. Several of these electrode combinations are placed across the platen to increase the total area of the cathode. To ensure uniformity across the wafer, the electrodes and the wafer move relative to each other.

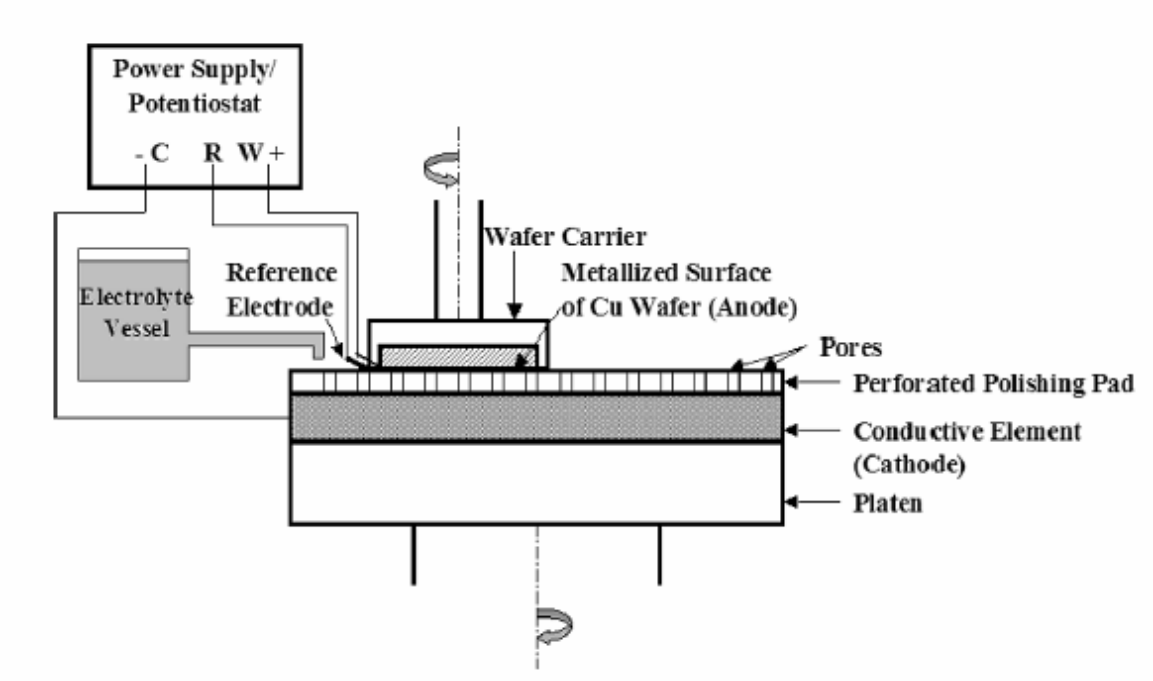

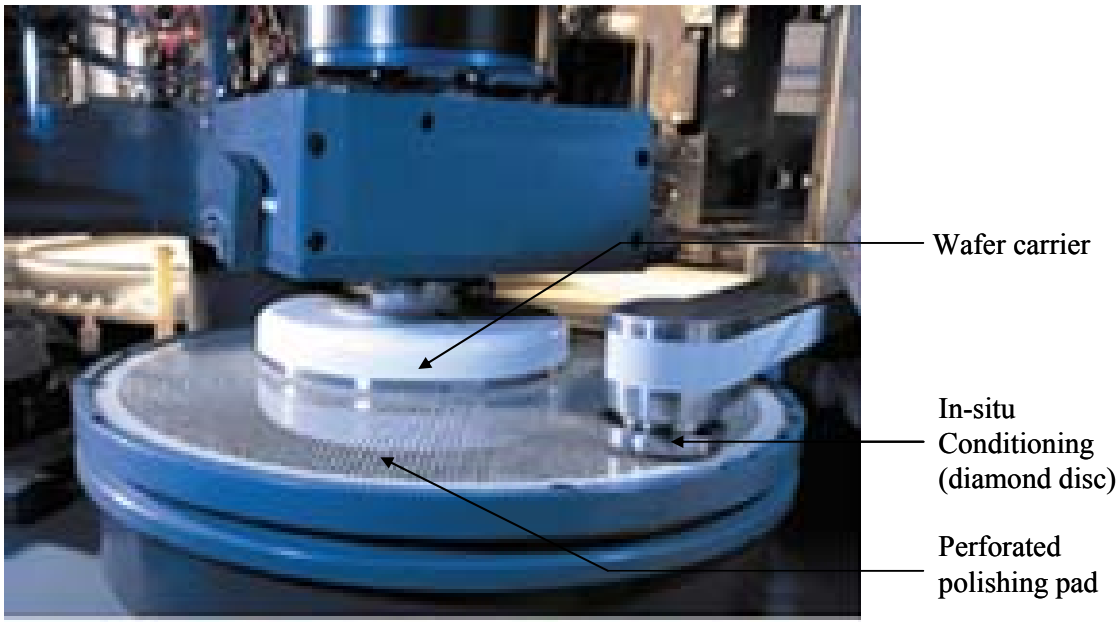

Figure 2.22: Applied's Reflexion LK 300 mm ECMP tool showing platen 1 [2.63].

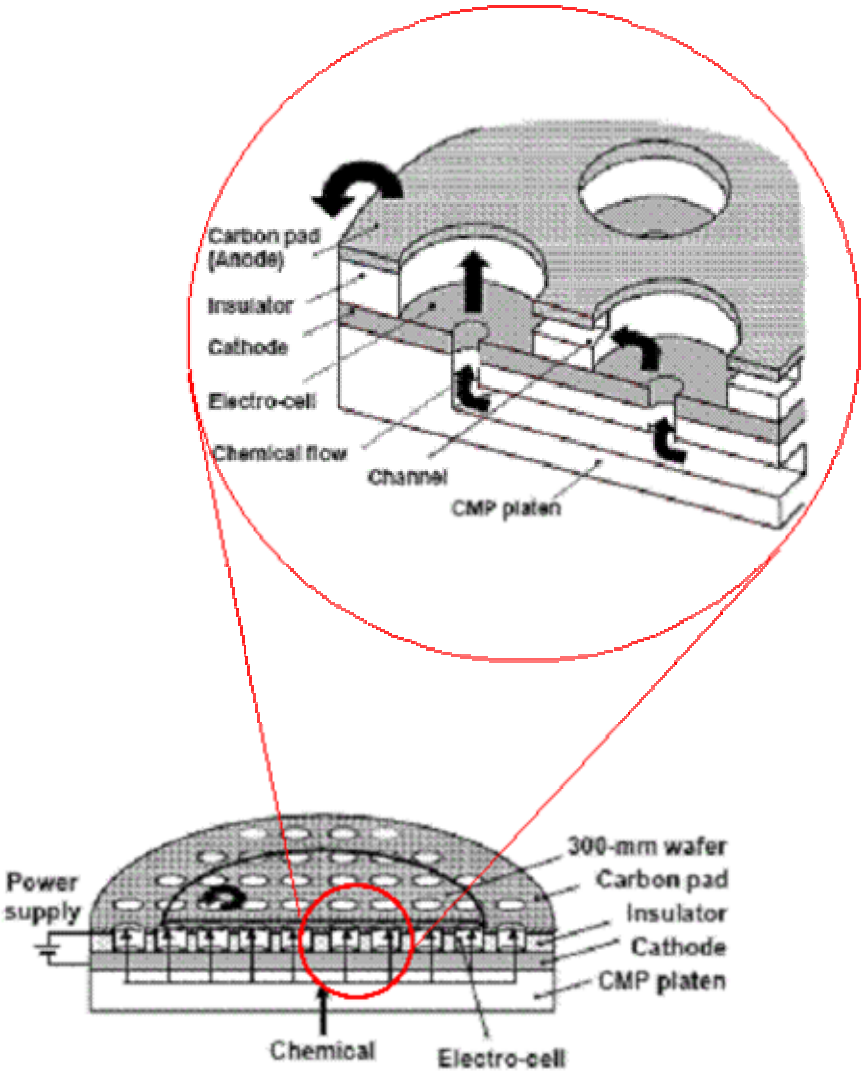

Figure 2.23: Conductive carbon pad used for polishing copper in the fabrication of Cu/low-k interconnect structures [2.64]. [Inset: Electro-cell structure fabricated in the carbon pad].

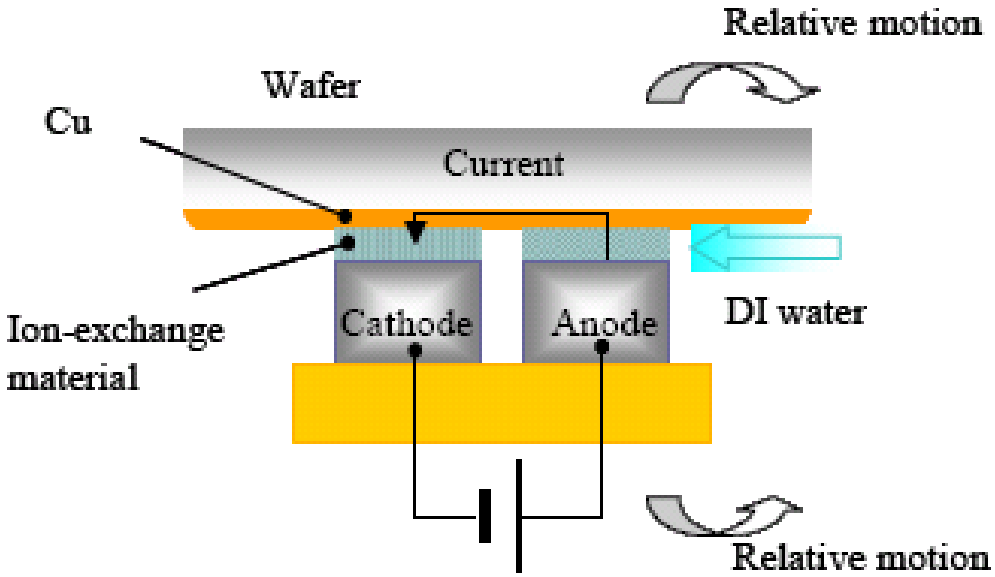

Figure 2.24: Schematic of the pad/electrode structure used by Wada et al. [2.65].

2.3.3. Chemical Systems for Copper ECMP

The chemical system used for ECMP typically contains ingredients to dissolve and complex the metal, and a corrosion inhibitor which is required to protect low lying areas by forming a passive film while higher areas are selectively removed through pad contact.

Kwon et al. [2.66] used KOH based electrolytes and studied the effect of additives such as peroxide and citric acid on ECMP of copper. Polishing experiments were performed at 1 psi. The static and dynamic removal rates were measured as a function of KOH concentration and applied overpotential. They found that the removal rate of copper was saturated at about 60 nm/min in 5% KOH solution. Unfortunately, the literature does not indicate the pH values. This rate was constant as a function of applied overpotential values (0.1V, 0.3V and 0.5V) in the passivation region. The addition of peroxide decreased both the static and dynamic removal rate of copper. For example, the addition of 5% H_2O_2 to the solution containing 5% KOH, decreases the removal rate to 25 nm/min at an overpotential of 0.3V. This decrease in rate was attributed to the formation of thick and dense copper oxide formed at higher concentrations of H_2O_2. However, the addition of 0.3M citric acid to 5% KOH electrolyte increased the dynamic removal rate to 100 nm/min. Figure 2.25 (a) show the effect of citric acid concentration on the removal rate of copper in solution containing 5% KOH and 1% H_2O_2 at an overpotential of 0.3 V. At low concentrations of citric acid ($\leq$ 0.2 M), the removal rate is 50 nm/min. The increase of citric acid concentration to 0.3 M increased the removal rate to 250 nm/min, which was a five fold increase of removal rates when compared to that in 0.2 M citric acid due to the enhanced complexation of Cu ions by citrates. The effect of peroxide concentration

on the removal rate of copper in citric acid and KOH based electrolyte is shown in Figure 2.25 (b). In solution containing 5% KOH and 0.3M citric acid concentration, increasing the peroxide concentration from 1% to 5%, increases the removal rate to 350 nm/min. At 10% H_2O_2, the removal rate decreases to 150 nm/min. The decrease in removal rate was attributed to the thick and dense copper oxide formation which may prevent electrochemical reaction.

(a)

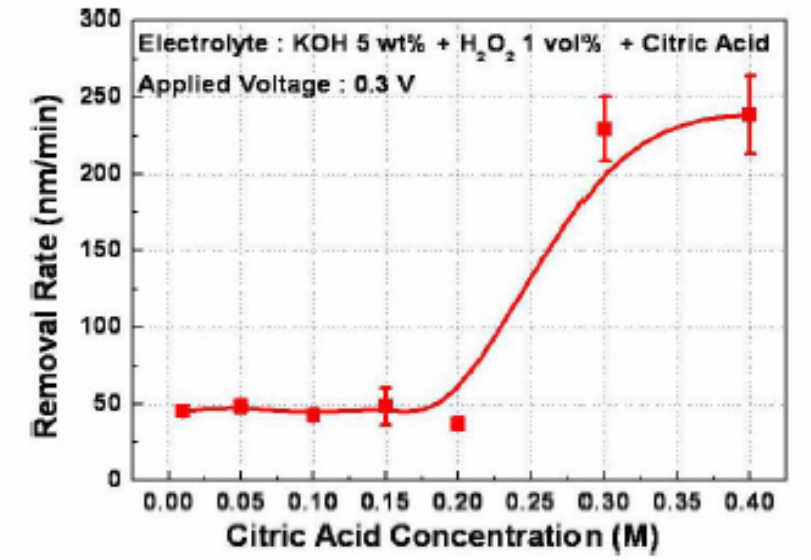

(b)

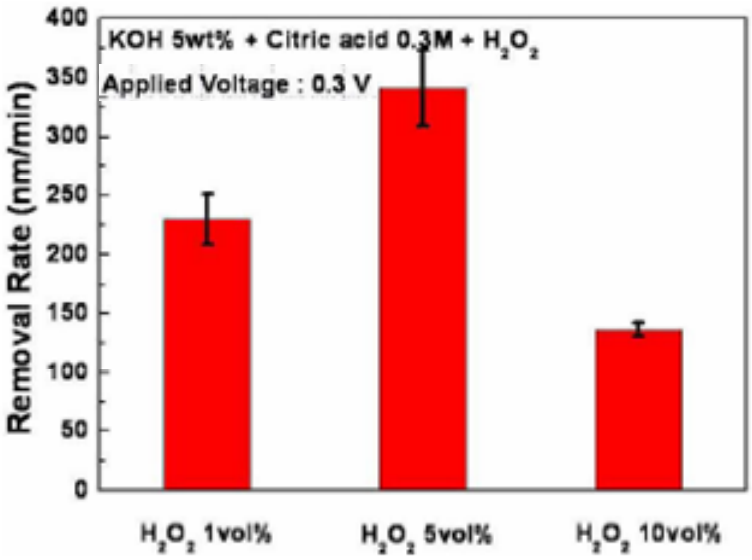

Figure 2.25: Removal rate of copper as a function of (a) citric acid concentration and (b) peroxide concentration in KOH based electrolyte [2.66].

Tamilmani [2.36] evaluated citric acid based chemistries for ECMP of copper. Citric acid ($C_6H_8O_7$ or H_3L) is a tribasic acid with pKa values 2.87, 4.35 and 5.69. The chemical structure of citric acid is shown below.

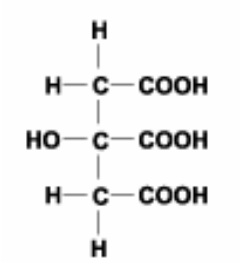

Figure 2.26: Chemical structure of citric acid

Literature indicates that the presence of citric acid in the slurry would favor copper dissolution through the formation of complexes [2.67]. Cupric ions forms a cationic complex, $Cu(H_2L)^+$ in the pH range of 3-4 and the doubly charged anionic complex, $Cu(H_{-1}L)^{2-}$ in the pH range from 5-11 [2.67, 2.68]. Figure 2.27 (a) compares the actual dissolution rates and rates estimated from the current profile. At 0.01M citric acid (pH 4), the dissolution rate measured by atomic absorption spectroscopy (AA) and electrochemical measurements (EC) under OCP condition was less than 10 Å/min. The dissolution rates gradually increased with an increase in anodic overpotentials (η). The addition of 2 M H_2O_2 to 0.01M citric acid solution increased the copper dissolution rate (AA) to 600 Å/min even at OCP conditions, but the rate obtained from electrochemical measurements for the same condition was only 20 Å/min. The copper dissolution rate (AA) reached a plateau value of approximately 800 Å/min at an overpotential of 150 mV. The electrochemical rates showed a dependence on the overpotential but were very low compared to the actual dissolution rates. Tamilmani attributed the difference in removal rate to the mechanical removal of copper through grain boundary attack [2.36].

Figure 2.27 (b) compares the removal rates (physical removal rate, AA) of copper in 0.01M citric acid solution containing 2M hydrogen peroxide and 0.5% silica particles under both abrasion and no abrasion conditions. The removal rates under abrasion conditions are higher, of the order of 400 Å/min, compared to the dissolution rates (no abrasion) under the same conditions. Also, the removal rates are equal at both 2 psi and 9 psi, suggesting that the removal rate increases only by pad contact and is independent of pressure above 2 psi. The polish rates increase with overpotentials (950 Å/min at OCP and 1200 Å/min at an overpotential of 450 mV), but the increase is not very large (250 Å/min over a potential range of 450 mV). Thus the citric acid based chemistry does not provide a large improvement in the removal rates under ECMP conditions.

The addition of a corrosion inhibitor in the electrolyte can allow for selective planarization of high lying regions while protecting the low lying regions of the surface. Organic compounds which can form protective films when undergoing oxidation may be suitable for ECMP. One such compound is thiosalicylic acid (TSA), which has been found to be useful for copper under ECMP conditions. The use of TSA as an inhibitor for copper in oxalic acid solutions was investigated by Lowalekar [2.24]. The static dissolution rates of copper as a function of oxalic acid concentrations and applied overpotentials are tabulated in Table 2.7. At OCP condition, the dissolution rate of copper was very low at all oxalic acid concentrations. The copper dissolution rate as high as 830 nm/min was obtained in 0.5M oxalic acid solution at an overpotential of 750 mV. Lowalekar further investigated the effect of two inhibitors such as thiosalicylic acid (TSA) and BTA on copper dissolution in oxalic acid solution under polishing conditions

(load ~ 2 psi). Figure 2.28 shows a comparison of BTA and TSA as inhibitors for copper exposed to 0.3 M oxalic acid solution at pH 4. The copper removal rate as high as ~ 240 nm/min with zero static dissolution rate was obtained in 0.3 M oxalic acid solution containing 0.005 M TSA (pH 4) at a current density of 12 mA/cm^2. In comparison, for 0.005 M BTA, the static dissolution rate of copper was 65 nm/min and the removal rate was 235 nm/min. Similarly, the static dissolution rate and removal rate of copper in solution containing 0.001 M BTA were 70 nm/min and 275 nm/min respectively. However, no static dissolution of copper was seen in a solution containing 0.005 M TSA, while a rate of 60 nm/min was seen in those containing 0.001 M TSA. Their results show that the inhibition efficiency of TSA is 100% even for a higher overpotential of 750 mV (which corresponds to a current density of 12 mA/cm^2), while for BTA, the efficiency is only 88% under the same overpotential.

Lowalekar explored the mechanism of inhibition by simultaneous recording of current as well as mass changes obtained from Quartz Crystal Microbalance (QCM) during the application of potential to electrodeposited copper films [2.24]. TSA oxidizes at high anodic potentials to form a *disulfide* which acts a passive film to prevent static copper dissolution.

One of the main requirements of ECMP is that the majority of applied current (charge) should be used in the oxidation of the metal of interest. Any side reactions such as oxidation of organic constituents and even water would be detrimental to the overall current efficiency. However, in cases where a redox inhibitor is used in the formulation, a part of the applied current has to be sacrificed for the oxidation of inhibitor.

(a)

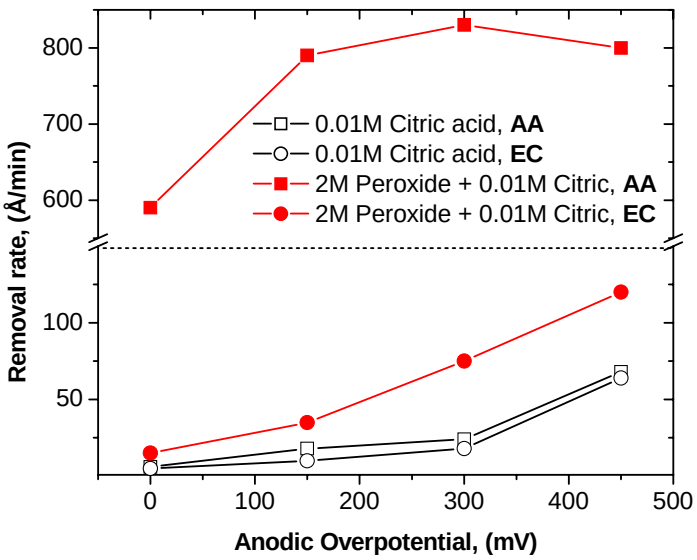

(b)

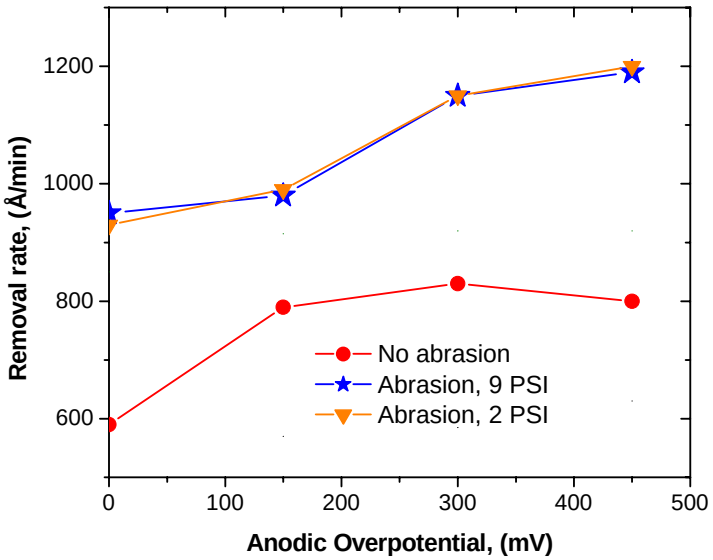

Figure 2.27: Removal rates of copper in citric acid chemistries under both abrasion and no abrasion conditions. a) 0.01M citric acid in the presence and absence of 2M hydrogen peroxide, b) 0.01M citric acid solution containing 2M hydrogen peroxide and 0.5% silica particles [2.36].

Oxalic acid concentration (M)	Static dissolution rate(Å/min) at η			
	0 mV	300 mV	500 mV	750 mV
0.1	1	600	1280	1890
0.3	2	1240	2910	5620
0.5	2	1700	4090	8260

Table 2.7: Dissolution rate of copper as a function of oxalic acid concentration and applied overpotential [2.24].

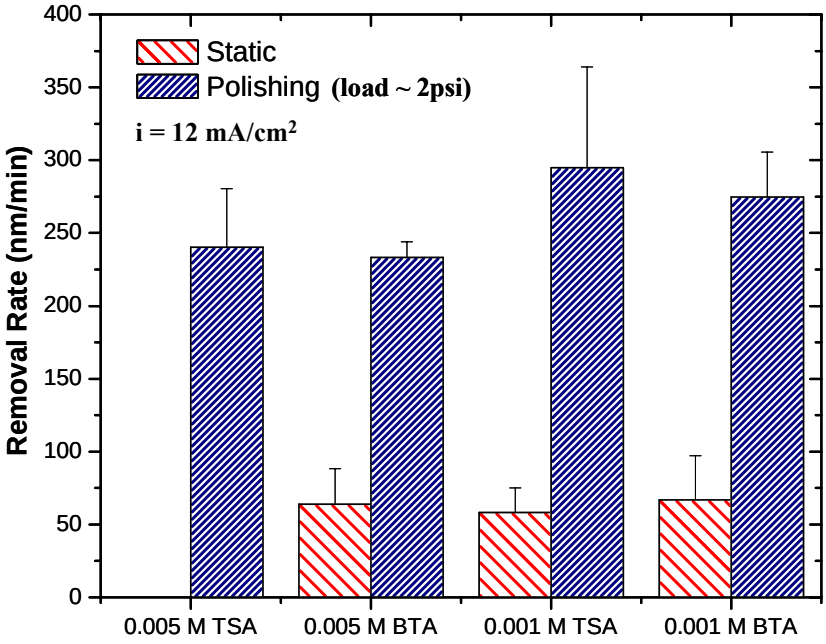

Figure 2.28: Comparison of BTA and TSA as inhibitor for copper exposed to 0.3 M oxalic acid solution at pH 4 [2.24].

The use of ammonium dodecyl sulfate (ADS) as an inhibitor for copper in solution containing 1% glycine and 1% peroxide solutions at pH 4 was investigated by Hong et al. [2.69]. Figure 2.29 shows the inhibition efficiencies of ADS and BTA at overpotentials of 0.1 and 1 V, in the absence of mechanical polishing. At an overpotential of 0.1V, the inhibition efficiency for ADS and BTA at a concentration of 0.01M is roughly 85%. As the concentration of BTA deceased to 0.001M, the efficiency is decreased to nearly 10%. However, ADS retain the same efficiency even at 0.001M concentration. At a higher overpotential of 1 V, the inhibition efficiency for 0.01M ADS and 0.01M BTA has decreased to 75% and 40%, respectively. It is clear that the inhibition efficiency decreases as the overpotential is increased in both ADS and BTA. This could be attributed to the fact that as the overpotential is increased, the passive film is more likely to break, resulting in copper dissolution.

The corrosion parameters of copper and inhibition efficiencies of ADS and BTA are listed in Table 2.8 [2.69]. IE_0 and IE_E represent the inhibition efficiencies at open circuit potential (OCP) and applied overpotential values, respectively. In solution containing ADS, the highest inhibition efficiency of ~ 85% was obtained at OCP and 0.1V overpotential. In the case of BTA, the efficiency is less than 35% under all conditions. The mixed ADS-BTA layer acts as a good inhibitor at OCP and 0.1V overpotential. However, at an overpotential of 1V, the inhibition efficiency is much less ~ 35%. These results indicate that ADS is a better inhibitor compared to conventionally used BTA for ECMP of copper.

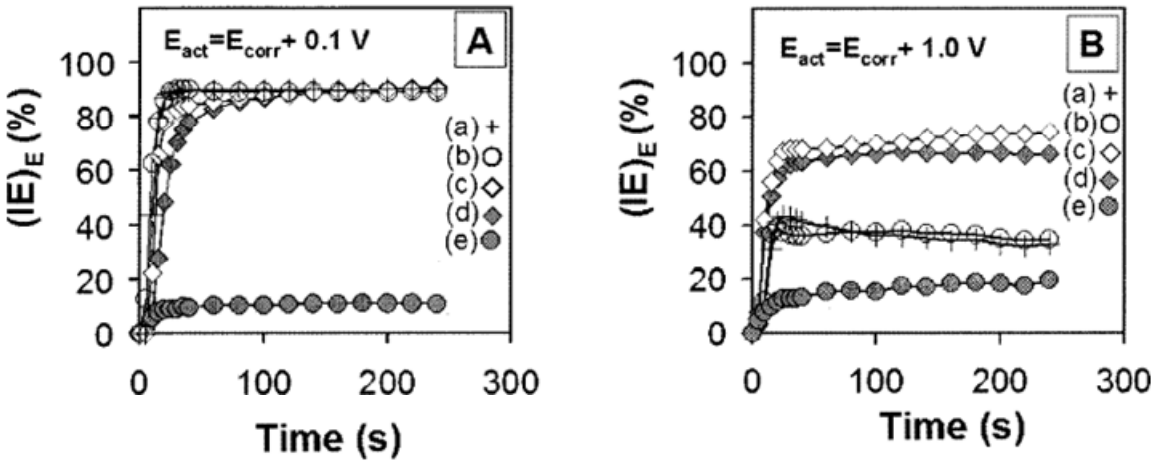

Figure 2.29: Inhibition efficiency, $(IE)_E$ of ADS and BTA at an overpotential of 0.1V and 1V measured as a function of sample immersion time in 1% glycine containing 1% H_2O_2 (pH 4) and (a) 10^{-3}M ADS + 10^{-3}M BTA (b) 10^{-2}M BTA (c) 10^{-2}M ADS (d) 10^{-3}M ADS and (e) 10^{-3}M BTA [2.69].

Corrosion parameter	Reference slurry, (Ref.)[a]	Ref. +1 mM ADS	Ref. +1 mM BTA	Ref. +1 mM ADS +1 mM BTA
E_{corr} (V vs. SCE)	0.27	0.36	0.28	0.29
i_{corr} (μA cm^{-2})	440	66	290	5.3
$[IE]_0$	-	85.0	34.1	98.8
$[IE]_E$	-	84.9[b]	10.5[b]	89.2[b]
		65.6[c]	16.3[c]	37.0[c]

[a] Ref. —1 wt % glycine+5 wt % H_2O_2 at pH 4.0.
[b] Measured at E_{corr} + 0.1 V.
[c] Measured at E_{corr} + 1.0 V.

Table 2.8: Corrosion parameters of copper and inhibition efficiencies of ADS and BTA [2.69].

2.3.4. Chemical Systems for Copper Electrochemical Polishing (ECP)

Some of the chemical system used for ECMP are based on electrochemical polishing (ECP) formulations. Wada et al. [2.65] investigated the ECP of copper in de-ionized water (DI). A specially designed pad/electrode system described in Section 2.3.2 was used. The process does not use an electrolyte solution for removing copper, but instead acts through the electrochemical interaction of OH^- ions in DI water and the surface atoms of copper film. Schematic representation showing the mechanism of electropolishing of copper in DI water is shown in Figure 2.30. Wada et al. proposed that the contact between the high lying areas of the film and the ion exchanger (between the wafer and the cathode) increases the conductivity of DI water. This resulted in a higher removal of the copper film. However, the low-lying areas were not in contact with the ion exchanger; hence, the conductivity of DI water remained low. Thus, removal in low lying areas takes place very slowly. Due to this difference, the high lying areas of the film were selectively removed, thereby achieving planarity.

Copper removal rate was characterized as a function of pressure, current density, and relative speed between the wafer and the electrode. It was found that pressure and relative speed had virtually no effect on the copper removal rate, while the rate increased linearly with applied current density. The results indicated that copper removal rates as high as 800 nm/min to 1600 nm/min can be obtained. In addition, a very high degree of planarity was achieved. Since this processing method is based on electrochemical interactions, copper can be processed without any mechanical damage or erosion. Also, the use of DI water would reduce the cost, as no post-processing of the waste fluid is required.

Huo et al. [2.70, 2.71] studied the feasibility of ECP of copper in solutions of phosphoric acid, ethylene glycol, hydroxyethylidenediphosphonic acid (HEDP), sodium chloride and sulfuric acid, with or without organic and inorganic additives. The I-V characteristics of copper carried out using a rotating disk electrode (RDE) showed a limiting current plateau region for most of these solutions. Polishing experiments were carried out on copper disks under anodic potential conditions. The copper surface, before and after ECP, was characterized using atomic force microscopy (AFM) for surface roughness (R_a). Table 2.9 lists the removal rate (RR) and surface roughness under different conditions. Polishing in solutions of phosphoric acid, HEDP, and phosphoric acid containing additives such as CuO, ethylene glycol and sodium tripolyphosphate, resulted in a smooth copper surface (R_a < 20 nm). However, high surface roughness (R_a > 20 nm) was seen after polishing in ethylene glycol-sodium chloride, sulfuric acid and sulfuric acid-sodium nitrate solutions. Further experiments on patterned copper films in phosphoric acid and HEDP solutions showed that the protruding areas on the film were not planarized in phosphoric acid while a good planarization was obtained in HEDP solutions due to the formation of a salt film.

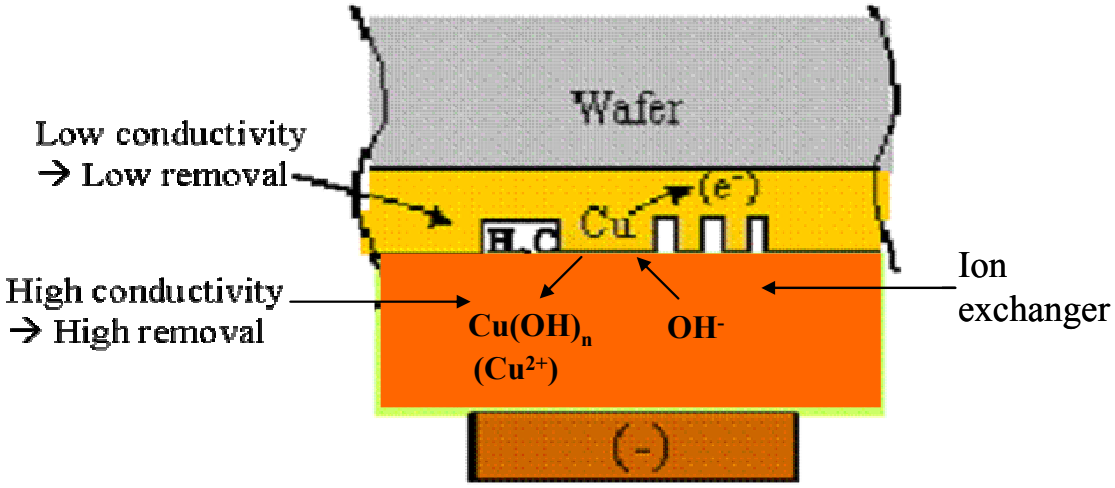

Figure 2.30: Schematic representation showing the mechanism for electropolishing of copper in DI water as proposed by Wada et al. [2.70].

Solution	i_L, mA	RR, µm/min	R_a, nm
30-100% H_3PO_4 + 0-2 M CuO	20-200	0.44-4.4	5-29
70% H_3PO_4 + 5-25% ethylene glycol	14-50	0.3-1.1	5-8
70% H_3PO_4 + 0.1-0.5 M $Na_5P_3O_{10}$	32-50	0.7-1.1	7-17
20-80% HEDP + 10-30% H_3PO_4	14-167	0.3-3.7	6-243
20-100% ethylene glycol + 1-2 M NaCl	20-50	0.44-1.1	63-91
20% H_2SO_4 + 0-2 M $NaNO_3$	70-80	1.54-1.75	72-279

Table 2.9: Summary of copper disk electropolishing data [2.70, 2.71].

2.3.5. Static Etching

In an ideal ECMP process, planarization can be achieved if the low-lying areas are protected while the higher lying areas are actively removed. However, this is not the case when strong oxidizers such as nitric acid or hydroxylamine are used as an electrolyte solution. These aggressive chemistries can dissolve copper very rapidly which can reduce the removal rate selectivity between high and low lying areas. Schematic representation of static etching of copper in an aggressive solution during polishing is shown in Figure 2.31 [2.72]. M_1 is the thickness of the metal on the inter-layer dielectric (ILD) and M_2 is the thickness of the metal in the trench. During polishing, M_1 is reduced due to combined chemical and mechanical effect. At the same time, M_2 can also decrease due to the etching action of aggressive chemistry. This phenomenon is known as static etching. With further polishing, the thickness of the metal, M_2, in the trench falls below the dielectric step height, while M_1 still gets reduced. Achieving planarity under this condition is very difficult. Static etching is of particular concern in chemistries where the etch rates are higher. Since copper is electrochemically active, static etching is a major concern in copper ECMP.

2.3.5.1 Role of inhibitor

Static etching problems can be eliminated or reduced by the addition of inhibitors in the electrolyte solutions. Inhibitors that can form a passive film are critical for the success of the ECMP process. Figure 2.32 shows the change in topography of copper in the presence of inhibitors during the ECMP process [2.72]. During polishing, the protective film formed by the inhibitors is removed in higher areas through pad contact,

while it remains intact in low lying regions. Thus the polishing proceeds by the reduction of M_1, while no or very small reduction of M_2 takes place. The planarization is finally achieved when M_1 becomes equal to M_2. The nature and properties of passive film affect the downforce pressure required for passive film removal, the copper removal rate, and the extent of dishing. Some of the major requirements of a passive film for ECMP application are: (1) Passive film must have excellent chemical stability but poor mechanical stability, so that it can be removed easily by the application of a very small downforce, and (2) It must be stable at applied anodic potentials.

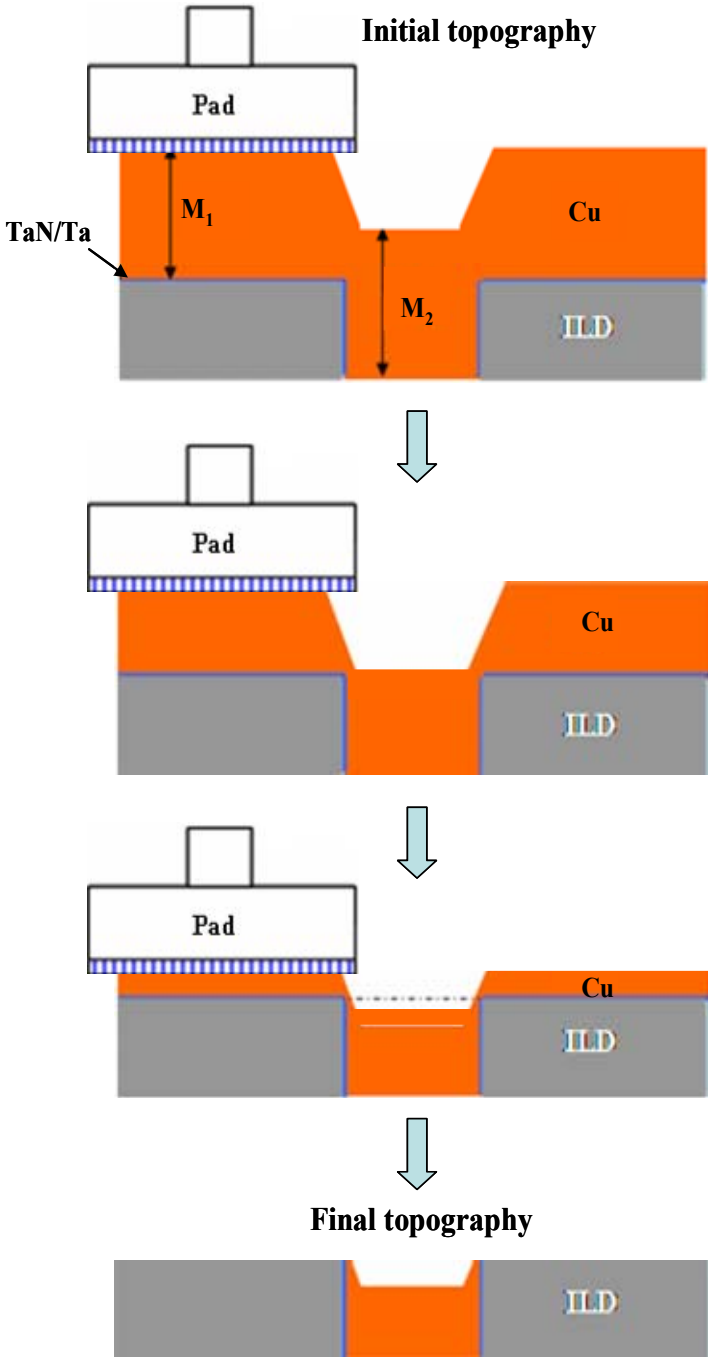

Figure 2.31: Change in topography of copper while polishing in aggressive chemistry in the *absence of inhibitor* [2.72].

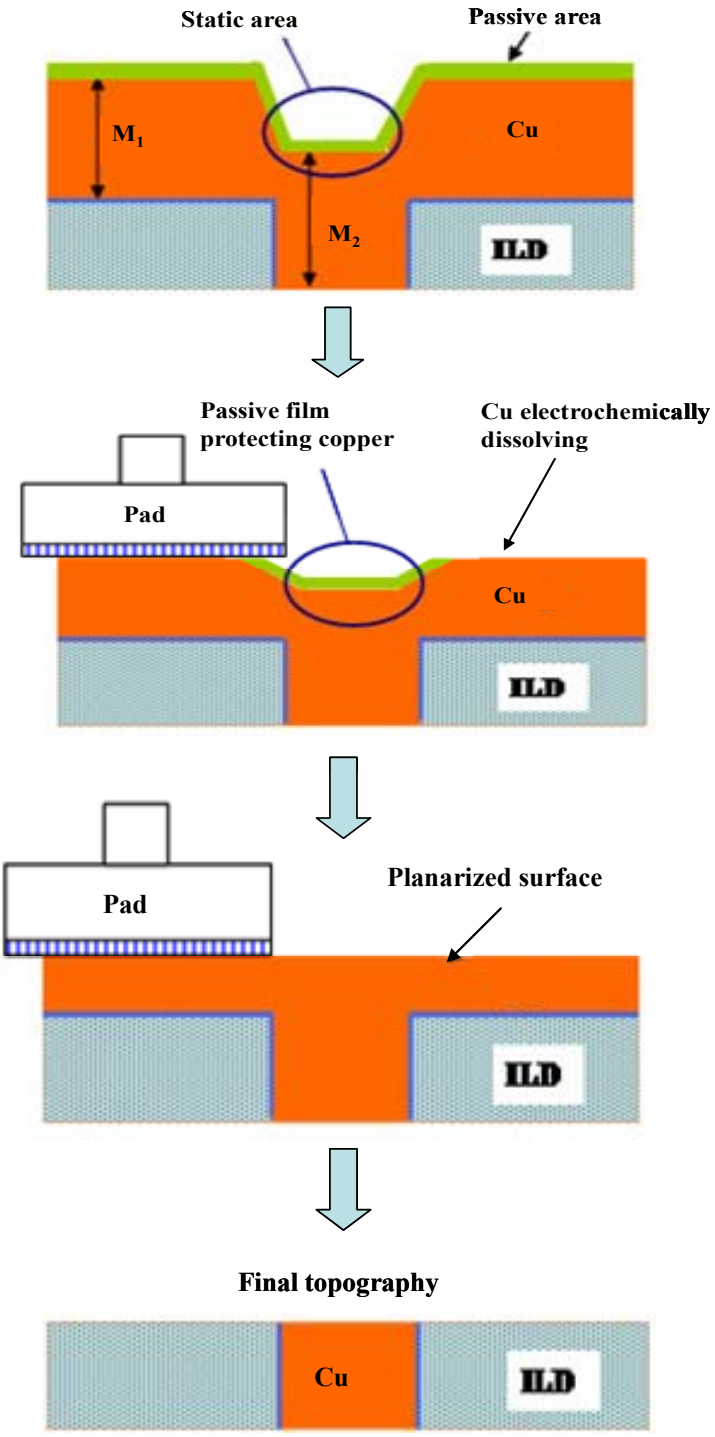

Figure 2.32: Change in topography of copper while polishing in the *presence of an inhibitor* [2.72].

2.3.6. Chemical Systems for Tantalum ECMP

The development and implementation of a full-sequence ECMP process, which includes the removal of the barrier layer as well, is in its infancy. Chemical systems that exhibit a 1:1 selectivity between the barrier layer and copper would be ideal for the barrier removal step of ECMP. Tantalum is a refractory metal and readily passivates in aqueous solutions. Conventional Ta CMP is done using silica slurries with high (~10 weight %) solid contents at alkaline pH values. It has been reported that the removal of Ta is predominantly a 'mechanical' process which involves the removal of the native oxide formed on the surface [2.53]. ECMP formulations, as mentioned earlier, are designed to be more chemically active with very small or no solid content. Tantalum, being a refractory metal, is not attacked by many chemical systems and hence poses challenges to the development of ECMP formulations.

The use of 3, 4-dihydroxy benzene sulfonic acid as an oxidizer for tantalum CMP has been reported in two recent patents [2.73, 2.74]. It is a weak acid with a pKa of 12.2 [2.75]. Sulfonic acids have also found use in electrochemical etching and polishing of Ta [2.76, 2.77]. Additionally, aryl sulfonic acids such as dihydroxy benzene disulfonic acid (aka Tiron) form strong complexes with refractory metals [2.78]. Further, catechol (dihydroxybenzene) is known to complex tantalum particularly in methanolic solutions [2.78]. A recent patent has reported the use of a peroxide based electrolyte containing inorganic additives (e.g. phosphoric acid) and a small amount of abrasives (e.g. silica particles) at alkaline pH for ECMP of tantalum [2.79]. An oxidizer free electrolyte containing sulfuric acid and a chelating agent such as ammonium citrate with abrasive particles at pH 8 - 9 has also been found useful for Ta ECMP [2.80].

2.4. Electrochemical Measurements

2.4.1. Potentiodynamic Polarization Method

Potentiodynamic polarization can provide significant useful information regarding the corrosion mechanisms, rate and susceptibility of specific materials to corrosion in designated environments. This method involves changing the potential of the working electrode and monitoring the current response. Depending on the magnitude and direction of the potential, this technique can be further classified into sub techniques such as anodic polarization, linear polarization, Tafel polarization, etc. The theories and steps involved in calculations are described below.

A charge transfer reaction representing corrosion of metal M is shown in equation 2.1.

$$M \leftrightarrow M^{+} + e^{-} \qquad (2.1)$$

The amount of current (I, Ampere) or current density (i, Ampere/cm^2) produced from the charge transfer reaction is given by the Bulter-Volmer equation shown in equation 2.2 [3.81-3.84].

$$i = i_o \left\{ \exp\left[\frac{\alpha \text{ n F } \eta}{\text{R T}} \right] - \exp\left[-\frac{(1-\alpha) \text{ n F } \eta}{\text{R T}} \right] \right\} \qquad (2.2)$$

where,

i = net current density

i_0 = exchange current density

α = anodic transfer coefficient

n = number of electrons involved in charge transfer reaction

F = Faraday's constant (96500 C/mol)

η = overpotential {η = E (applied potential) – E_{eq} (equilibrium potential)}

R = gas constant (8.314 J/ mol. K)

T = absolute temperature (K)

When the absolute value of measured current density is plotted against overpotential (η) on a semi-logarithmic scale, the resulting plot is known as a Tafel plot. A Tafel plot obtained for $i_0 = 10^{-5}$ A/cm^2, n = 1, $\alpha = 0.5$ and T = 298 K is shown in Figure 2.33 [2.85]. If the overpotential (η) is greater than ± 100 mV, a linear relationship known as a Tafel relationship is established between η and log (i), which is shown in equations 2.3 and 2.4 [2.86, 2.87].

$$Anodic: \eta_a = \beta_a \log\left[\frac{i_a}{i_o}\right], where\ \beta_a = 2.303\frac{RT}{\alpha n F} \quad (2.3)$$

$$Cathodic: \eta_c = -\beta_c \log\left[\frac{i_c}{i_0}\right], where\ \beta_c = 2.303\frac{RT}{(1-\alpha) n F} \quad (2.4)$$

where

β_a and β_c represents anodic and cathodic Tafel slopes, respectively.

η_a and η_c represents anodic and cathodic overpotentials, respectively.

Anodic and cathodic reactions in corroding systems typically involve different redox couples. For example, the Figure 2.34 shows the corrosion of copper in aerated acidic solutions [2.87]. The anodic and cathodic reactions for this system are shown in equations 2.5 and 2.6 respectively.

Anodic reaction: $Cu \rightarrow Cu^{2+} + 2\ e^-$ (2.5)

Cathodic reaction: $0.5\ O_2 + 2\ H^+ + 2\ e^- \rightarrow H_2O$ (2.6)

The anodic reaction is the oxidation of copper and the cathodic reaction is the reduction of oxygen. The potential at which the O_2/H_2O cathodic curve intersects the Cu^{2+}/Cu anodic curve is known as the corrosion potential (E_{corr}). The corresponding current density at E_{corr} is known as the corrosion current density (i_{corr}). Figure 2.34 is also known as the mixed potential plot. The value of E_{corr} can be directly measured from the experiments, but the value of i_{corr} is calculated from the Tafel slopes.

The Tafel relationship of equation 2.3 and 2.4 can be used to calculate the anodic and cathodic current densities (i_a & i_c).

$$i_a = i_{\text{corr}} 10^{\Delta\eta/\beta_a} \text{ and } i_c = i_{\text{corr}} 10^{-\Delta\eta/\beta_c} \tag{2.7}$$

The net applied current density, i_{applied},

$$i_{\text{applied}} = i_a - i_c = i_{\text{corr}} 10^{\Delta\eta/\beta_a} - i_{\text{corr}} 10^{-\Delta\eta/\beta_c} = i_{\text{corr}} \left(10^{\Delta\eta/\beta_a} - 10^{-\Delta\eta/\beta_c} \right) \tag{2.8}$$

Using the Maclaurin series, the i_{applied} of equation 2.8 can be approximated as follows

$$i_{\text{applied}} = i_{\text{corr}} \left(\left(1 + \frac{2.303 \times \Delta\eta}{\beta_a} \right) - \left(1 - \frac{2.303 \times \Delta\eta}{\beta_c} \right) \right) = i_{\text{corr}} 2.303 \times \Delta\eta \left(\frac{1}{\beta_a} + \frac{1}{\beta_c} \right) \tag{2.9}$$

$$i_{\text{corr}} = \frac{i_{\text{applied}}}{2.303 \times \Delta\eta} \left(\frac{1}{\beta_a} + \frac{1}{\beta_c} \right)^{-1} = \frac{i_{\text{applied}}}{2.303 \times \Delta\eta} \left(\frac{\beta_a \beta_c}{\beta_a + \beta_c} \right) \tag{2.10}$$

Equation 2.10 is known as the Stern-Geary equation [2.87]. Substituting the term $i_{\text{applied}}/\Delta\eta$ in equation 2.10 by $1/R_p$, where R_p is the polarization resistance, then the Stern-Geary equation then becomes

$$i_{\text{corr}} = \frac{1}{2.303 \times R_P} \left(\frac{\beta_a \beta_c}{\beta_a + \beta_c} \right) \tag{2.11}$$

Once the values of R_p, β_a and β_c are obtained from the polarization plot, the corrosion current density (i_{corr}) can be calculated using equation 3.11. The removal can than be estimated from the corrosion current density using Faraday's Law given by equation 2.12.

$$Film\ removal\ rate, \left(\frac{\text{Å}}{\text{min}} \right) = \frac{i_{corr}}{nF} \times \frac{Molecular\ Weight}{\rho_M\,(density)} \times \frac{60\ s}{\text{min}} \times \frac{\text{Å}}{10^{-8}\,\text{cm}} \tag{2.12}$$

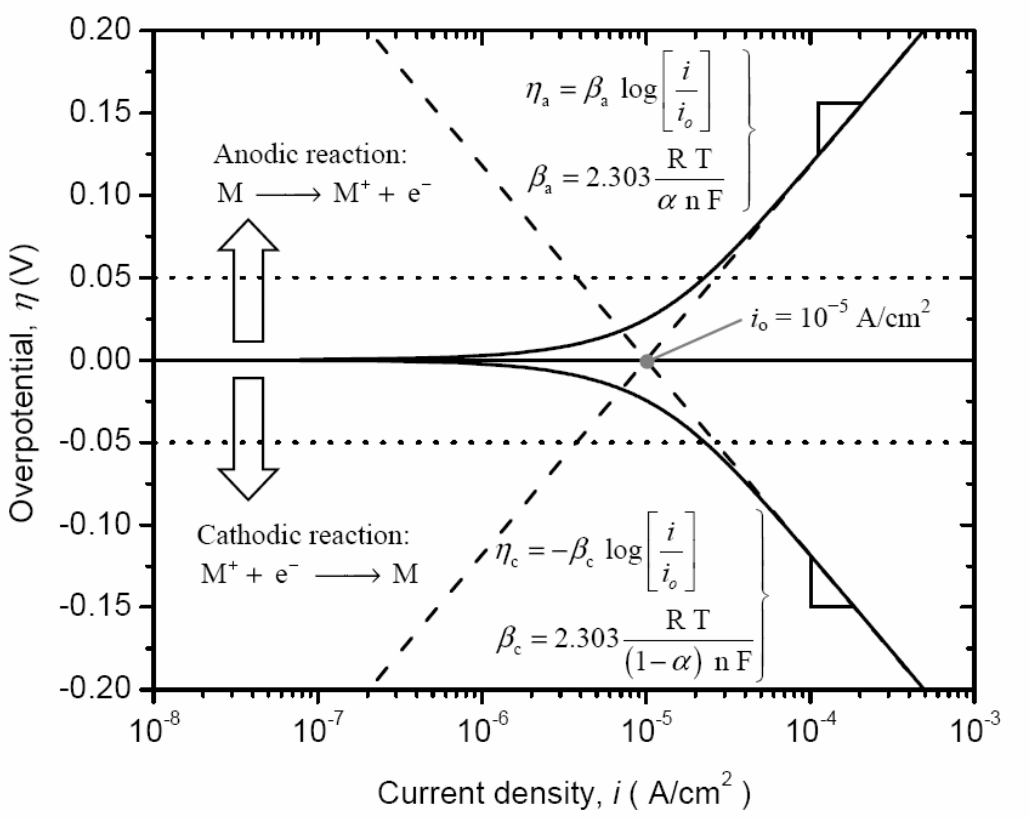

Figure 2.33: Tafel plot for an ideal system showing Tafel slopes [2.85].

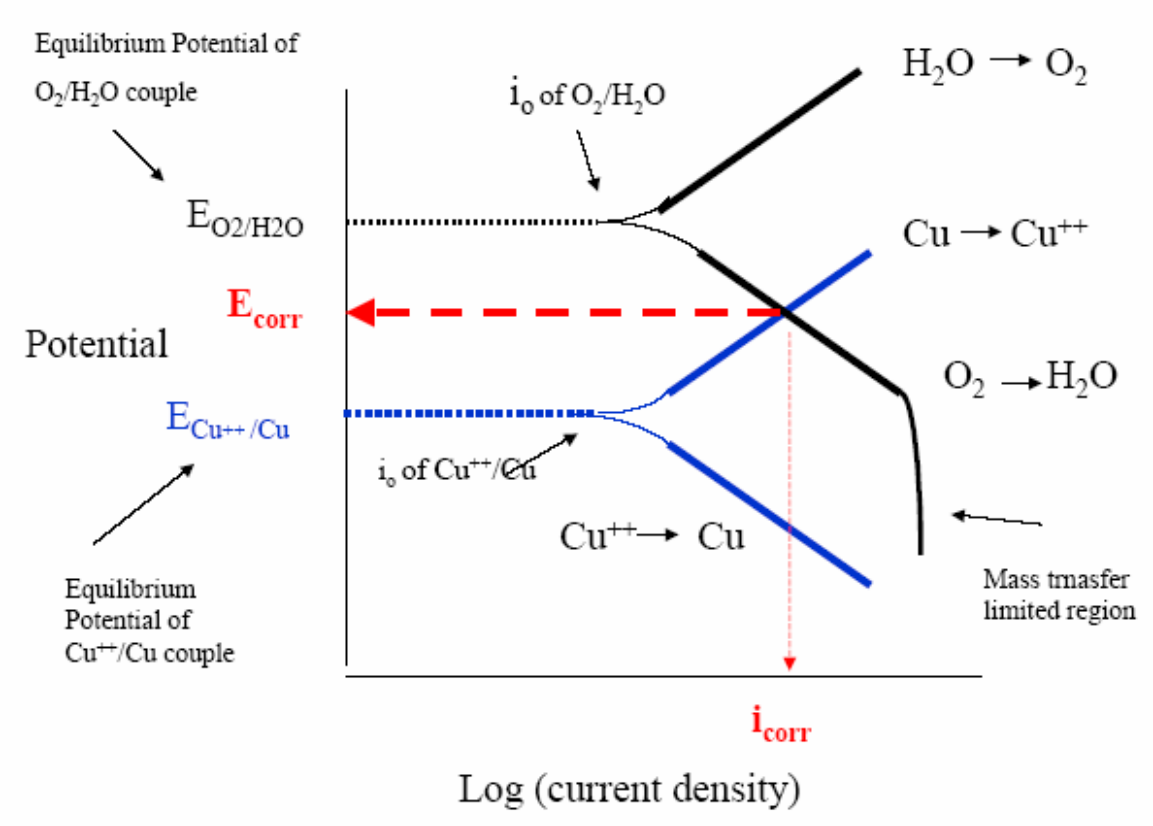

Figure 2.34: Tafel plot of mixed electrode system of oxygen and copper electrodes [2.87].

2.4.2. Cyclic Voltammetry

Cyclic voltammetry (CV) is a potential sweep technique that measures the current with applied potential in an unstirred solution so that the measured current is limited by analyte diffusion at the electrode surface. The electrode potential is ramped linearly to a more positive potential, and then ramped in reverse back to the starting voltage. The forward scan produces a current peak for any analytes that can be oxidized through the range of the potential scan. The current starts to increase as the potential reaches the oxidation potential value, but then falls off as the concentration of the analyte is depleted close to the electrode surface. As the applied potential is reversed, it will reach a potential that will reduce the product formed in the first oxidation reaction, and produce a current of reverse polarity from the forward scan [2.88]. This reduction peak will usually have a similar shape to the oxidation peak. The peak current, i_p, is described by the Randles-Sevcik equation:

$$i_p = (2.69 \times 10^5)\, n^{3/2}\, A\, C\, D^{1/2}\, v^{1/2}$$

where n is the number of moles of electrons transferred in the reaction, A is the area of the electrode, C is the analyte concentration (in moles/cm^3), D is the diffusion coefficient, and v is the scan rate of the applied potential.

Assuming a single electron transfer reaction, the ideal potential difference between the oxidation and reduction peak is 59 mV for a reversible reaction [2.88]. However, in practice, the difference is typically 70-100 mV. Larger differences, or nonsymmetric reduction and oxidation peaks, are an indication of a nonreversible

reaction. These parameters of cyclic voltammograms make CV most suitable for characterization.

2.5. Solution Analysis

2.5.1. Atomic Absorption Spectrophotometry (AAS)

AAS uses the absorption of light to measure the concentration of gaseous phase atoms [2.89]. Since samples are usually liquids, the analyte atoms or ions must be vaporized in a flame or graphite furnace. The detection of metals occurs by passing an ultraviolet or visible light through the ionized flame and into a photomultiplier detector. The atoms absorb the light and make transitions to higher electronic energy levels. During ionization, absorption of light occurs at a characteristic wavelength for each element. The concentration of the analyte is determined from the amount of absorption. Applying the Beer-Lambert law directly in AAS is difficult due to variations in the atomization efficiency from the sample matrix, and nonuniformity of concentration and path length of analyte atoms (in graphite furnace AAS) [2.89]. Concentration measurements are usually determined from a working curve after calibrating the instrument with standards of known concentration.

2.5.2. Inductively Coupled Plasma Mass Spectrometry (ICP-MS)

ICP-MS is a very powerful technique for trace (ppb range) elemental analysis. In ICP-MS, plasma which is formed from Argon gas is used to atomize and ionize the elements in the solution. The resulting ions are then passed through a series of apertures into the high vacuum mass analyzer. The isotopes of the elements are identified by their

mass-to-charge ratio (*m/e*), and the intensity of a specific peak in the mass spectrum is proportional to the amount of that isotope (element) in the original solution [2.90]. The removal rate was then calculated from metal concentration in solution.

CHAPTER 3: METHODS AND MATERIALS

3.1. Experimental Methods

3.1.1. Bench Top Electrochemical Mechanical Abrasion Cell (EC-AC) Tool

A specially designed laboratory scale electrochemical abrasion cell (EC-AC) was used for all the polishing and electrochemical studies (Figure 3.1). A schematic diagram of a cross-sectional view of the EC-AC tool is shown in Figure 3.2. The EC-AC tool can be viewed as an "upside-down" version of an industrial CMP tool. The main advantages of this design are: (1) it provides flexibility of performing polishing and electrochemical experiments on electroplated copper films deposited on silicon wafers and (2) the electrolytes used during experiments can be collected for solution analysis. The tool can be divided into two parts: (1) the top part consists of a pad, a counter electrode (cathode), a stepper motor, and the load cells, and (2) the bottom part consists of a perfluoroalkoxy (PFA) cell, a sample, and a brass table with a bottom stepper motor. The tool was designed to control pressures as low as ~ 0.5 psi and accommodate samples of 6 cm in diameter.

A typical ECMP experiment was conducted as follows: A diced sample (Cu or Ta film deposited on wafer) 7 cm x 7 cm in size was placed on the circular copper plate attached to the rotating table. An electrical contact was established by applying conductive silver paint on the backside and around the wafer edges. This made the sample into a working electrode, which was connected to the potentiostat by means of a carbon brush which continuously touched the copper plate during rotation. Care was taken to ensure that electrical continuity was maintained during the experiments. A cell

made from PFA was used to hold the polishing solution and was securely fastened to the rotating table with four screws. A Viton® o-ring was used as a seal to prevent the electrolyte from leaking out of the cell and to hold the sample in place during rotation. After the set-up was assembled, the electrical continuity between the sample and the copper plate was tested.

The top part of the EC-AC tool was then assembled. A three-electrode setup was used for all electrochemical experiments. The reference electrode was a calomel electrode and the counter electrode was a stainless steel (316L) disc (diameter ~ 3 cm), to which a perforated polishing pad was affixed. A perforated Rohm and Hass IC1010 pad (with K-grooves) stacked on Suba IV was used for polishing experiments. The pad holder was then attached to the shaft of the top stepper motor using a setscrew. The center of the pad/electrode was offset from the center of the wafer sample such that 70% of the sample was polished. This is schematically shown in Figure 3.3. After the assembly of the abrasion cell, 100 ml of electrolyte was poured into the PFA cell. The polishing pressure was fixed at 0.5 psi for all experiments. The pad (diameter ~ 3.2 cm) was rotated at 240 rpm and the wafer sample was rotated at 222 rpm using two different computer controlled stepper motors. Electrochemical data were obtained using PARC 273A and 2273 potentiostat.

Figure 3.1: Typical setup of the laboratory scale electrochemical abrasion cell (EC-AC) tool.

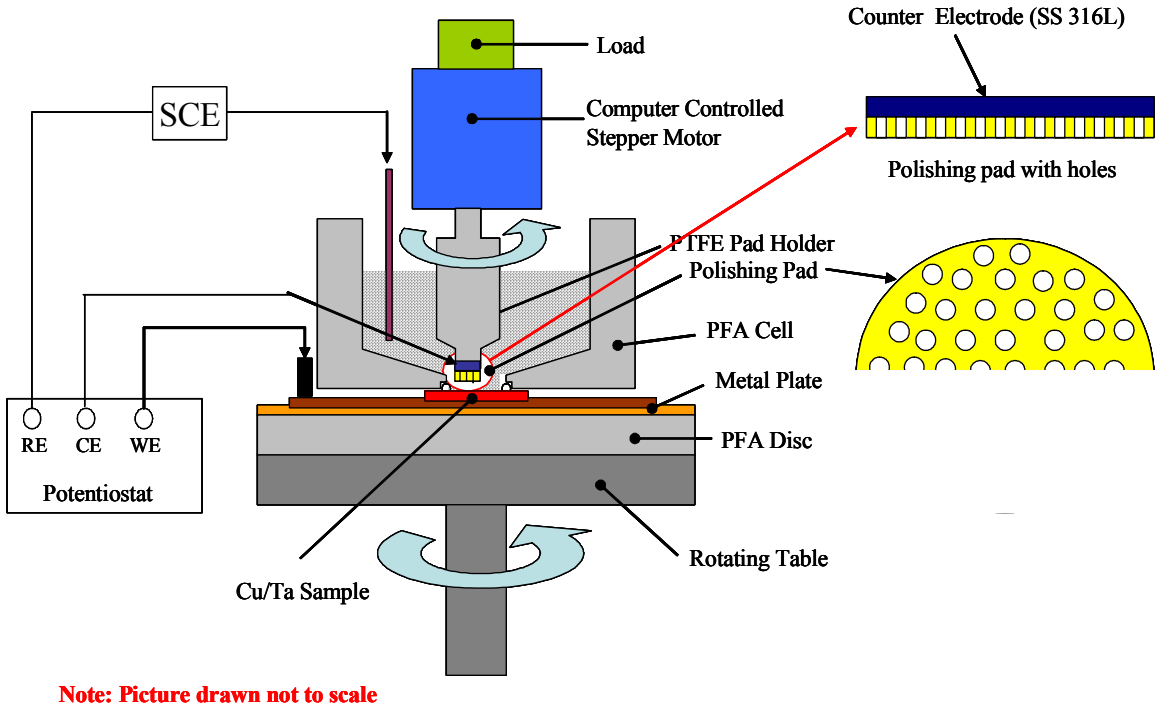

Figure 3.2: Cross-sectional view of the bench top electrochemical abrasion cell (EC-AC) tool.

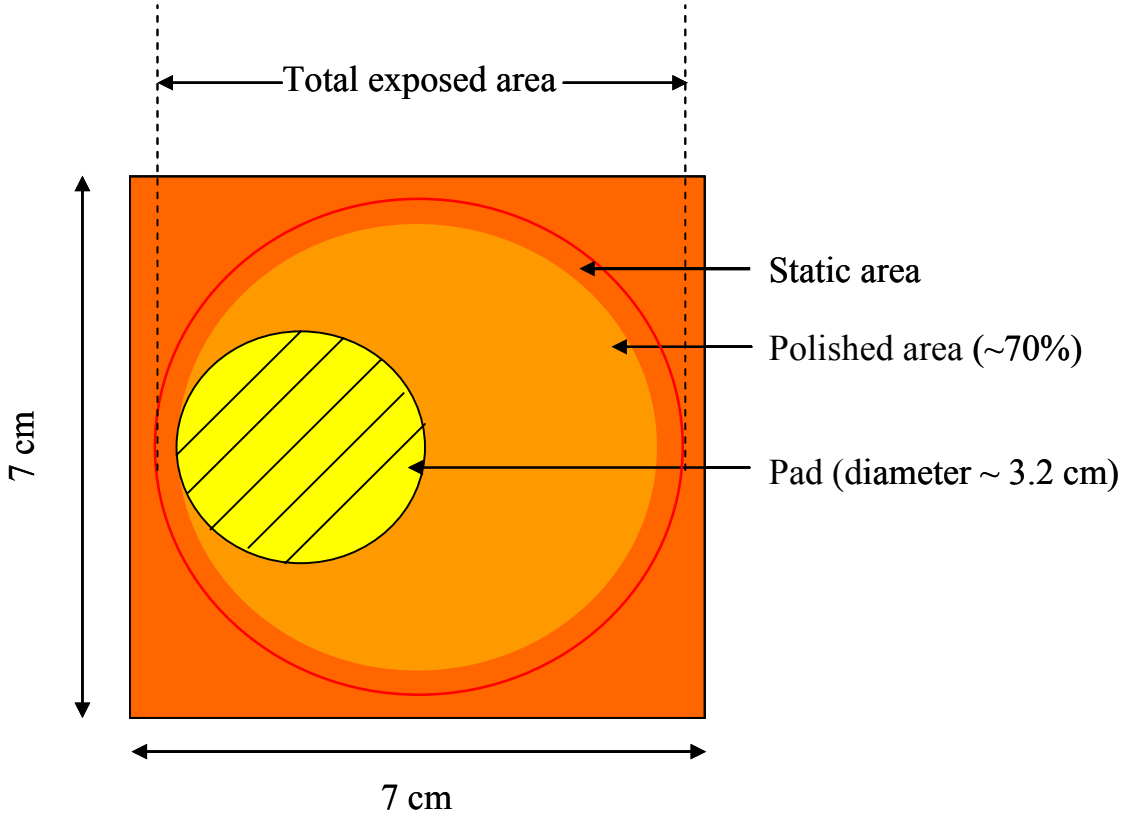

Figure 3.3: Schematic representation showing the offset between the pad and the sample.

3.2. Quartz Crystal Microbalance (QCM)

The effect of anodic polarization on copper dissolution in hydroxylamine based chemical system was investigated using a Research Quartz Crystal Microbalance (model RQCM from Maxtek Inc) technique to evaluate their use in ECMP processes. It is an extremely sensitive sensor capable of measuring the frequency change which is then converted to mass change using Sauerbrey equation given below [3.1]. The change in oscillation frequency (Δf) of the crystal (QCM electrode surface) to the mass change (Δm) per unit area at the electrode surface is,

$$\Delta f = \frac{-2\,\Delta m\,(f_0)^2}{n\,A\sqrt{\mu\rho}}$$

where,

f_0 is the fundamental frequency of the crystal,

n is the order of the harmonic,

μ is the shear modulus of quartz (2.947×10^{11} g cm^{-1} s^{-2}),

ρ is the density of quartz.

According to the manufacturer, the mass resolution for this RQCM is roughly 0.4 ng/cm^2. Quartz crystals used in this study were AT-cut disks of 1-inch diameter and of 5 MHz nominal oscillation frequency. On both sides, gold was deposited over a thin layer of chromium as shown in Figure 3.4 [3.1]. Typically, one side of the electrode is exposed to the chemistry of interest while the other side serves as electrode contact. The exposed area of the front electrode was 1.37 cm^2. The roughness (R_a) of the gold coating measured by atomic force microscopy (AFM) was found to be 2 nm.

QCM was interfaced with a Potentiostat/Galvanostat (EG&G PARC 273A) to make the measurements. An immersion type crystal holder was used for all experiments.

A typical experimental setup is shown in Figure 3.5 [3.1]. A saturated calomel electrode and a platinum plate were used as reference and counter electrodes, respectively.

Copper was electroplated on the gold surface at room temperature from a commercial copper plating solution (0.27 M cupric sulfate) obtained from Shipley ST2001 at a current density of 2 mA/cm^2. The freshly deposited copper film (2μm thickness) was rinsed thoroughly in de-ionised (DI) water, dried using nitrogen gas and immediately used in dissolution experiments. Copper was freshly deposited for each investigation and all dissolution experiments were performed in a beaker containing 150 ml of solution at room temperature with constant stirring.

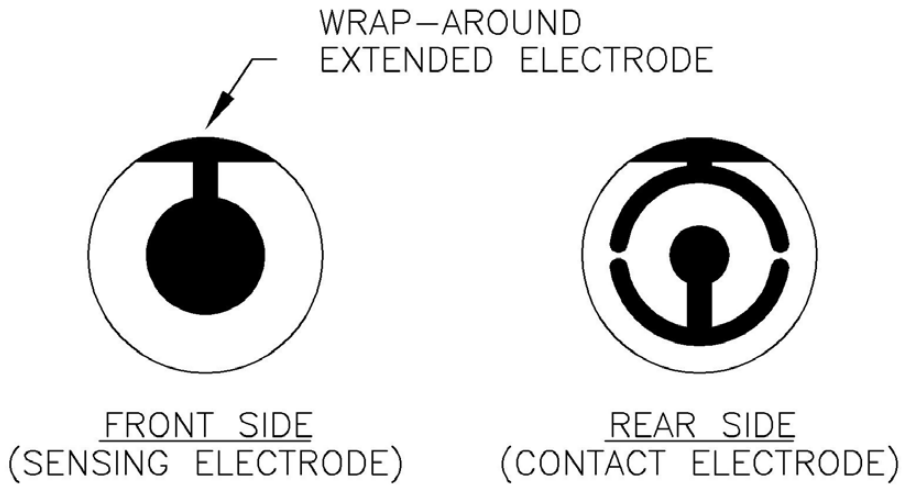

Figure 3.4: Schematic representation of the front and rear side of the gold coated quartz crystals [3.1].

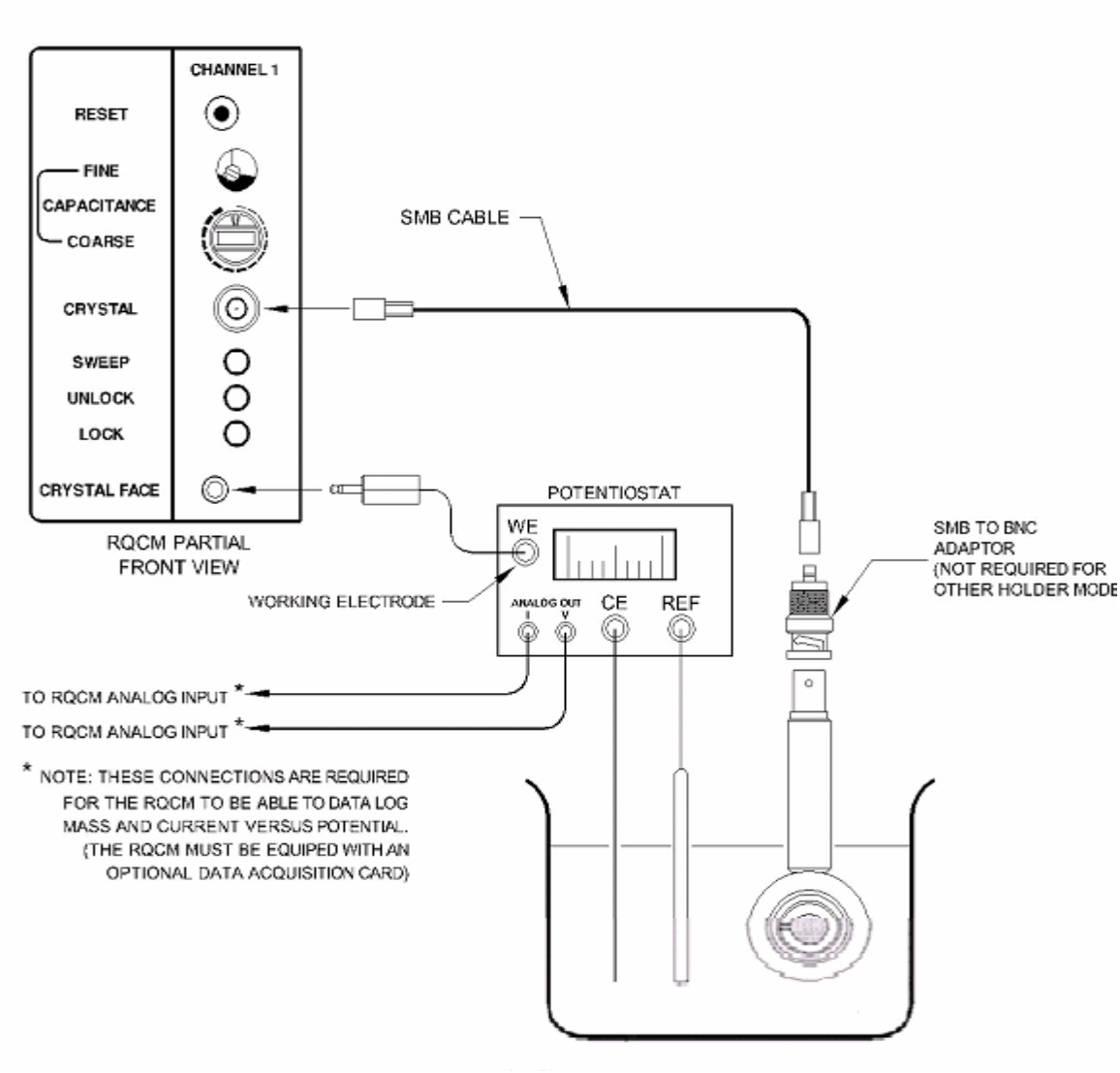

Figure 3.5: Schematic representation of QCM interfaced with a potentiostat [3.1].

3.3. Electrochemical Measurements

The electrochemical measurements were performed using Princeton Applied Research potentiostats (Models 263A, 273A and 2273). A three-electrode setup was used for all electrochemical measurements. The counter electrode was a platinum or stainless steel (316L) and the reference was a saturated calomel electrode (SCE, Hg/Hg_2Cl_2) obtained from Aldrich Chemicals and VWR International, respectively. Tantalum films of thickness 1000 Å deposited on carbon doped oxide were used for the experiments. Electrodeposited copper films of thickness 1 μm on a film stack of tantalum (250 Å)/SiO_2/Si were kindly provided by Semitool Corporation. Patterned test structures were fabricated at Intel Corporation, Santa Clara. A schematic representation of the patterned test structure is shown in Figure 3.6. The as-received test structure consists of copper filled trenches deposited on Ta/TaN barrier stack in a matrix of low-k dielectric material. CMP was done to remove the copper on platen 1 and 2, and stopping on the tantalum barrier layer. The width of copper lines and spaces are ~ 200 and 300 nm, respectively.

Microelectronic grade hydroxylamine solution (17M) and hydrogen peroxide (30%) were provided by EKC Technology and J.T. Baker, respectively. Potassium salt of 2, 5 dihydroxybenzene sulfonic acid (DBSA, 99%), benzotriazole (99%) and salicylhydroxamic acid (SHA), were obtained from Aldrich Chemical Company. Nitric acid and tetra methyl ammonium hydroxide (TMAH) were used to adjust the pH of the solutions. Colloidal silica particles of size 80 nm were obtained from Precision Colloids. Polishing of tantalum films was carried out in DBSA solutions with and without colloidal silica particles. The electrochemical data were recorded and analyzed using PAR Model 352/252 Corrosion Analysis Software Version 2.23/ Powersuite Software Version 2.58.

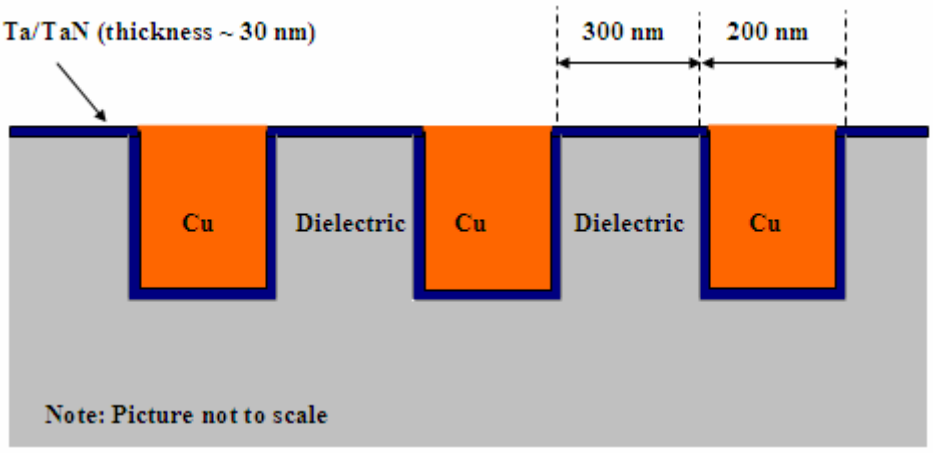

Figure 3.6: Schematic representation of the patterned test structure.

3.3.1. Tafel Polarization

Tafel polarization experiments were performed during polishing by perturbing the system from -250 mV to +250 mV with respect to open circuit potential (OCP) value. Ideally, Tafel experiments should ideally be done at low scan rates, less than 1 mV/sec, but due to the thin tantalum films used in the experiments, a higher scan rate of 5 mV/s was used to ensure that the polarization was complete before the film was completely dissolved. Tafel slopes were obtained from the plots and used to calculate the corrosion current density (i_{corr}).

3.3.2. Anodic Polarization

The I-V characteristics of tantalum films during polishing were obtained by anodic polarization from OCP to an over potential of 1V. The potential was scanned at a rate of 5 mV/s.

3.3.2.1. Potentiostatic Experiments

Anodic dissolution of electroplated copper films in hydroxylamine based solutions was carried out under the potentiostatic mode. Experiments were carried out by holding the working electrode at constant potentials and monitoring the current response with time. Polishing experiments were carried out by holding copper samples at different anodic overpotentials (250 mV, 500 mV and 750 mV) to simulate ECMP conditions. The current response was used to estimate the electrochemical removal rate.

3.3.2.2. Galvanostatic Experiments

Polishing of tantalum films was carried out in DBSA solutions under the galvanostatic mode. In the galvanostatic mode, constant current was applied to the

working electrode and the potential was monitored with time. Constant anodic currents of 0.1 mA/cm^2, 0.25 mA/cm^2 and 0.5 mA/cm^2 were applied to tantalum films during polishing. The total removal rate which consists of mechanical as well as electrochemical removal of tantalum was then compared to the electrochemical removal rate calculated from the applied current using equation (2.12).

3.4. Cyclic Voltammetry

Cyclic voltammetry experiments were carried out to characterize the tantalum films. Oxidation of tantalum was studied by scanning the potential from OCP to 1.5 V with respect to OCP and then reversing back to OCP. The scan rate was set at 100 mV/sec. Tantalum samples were dipped in dilute HF to remove any native oxide formed on the surface followed by DI water rinsing and dried in nitrogen gas. The electrolyte solution was deoxygenated by purging with nitrogen to prevent surface passivation due to dissolved oxygen.

3.5. Chemical and Physical Analysis

3.5.1. Atomic Absorption Spectrophotometry (AAS)

The concentration of dissolved copper in solution was determined by using a Perkin-Elmer Model 2380 Atomic absorption spectrophotometer that uses a hollow cathode lamp of wavelength, λ = 324.8 nm. This technique aspirates a sample of the analyte into acetylene-air mixture flame. The temperature of the flame is typically around 2300 ^{o}C. At this temperature, ionization of metal ions takes place. Before analyzing the concentration of unknown solution, a linear calibration curve was obtained by measuring

the absorption of solutions with five known copper concentrations (0.1, 0.5, 1.0, 3.0, and 5.0 ppm). These individual calibration standards were prepared from a 1000 ppm copper standard solution purchased from Alfa-Aesar Chemicals. The linear calibration range of copper was 0.1 to 5.0 ppm. The calibration curves had a coefficient of determination (R^2) of 0.99. The unknown solutions were acidified with a known amount of concentrated nitric acid to adjust the solution pH to < 1. For solutions with a copper concentration above 5.0 ppm, it was diluted with DI water and the absorption was then measured.

3.5.2. Inductively Coupled Plasma Mass Spectrometry (ICP-MS)

In the absence of abrasive particles, after polishing tantalum films, the solutions were acidified by adding 5 ml each of 49% HF and 16M HNO_3 to dissolve any metallic tantalum, if any. In the presence of abrasive particles, the particles were allowed to settle and then centrifuged at 5000 rpm for 2 hours. This procedure led to the complete removal of particles from the solutions. The solutions were then acidified by adding 5 ml each of 49% HF and 16M HNO_3 to dissolve any metallic tantalum, if any. The solution was analyzed using a Perkin Elmer ELAN DRC II inductively coupled plasma-mass spectrometer (ICP-MS). The linear calibration range of tantalum was 1 to 50 ppb. All calibration curves established prior to analysis had a coefficient of determination (R^2) of 0.99.

3.5.3. pH and Conductivity Measurements

All pH measurements were obtained using Orion Model 920A and Model 1230 meters. For pH measurements, an epoxy body single junction (Ag/AgCl reference electrode) with built-in thermistor for automatic temperature compensation pH probe was used. The meters and the probes were all purchased from Thermo Orion and were

calibrated using freshly prepared standard buffer solutions on a regular basis. For conductivity measurements, an epoxy body graphite electrode Orion 013010 with built-in thermistor for automatic temperature compensation was used.

3.5.4. Surface Profile Measurements

The surface topography was measured using a Veeco Dektak 6M profiler. This instrument used a diamond stylus tip with a radius of 12.5 μm. When the stylus is moved across the sample, any changes in the topography cause the stylus to move in the vertical direction. The piezo-electric material converts the mechanical movement of the stylus to electrical signals, which are then converted back into vertical distance. In the case of samples with blanket copper or tantalum film, the portion exposed to polishing and the unexposed portion were scanned in a single line. The difference in thickness gives the amount of material removed during polishing.

3.5.5. Atomic Force Microscopy (AFM)

The surface topography of copper film exposed to various chemistries was examined using a Digital Instruments Nanoscope AFM. The topographic measurements were done in tapping mode and the data analysis was performed using DI Nanoscope Version 5.12R4 Software. Tapping mode imaging was implemented in ambient air by oscillating the cantilever assembly near the resonant frequency using a piezoelectric crystal. The oscillating tip is then moved toward the surface until it begins to lightly touch or tap the surface. During scanning, the vertically oscillating tip alternately contacts the surface and lifts off at a frequency of 50,000 to 500,000 cycles per second. As the oscillating cantilever begins to intermittently contact the surface, the cantilever

oscillation is necessarily reduced due to energy loss caused by the tip contacting the surface. The reduction in oscillation amplitude is used to identify and measure surface topography.

3.5.6. Focused Ion Beam (FIB) - Scanning Electron Microscope (SEM)

The cross section of patterned test structure was studied using Nova 200 NanoLab ultra high resolution scanning electron microscope (SEM) equipped with focused ion beam (FIB) capability. The sample area of interest was coated with platinum of thickness ~ 500 nm and then cross sectioned by FIB etching of platinum film and the underlying test structure. Coating the sample with platinum is necessary to prevent charging effects as well as to minimize damage to sample during FIB etching. The sample was then imaged using secondary electron mode at a high magnification of 250,000x.

3.5.7. Four Point Probe

The thickness of the copper films after polishing was characterized using a four-point probe technique. This technique measures the sheet resistance of thin films, which can be used to calculate film thickness. Removal rate of copper was calculated from thickness measurements made with a Mitsubishi LORESTA AP super-intelligent four point probe resistivity meter (Model MCP T400). It can measure resistance in the range of 0.001×10^{-2} Ω to 1.99×10^{7} Ω. As shown in Figure 3.7, it consists of four equally spaced tungsten metal tips which are brought into contact with the surface of the sample to be measured. A high impedance current source is used to supply current through the outer two probes, while a voltmeter measures the voltage across the inner two probes to determine the sample resistivity [3.2]. If probes with uniform spacing s are placed on a film with thickness t, then the resistivity, ρ, is given by

$$\rho = \left(\frac{\pi t}{\ln 2}\right)\frac{V}{I} \qquad \mu\Omega - cm \quad (s >> t)$$

Then the sheet resistance, R_s of a thin film is

$$R_s = \frac{\rho}{t} = \left(\frac{\pi}{\ln 2}\right)\frac{V}{I} = 4.53\frac{V}{I}$$

It is important to note that R_s is independent of any geometrical dimension and is therefore a function of the material alone. The unit of R_s is Ω/□ (ohms-per-square).

For copper samples, sheet resistance was measured at about 8 points in the polished area and about four points in the unpolished area. Film thickness (in nm) was calculated by dividing the bulk resistivity of copper (2.1 μΩ-cm) by the sheet resistance.

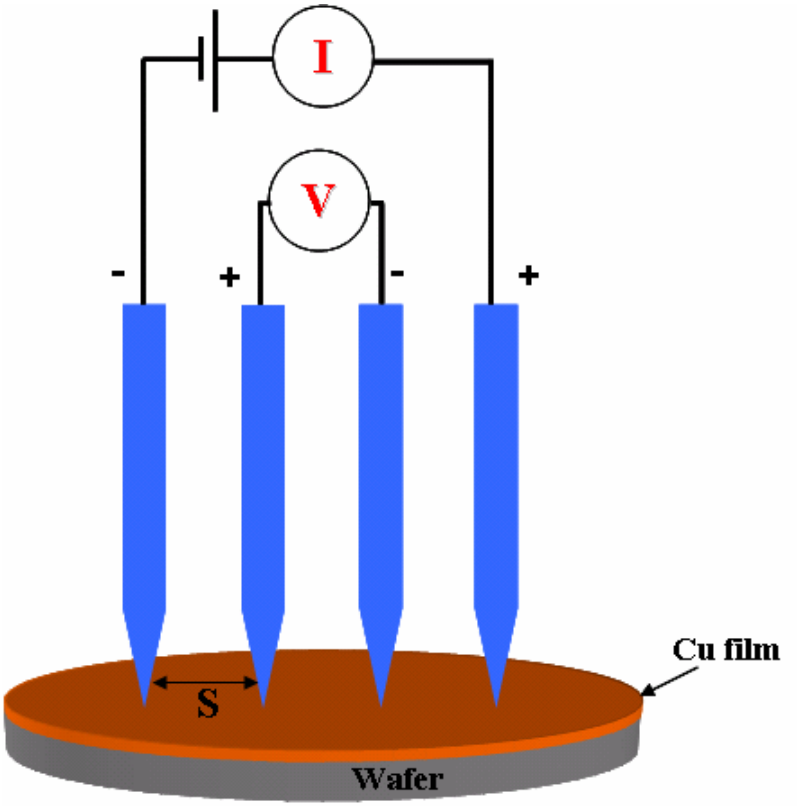

Figure 3.7: Schematic representation of a four point probe technique [3.2].

CHAPTER 4: RESULTS AND DISCUSSION

4.1. Potential-pH Diagrams

4.1.1. Copper - Hydroxylamine - Water System

The potential-pH diagram for the Cu-hydroxylamine-water system for a dissolved copper activity of 10^{-4} and a hydroxylamine activity of 0.5 is shown in Figure 4.1. Copper forms 1:1 and 1:2 complexes, ($[Cu(NH_2OH)]^{2+}$ and $[Cu(NH_2OH)_2]^{2+}$), with hydroxylamine. The $Cu(NH_2OH)]^{2+}$ complex is stable around pH 4, while the $Cu(NH_2OH)_2]^{2+}$ complex is the predominant species in the pH range of 5-7. The stars indicate the overpotential values (0, 250 mV, 500 mV and 750 mV) for copper exposed to 0.5 M hydroxylamine solution at pH 4, 6 and 8. It may be noted that the stars indicated at pH 4 and 6 occur in the stability region of the copper hydroxylamine complex. This indicates that dissolution of copper by complex formation is thermodynamically favorable. Thus, the application of potential is likely to enhance copper dissolution. However, at pH 8, since the stars fall in the copper oxide stability region, dissolution of copper is not thermodynamically favorable. The dissolution rate of copper in hydroxylamine solution has been reported to be strongly dependent on pH and exhibits a maximum in the vicinity of pH 6 [2.47].

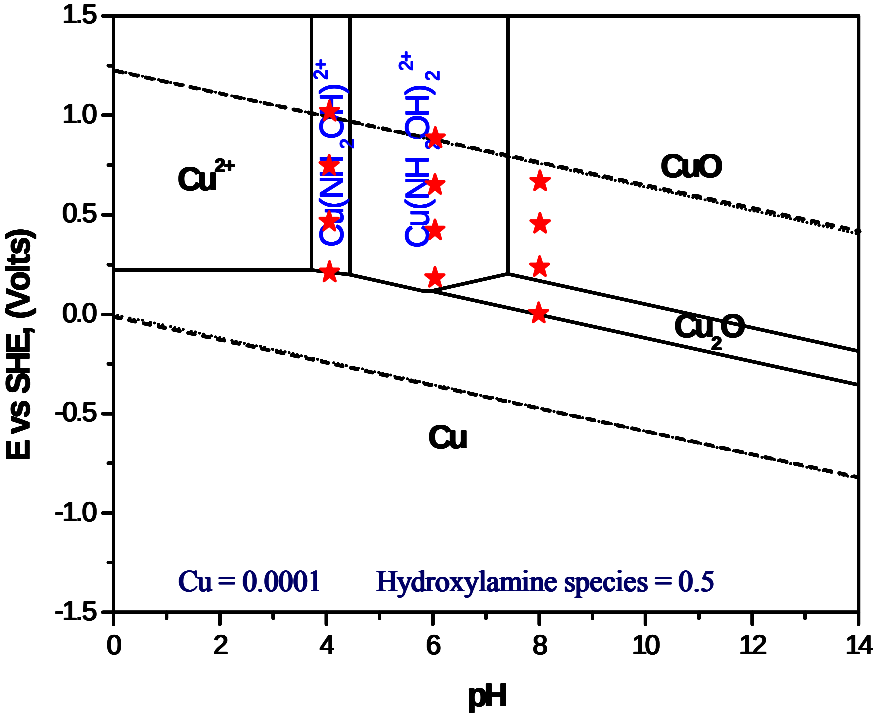

Figure 4.1: Potential-pH diagram for copper-hydroxylamine-water system (activity of the dissolved copper species = 10^{-4} and the activity of nitrogen species = 0.5).

Note: ★ indicates different overpotential values (0, 250mV, 500mV and 750mV).

4.1.2. Copper - BTA - Water System

Figure 4.2 shows the Cu-BTA diagram for an assumed copper activity of 10^{-4} and BTA species activity of 0.01. The BTA^- ion reacts with the cuprous ion to form a highly insoluble compound (Cu-BTA) in a wide pH range from 3-11. The Cu-BTA compound is stable in a narrow potential region. For example, the Cu-BTA compound is stable only in a potential range from 0 V (vs. SHE) to 0.45 V (vs. SHE) at pH 4. Above 0.45 V, copper is likely to exist in the form of Cu^{2+} at pH 4. The copper oxides dominate the alkaline region.

4.1.3. Copper - SHA - Water System

Figure 4.3 shows the potential-pH diagram of the copper-salicylhydroxamic acid (SHA) system (activity of copper species = 10^{-4}, activity of SHA species = 0.01). SHA forms a complex with copper ions in the form of $Cu(SHA)^+$ in the pH range of 1-10. The stability constant of the $Cu(SHA)^+$ complex has been reported to be ~ 10^9 [4.1]. It has been reported in the literature that metal-salicylhydroxamate complexes are often polymeric with phenolic OH or hydroxamate oxygen bridging groups [4.2]. However, there is no thermodynamic data available for the polymeric complex for incorporation into the software.

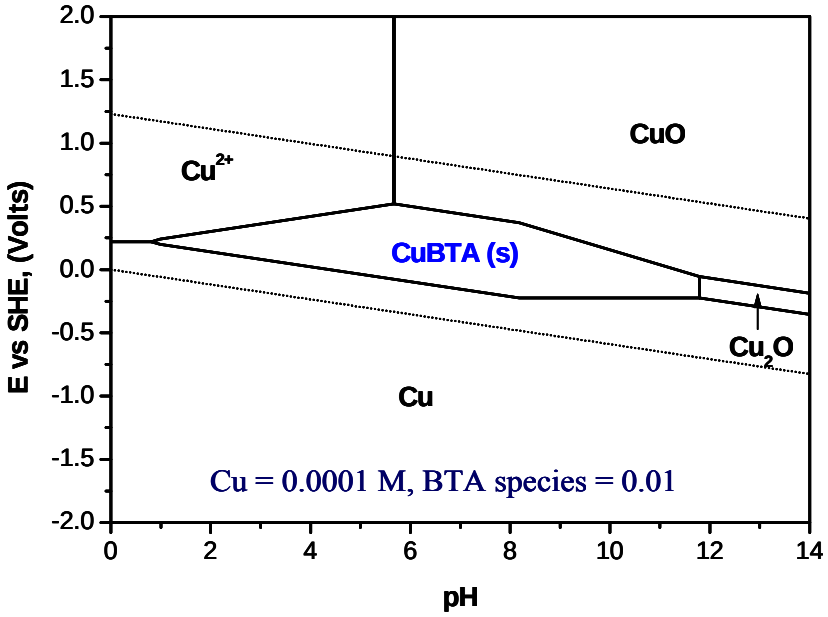

Figure 4.2: Potential-pH diagram for Cu-BTA-water system for activity of the dissolved copper species = 10^{-4} and BTA species = 0.01.

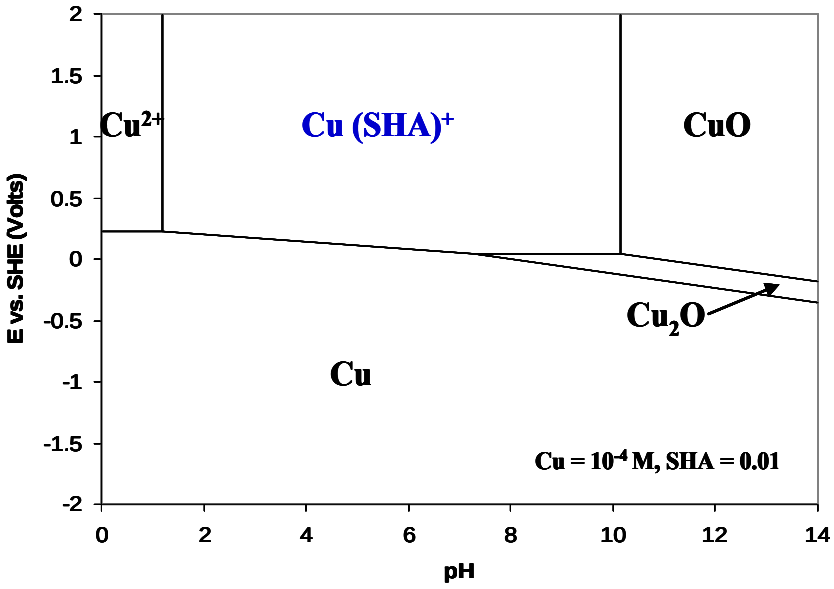

Figure 4.3: Potential-pH diagram for Cu-SHA-water system for activity of the dissolved copper species = 10^{-4} and SHA species = 0.01.

4.2. Evaluation of Copper Dissolution in Hydroxylamine Based Solutions using QCM

4.2.1. Effect of Potential and pH on Copper Dissolution

Figure 4.4 shows the effect of pH on the dissolution of electroplated copper film in 0.1M hydroxylamine solution at different anodic overpotentials (η). A mass decrease of 1 μg/cm^2 roughly corresponds to a copper dissolution rate of 11Å/min. At pH 4, under OCP conditions (~ -160mV vs. SCE), the dissolution rate is 30 Å/min. The rate increases to 100 Å/min at pH 6 (OCP = -170mV vs. SCE). A further increase in pH to 8 (OCP = -215mV vs. SCE) reduces the dissolution rate of copper to 5 Å/min.

At an anodic overpotential of 250mV, the dissolution rate of copper at pH 4 increases dramatically to approximately 600 Å/min. Interestingly, this level of overpotential increases the dissolution rates at pH 6 and 8 only slightly, to approximately 145 Å/min and 7 Å/min respectively. Even at higher overpotentials of 500 and 750mV, there is only a slight increase in the dissolution rate at pH 6 and 8; but the rate increases significantly to 1110 Å/min and 1730 Å/min respectively at pH 4.

The effect of increasing the hydroxylamine concentration to 0.5 M on the dissolution rate at different anodic overpotentials is shown in Figure 4.5. At OCP (20mV vs. SCE), the dissolution rate of copper in this solution at pH 4 is 55 Å/min. As was observed for 0.1M hydroxylamine solution, the dissolution rate in 0.5M hydroxylamine solution also shows a maximum value of the order of 500 Å/min at pH 6. At pH 8, the dissolution rate of copper reduces to 40 Å/min. The dissolution rate and the trend are in agreement with the report of Huang et al. who determined dissolution rates from the analysis of solutions for copper [2.47].

At an anodic overpotential of 250mV, the dissolution rate of copper at pH 4 and 6 increases drastically to ~ 2270 Å/min. At pH 8, the dissolution rate increases slightly to 620 Å/min. The dissolution rate exhibits a higher value at pH 4, of the order of 6030 Å/min for an overpotential of 750mV, but the rate decreases to 1200 and 920 Å/ min for pH 6 and 8, respectively. The dissolution rates of copper in hydroxylamine solutions at various pH under different anodic overpotentials are listed in Table 4.1.

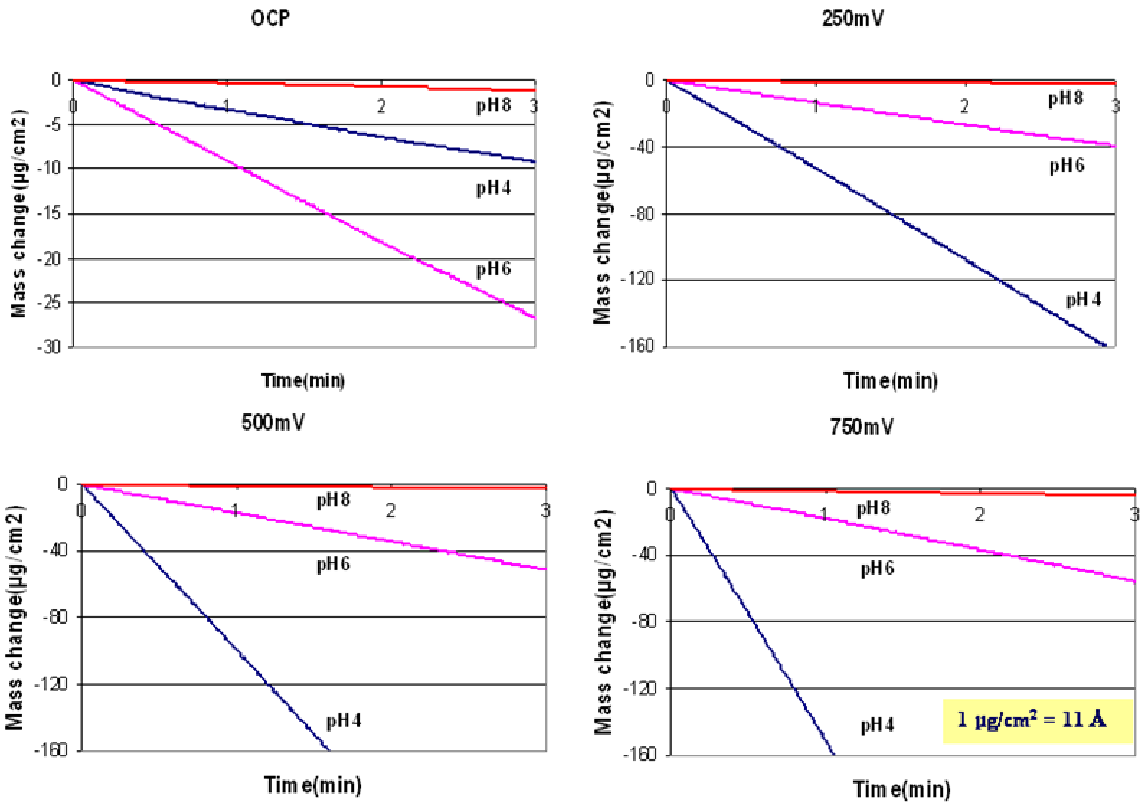

Figure 4.4: Effect of pH on the dissolution of electroplated copper thin films in 0.1M hydroxylamine solution at different anodic overpotentials. (Note: 1 µg/cm^2 = 11 Å)

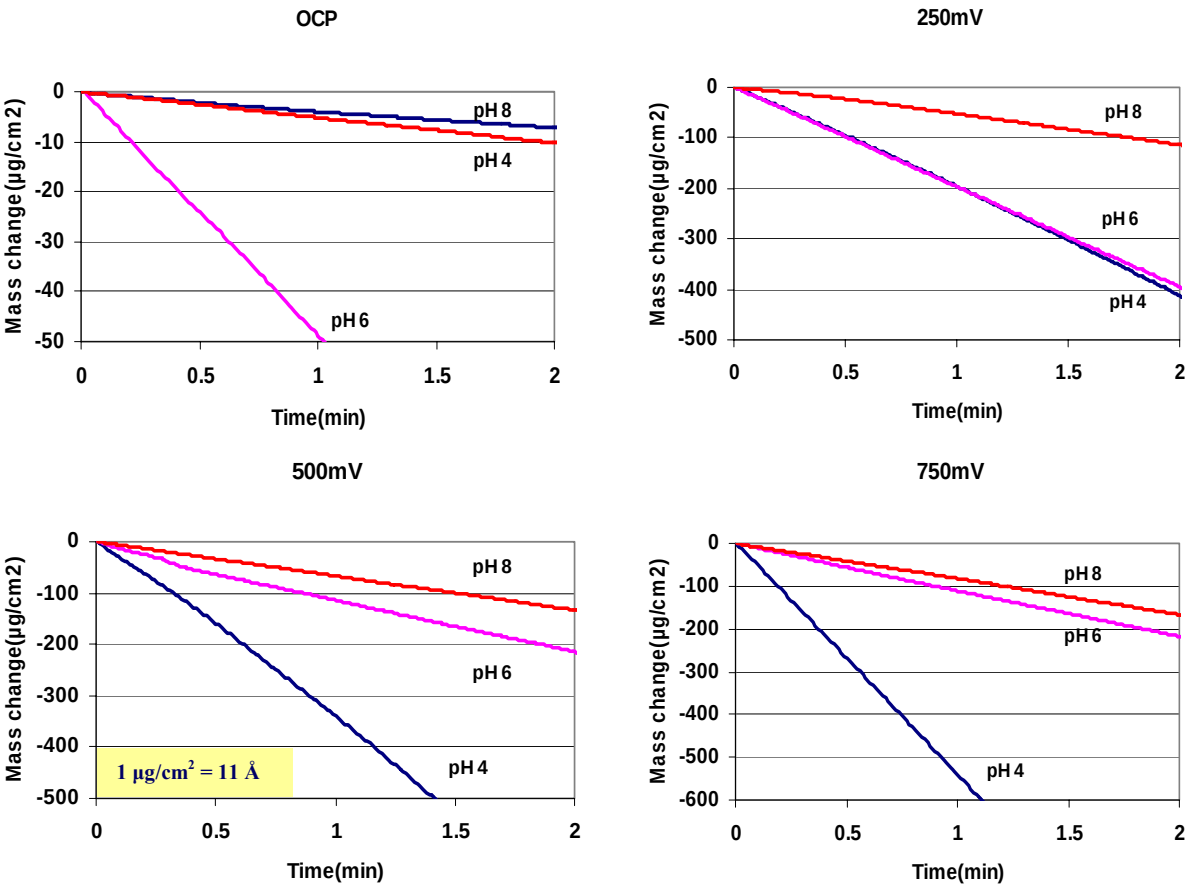

Figure 4.5: Effect of pH on the dissolution of electroplated copper thin films in 0.5M hydroxylamine solution at different anodic overpotentials.

NH_2OH	Overpotential (η)	Dissolution rate of copper (Å/min)		
		pH 4	pH 6	pH 8
0.1 M	OCP	30	100	5
	250mV	600	145	7
	500mV	1115	190	10
	750mV	1730	205	15
0.5 M	OCP	55	500	40
	250mV	2270	2200	625
	500mV	3940	1200	760
	750mV	6030	1200	920

Table 4.1: Dissolution rate of copper in hydroxylamine solutions at various pH under different anodic overpotentials.

The effect of applied potential and pH on the dissolution rate of copper in hydroxylamine solution can be explained by referring to the Pourbaix diagram (Figure 4.1), where the applied overpotentials are indicated by asterisks. At pH 8, based on the potential-pH diagram (Figure 4.1), copper oxides are thermodynamically more stable than copper-hydroxylamine complexes at all applied overpotentials. Copper removal at this pH will be limited by the thickness and porosity of the oxide film. At pH 6, the formation of 1:2 complexes is favorable, resulting in increased dissolution. Oxidation of hydroxylamine at higher anodic potentials will compete with copper dissolution and complexation, resulting in a reduction of rate as well as current efficiency. At pH 4, at lower overpotentials, the rate is limited by the formation of cupric ions, which are then complexed to form 1:1 complex ions. At higher overpotentials, because of a higher concentration of hydrogen ions at this pH, the rate dramatically increases. A schematic representation of copper dissolution mechanism at different pH is shown below.

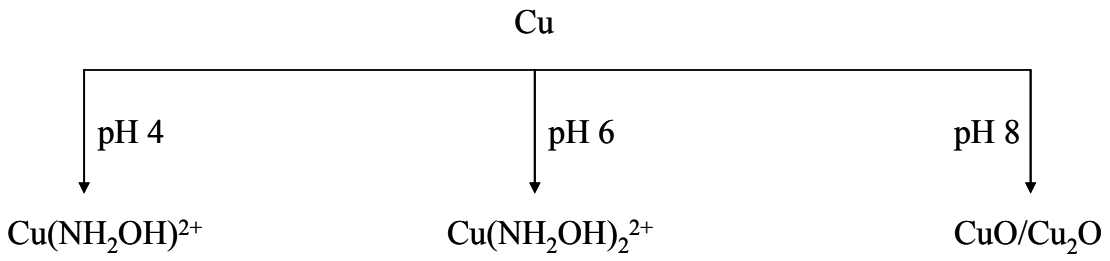

In order to determine whether the very high rate of dissolution at pH 4 was due to a higher hydrogen ion or hydroxylammonium ion concentration, an experiment was conducted at pH 4 without using hydroxylammonium ions. In this experiment, 0.4M KNO_3 was added as the supporting electrolyte to maintain the conductivity at the same

value (42.7mS/cm) as the 0.5 M hydroxylamine solution at pH 4. Figure 4.6 compares mass change of copper in the presence and absence of hydroxylammonium ions at pH 4 under different overpotentials. The presence of hydroxylammonium ions does not influence the initial (one minute) rate greatly, but in solutions without hydroxylamine, copper film was visually observed to peel off from the surface after approximately a minute. Additionally, copious gas evolution was also observed. Based on this observation, it may be said that without hydroxylammonium ions, the uniform dissolution of copper is not feasible.

The relationship between the applied overpotential and the measured current density using Butler-Volmer equation was then analyzed. During these experiments, the current density was simultaneously recorded. Figure 4.7 (a) and (b) shows the dependence of the dissolution rate of copper as well as the current density on anodic overpotential at various pH values in 0.1M and 0.5M hydroxylamine solutions, respectively. It may be seen that while the current density, as expected from the Butler-Volmer equation, increases exponentially with overpotential, the dissolution rate varies only linearly with overpotential. Table 4.2 lists the best fit lines under different conditions. This perhaps indicates that part of the current goes towards hydroxylamine oxidation (to nitrite and nitrate).

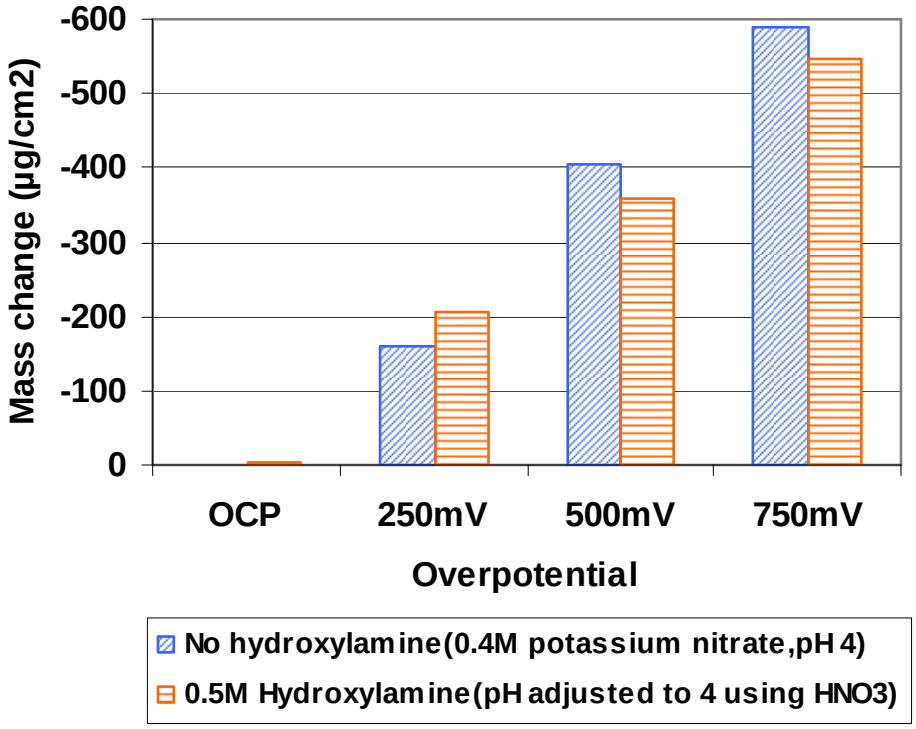

Figure 4.6: Comparison of mass change of copper as a function of overpotential in 0.5M NH_2OH and 0.4M KNO_3 solution at pH 4.

0.1M NH_2OH			0.5M NH_2OH		
pH	Dissolution rate	Current density	pH	Dissolution rate	Current density
4	2.3η $R^2 = 0.99$	$2.081e^{0.0023\eta}$ $R^2 = 0.97$	4	$7.6\eta + 233$ $R^2 = 0.99$	$9.879e^{0.002\eta}$ $R^2 = 0.99$
6	$0.17\eta + 106$ $R^2 = 0.97$	$0.853e^{0.0023\eta}$ $R^2 = 0.99$	6	$-2.3\eta + 2533$ $R^2 = 0.8$	$4.012e^{0.0023\eta}$ $R^2 = 0.99$
8	$0.01\eta + 4.6$ $R^2 = 0.97$	$0.055e^{0.0022\eta}$ $R^2 = 0.99$	6	$0.64\eta + 428$ $R^2 = 0.99$	$4.327e^{0.0024\eta}$ $R^2 = 0.99$

Table 4.2: Best fit lines under different conditions.

(a)

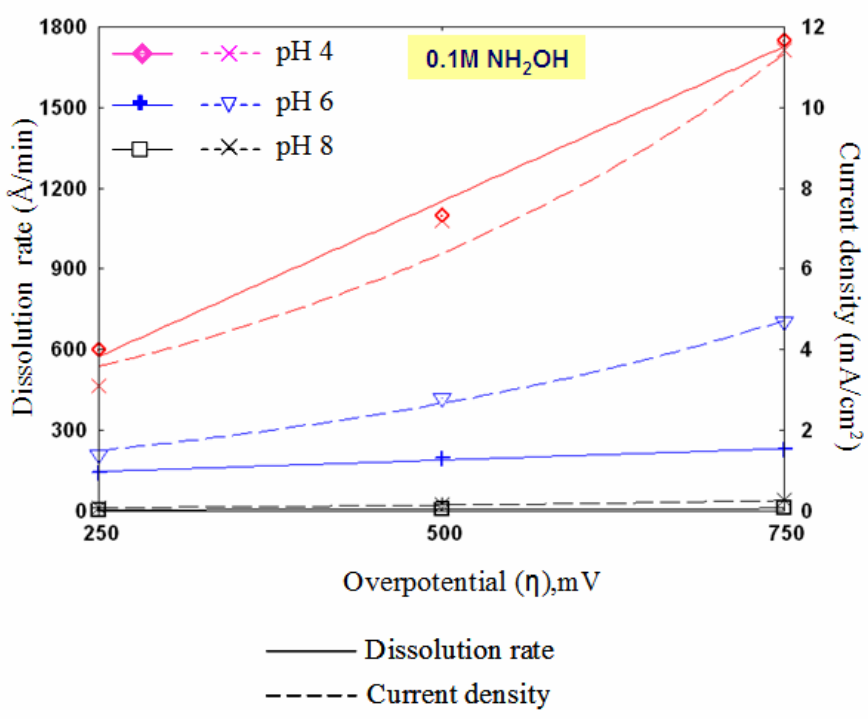

(b)

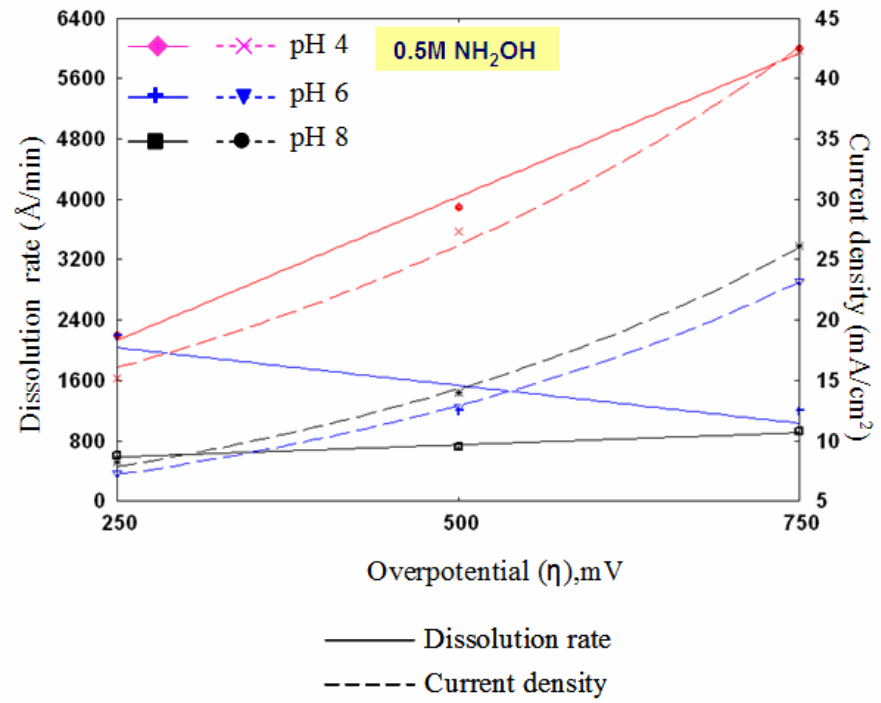

Figure 4.7: Current density and dissolution rate of copper as a function of overpotential in (a) 0.1M NH_2OH (b) 0.5M NH_2OH at different pH values.

4.2.2. Current Efficiency

Current efficiency was calculated from the expression

$$Current\ Efficiency(\%) = \frac{Actual\ dissolution\ rate}{Estimated\ dissolution\ rate} \text{ x } 100$$

The estimation of dissolution rate was made from measured current density using Faraday's law and assuming a two electron transfer process.

Figure 4.8 (a) and (b) shows the current efficiency as a function of overpotential in 0.1M and 0.5M hydroxylamine solutions at various pH values. At pH 4, for both hydroxylamine concentrations, the current efficiency is roughly 65% to 70% under all applied anodic overpotentials. Interestingly, at pH 6, the calculated current efficiency is low in 0.1 M hydroxylamine solution but is over 100% in the 0.5 M hydroxylamine solution at an overpotential of 250 mV. A current efficiency value in excess of 100% is an indication that non-electrochemical pathways may also be contributing to the removal of copper films. One such mechanism is intergranular corrosion resulting in selective copper grain removal, a phenomenon that has been observed in hydroxylamine systems by other researchers [2.36]. At pH 8, as the overpotential is increased from 250mV to 750mV, the current efficiency drops from 35% to 15%, which is perhaps due to the oxidation of hydroxylamine species. High current efficiencies greater than 70% at pH 4 up to an overpotential $\leq$ 500 mV makes this chemistry suitable for ECMP application.

(a)

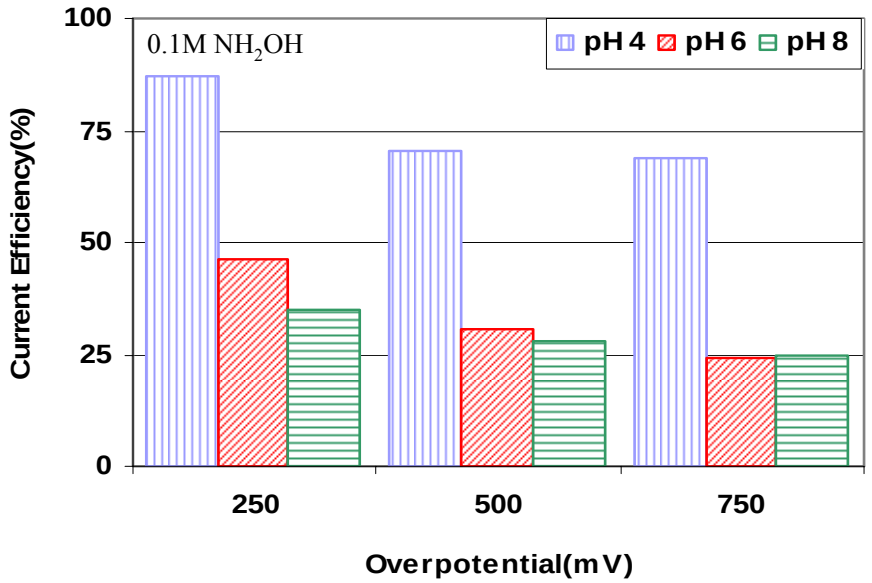

(b)

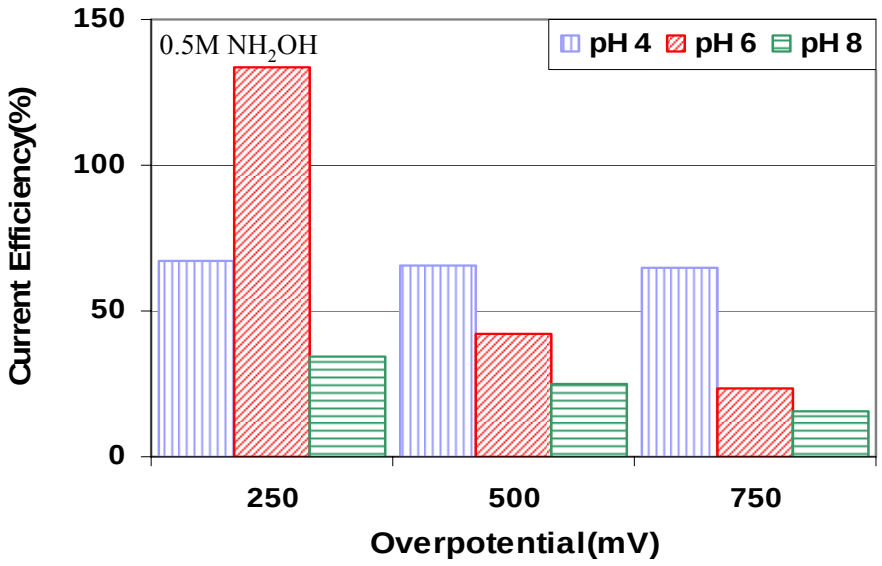

Figure 4.8: Current efficiency vs. overpotential in (a) 0.1M NH_2OH and (b) 0.5M NH_2OH solutions at various pH.

4.2.3. Effect of BTA on Copper Dissolution

Figure 4.9 shows the effect of different concentrations of BTA (0.001M, 0.005M and 0.01M) on copper dissolution in 0.5M hydroxylamine solution (pH 6) at different anodic overpotential values. Under open circuit potential (-10mV vs. SCE), the mass increases for 0.01M BTA, preventing the copper dissolution. In the case of 0.005M BTA, initially there was some copper dissolution at a rate of 8 Å/min, after which BTA inhibits further dissolution. At a lower concentration of 0.001M BTA, the dissolution rate increases significantly to 180 Å/min.

At an overpotential of 250mV, the mass increases for 0.01M BTA and protects copper. But there is a slight increase in copper dissolution of 14 Å/min for 0.005M BTA. If the BTA concentration is lower, 0.001M, the dissolution rate increases to 490 Å/min indicating film breakdown.

At higher overpotentials of 500mV and 750mV, BTA becomes less effective irrespective of any concentration compared to a lower overpotential. For example, the dissolution of copper at an overpotential of 500 mV and 750 mV in 0.01M BTA is 395 and 1000 Å/min, respectively. The dissolution rates of copper in 0.5M hydroxylamine solution maintained at a pH 6 for various overpotentials at different BTA concentrations are listed in Table 4.3. Thus 0.01M BTA is effective in preventing copper dissolution in 0.5M hydroxylamine (pH 6) at $\eta \leq 250$mV.

Overpotential (η)	Dissolution rate (Å/min) of copper in 0.5M hydroxylamine (pH 6)			
	0.001M BTA	0.005M BTA	0.01M BTA	No inhibitor
OCP	180	8	*	500
250 mV	490	14	*	2200
500 mV	670	460	395	1200
750 mV	1200	1100	830	1200

Table 4.3: Dissolution rate of copper in 0.5M hydroxylamine solution (pH 6) for various overpotential values at different BTA concentrations.

Note: * denotes that the mass is increasing

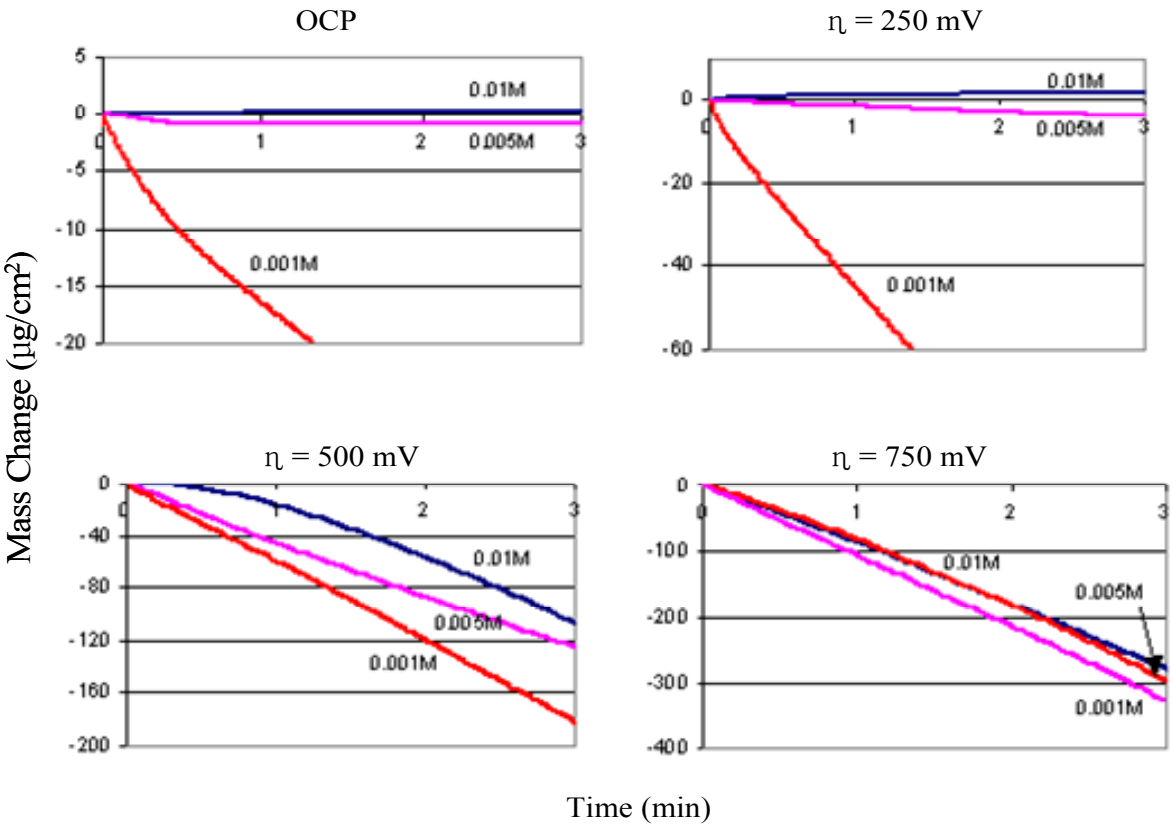

Figure 4.9: Effect of BTA concentrations on copper dissolution in 0.5M hydroxylamine solution (pH 6) at different anodic overpotential values.

4.2.4. Comparison of BTA and SHA on Copper Dissolution

The effects of 0.01M BTA and 0.01M SHA on copper dissolution in 0.5M hydroxylamine solutions at pH 4 and pH 6 under different anodic overpotential values are shown in Figures 4.10 (a) and (b) respectively. At pH 4, under OCP conditions, mass increases both in the case of BTA and SHA by ~0.14 $\mu g/cm^2$ and ~0.7 $\mu g/cm^2$, respectively, indicating adsorption/surface precipitation. At an overpotential of 250mV, the mass increases in the presence of BTA, whereas in the case of SHA, mass decreases, indicating copper dissolution. At higher overpotentials, both BTA and SHA become less effective in preventing copper dissolution. For example, the dissolution rate of copper in the presence of BTA and SHA at an overpotential of 750 mV is 5120 and 6000 Å/min, respectively. These results indicate that SHA is less effective than BTA at any given overpotential value at pH 4.

At pH 6, copper dissolution is observed in solutions containing SHA at $\eta \leq 250$ mV, as compared with complete inhibition observed in BTA. However, at overpotentials of 500 mV and 750 mV, SHA appears to be a much more effective inhibitor than BTA. It may be concluded from these results that the inhibitory properties of BTA and SHA decrease with increasing anodic overpotential. A summary of the results obtained is presented in Table 4.4.

Overpotential (η)	Dissolution rate (Å/min) of copper in 0.5M hydroxylamine					
	pH 4			pH 6		
	No inhibitor	0.01M BTA	0.01M SHA	No inhibitor	0.01M BTA	0.01M SHA
OCP	55	*	*	500	*	20
250 mV	2270	*	1300	2200	*	110
500 mV	3940	1390	3220	1200	395	290
750 mV	6030	5120	6000	1200	830	365

Table 4.4: Dissolution rate of copper in 0.5 M hydroxylamine solutions in the presence and absence of 0.01M BTA and 0.01M SHA at pH 4 and 6 under various overpotentials.

Note: * denotes that the mass increases

(a)

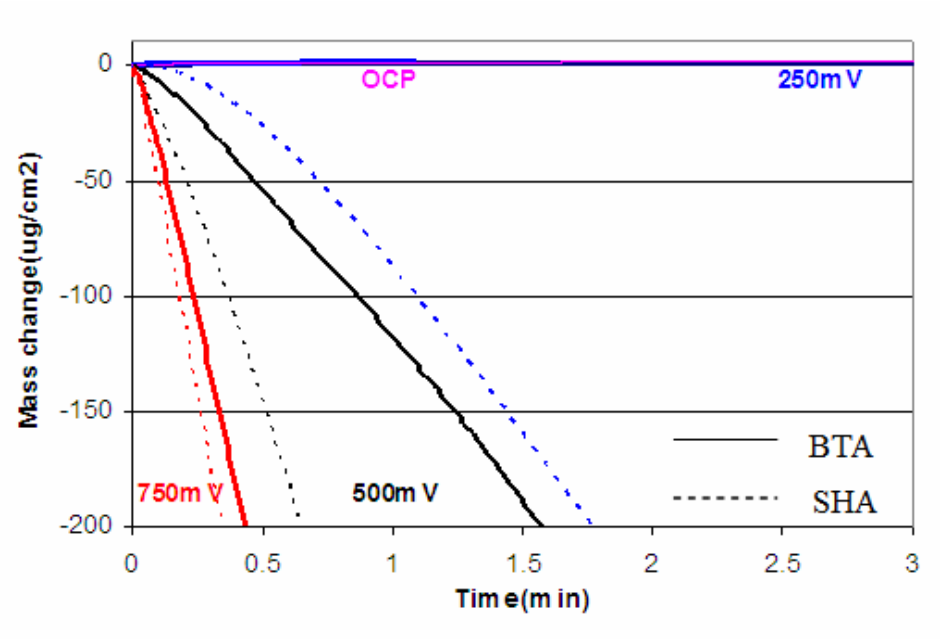

(b)

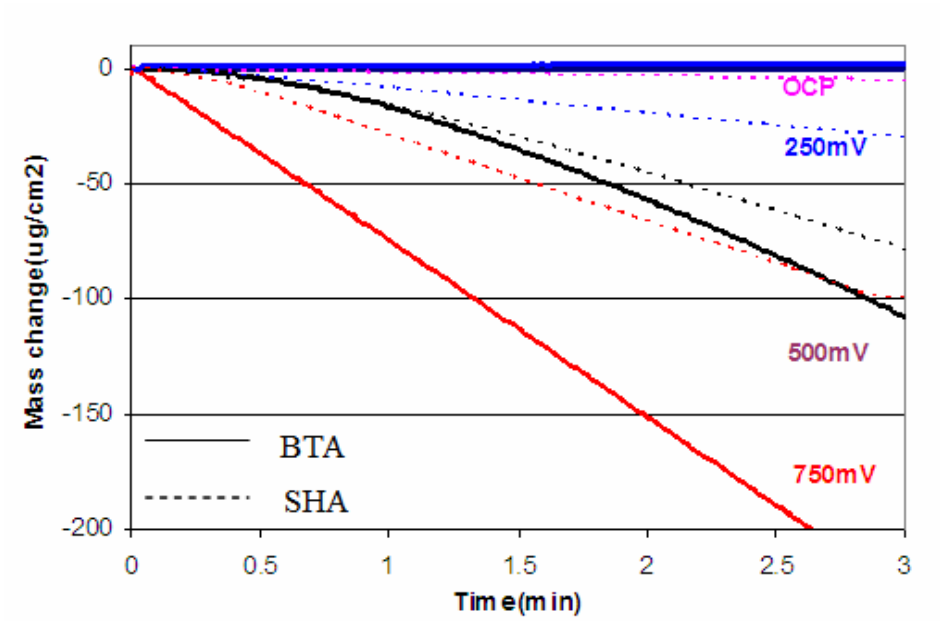

Figure 4.10: Effect of 0.01M BTA and 0.01M SHA on copper dissolution in 0.5M hydroxylamine solution (a) pH 4 and (b) pH 6 at different anodic overpotential values

4.2.5. Characterization of Copper Surface by AFM

The topography of the copper surface after exposure to hydroxylamine solutions at pH 4 and 6 was examined using an atomic force microscope (AFM). The average roughness (R_a) of as-received gold coated crystal and the copper plated crystal was 2 and 28 nm, respectively. At pH 4, under the OCP condition, the roughness of the copper film exposed to 0.5M hydroxylamine solution for 1 minute was 30 nm (figure not shown here). When polarized at an overpotential of 250mV, roughness drastically increased to 82 nm as shown in Figure 4.11. The effect of BTA on the topography of the copper surface was also studied. Figure 4.12 shows the AFM topographic image of the copper surface (25 μm x 25 μm) exposed to 0.5M hydroxylamine containing 0.01M BTA (pH 4) at an overpotential of 250mV for 1 minute. The addition of BTA to the solution reduces the roughness value to 40 nm, indicating that BTA is effective in controlling the dissolution of the copper film.

Similar studies of a copper surface exposed to 0.5M hydroxylamine solution at pH 6 under OCP conditions showed a surface roughness of 36 nm (figure not shown here). At an overpotential of 250mV, the roughness increased to 44 nm with evidence of grain boundary attack and loss of some copper grains as shown in Figure 4.13. This mechanical removal of copper may explain more than 100% current efficiency. The effect of 0.01M BTA on the topography of the copper surface that was polarized at an overpotential of 250 mV for 1 minute in 0.5M hydroxylamine solution is shown in Figure 4.14 (a). The surface roughness is about 22 nm, slightly lower than that of as-plated copper. Figure 4.14 (b) shows a closer view of the same image (1 μm x 1 μm). It can be seen that the surface is uniformly covered by small granular structures. The size of the

granular structure is too large to be a single BTA or Cu-BTA molecule, but indicates that the adsorbed BTA and Cu-BTA compounds group to form nodules.

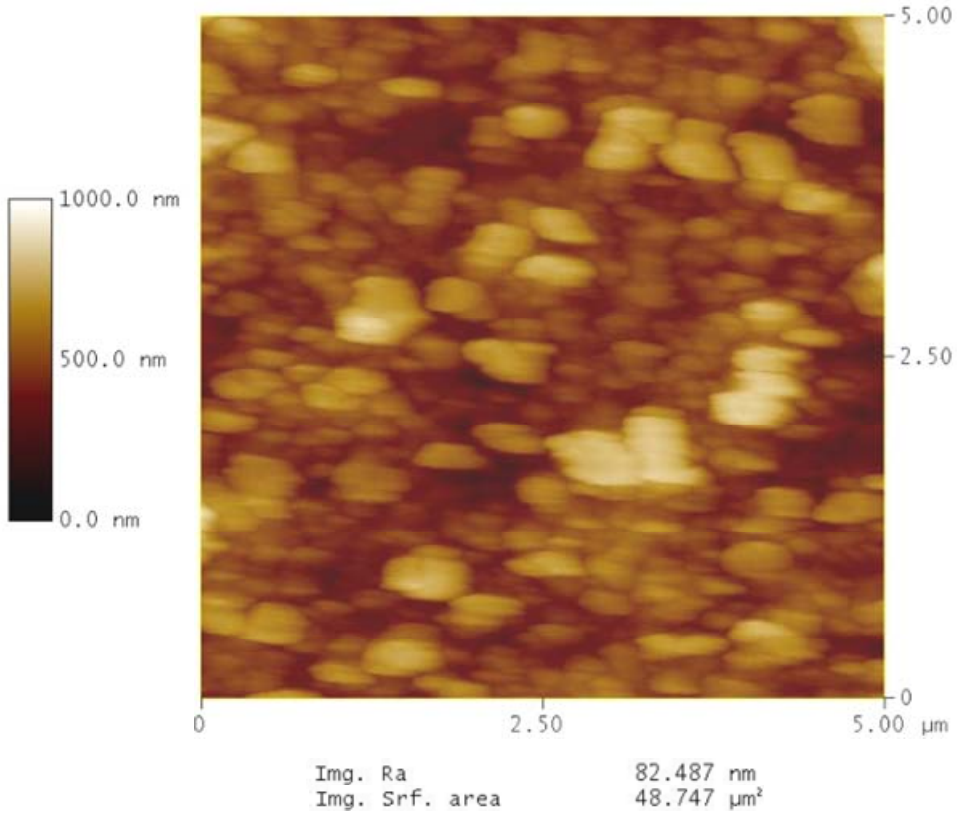

Figure 4.11: AFM topographic images of copper surface (5 µm x 5 µm) exposed to 0.5M hydroxylamine (pH 4) at an overpotential of 250mV for one minute.

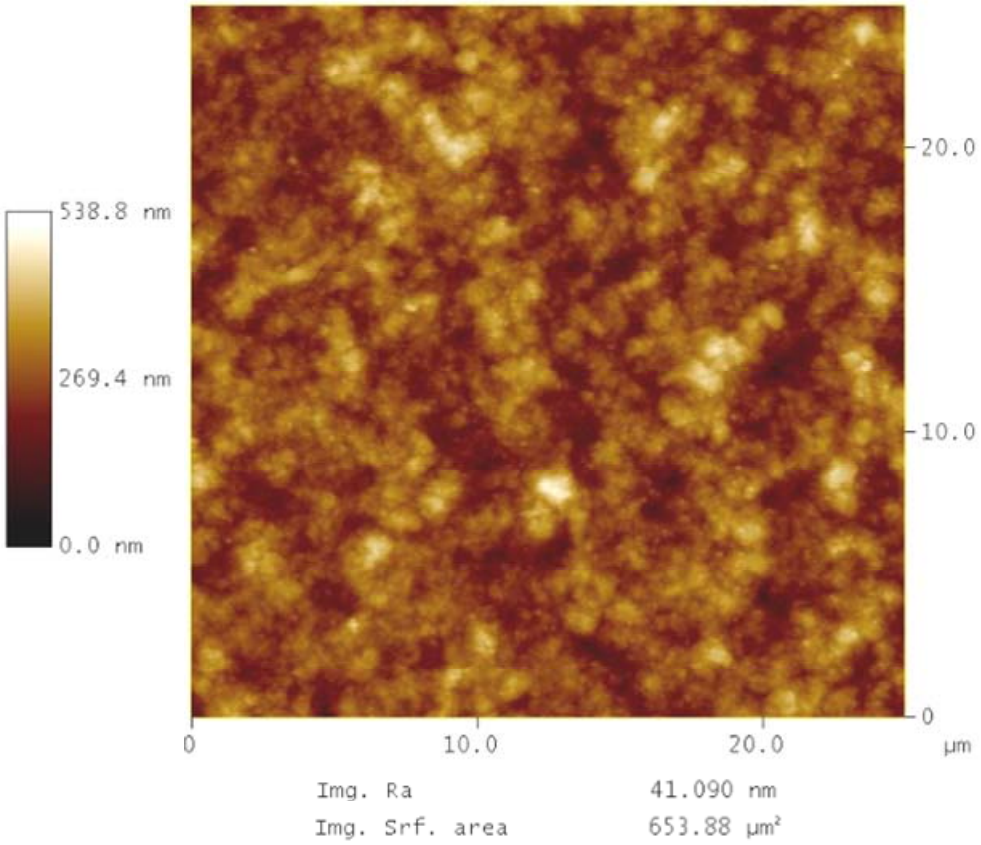

Figure 4.12: AFM topographic images of copper surface (25 µm x 25 µm) exposed to 0.5M hydroxylamine containing 0.01M BTA (pH 4) at an overpotential of 250mV for 1 minute.

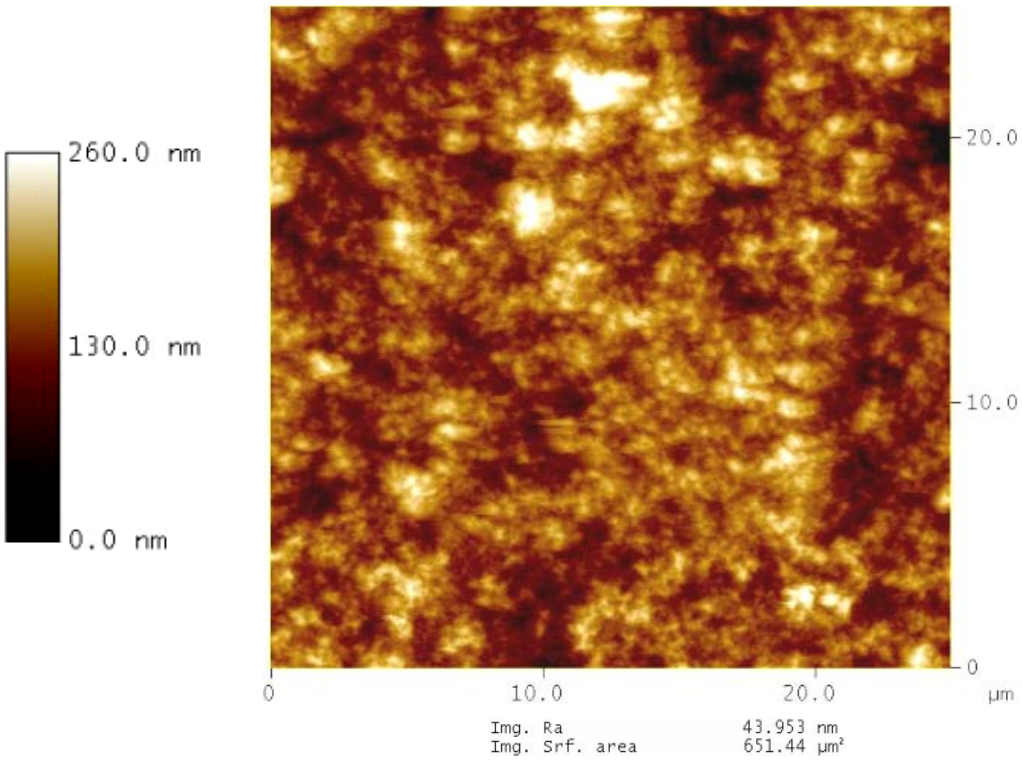

Figure 4.13: AFM topographic images of copper surface (25 µm x 25 µm) exposed to 0.5M hydroxylamine (pH 6) at an overpotential of 250mV for one minute.

(a)

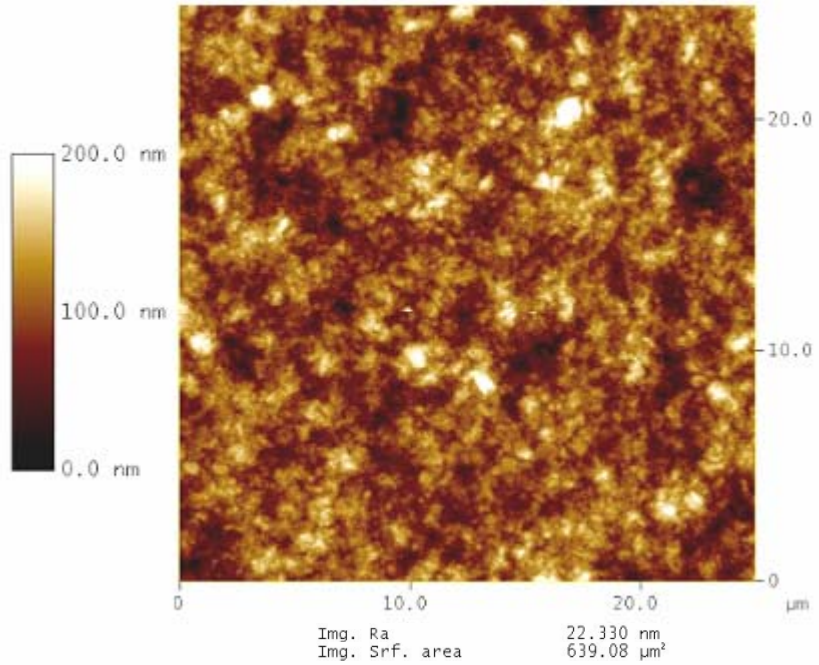

(b)

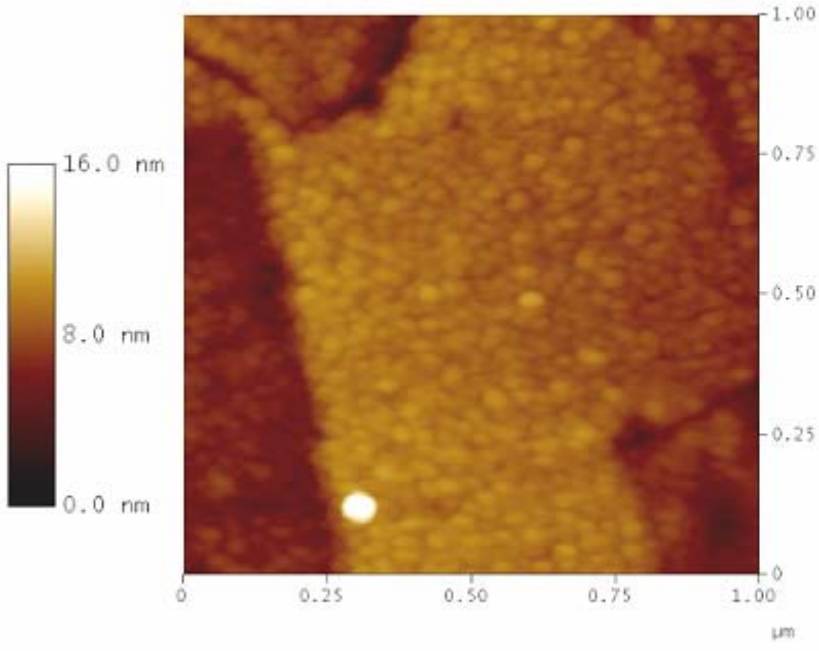

Figure 4.14: AFM topographic images of (a) copper surface (25 µm x 25 µm) exposed to 0.5M hydroxylamine containing 0.01M BTA (pH 6) at an overpotential of 250mV for 1 minute and (b) closer view of the same surface at 1 µm x 1 µm showing BTA nodules.

4.2.6. Inhibition Efficiency

Inhibition efficiency of BTA and SHA was calculated from the corrosion rates in the absence and presence of inhibitors. Figure 4.15 (a) shows the inhibition efficiency of BTA as a function of overpotential in 0.5 M hydroxylamine solution at pH 4 and 6. At OCP and an overpotential of 250mV, the inhibition efficiency is 100% at both pH 4 and 6. At an overpotential of 500mV, the inhibition efficiency drops to 65% and 67% for pH 4 and 6, respectively. At a higher overpotential of 750mV, the inhibition efficiency is 30% at pH 6 and 15% at pH 4. These results show that BTA becomes less effective in hydroxylamine solutions as overpotential is increased, indicating the unstable nature of the passive film on the copper surface. For ECMP of copper in 0.5M hydroxylamine solution at pH 4 and 6, BTA would be effective at a concentration of 0.01M if the applied overpotential is less than 500mV.

The inhibition efficiency of SHA as a function of overpotential is shown in Figure 4.15 (b). At pH 4, 100% inhibition efficiency is achieved under the OCP conditions. At overpotentials $\geq$ 250 mV, SHA is less effective compared to BTA, having almost zero inhibition efficiency at an overpotential of 750 mV. In the case of pH 6, ~ 95% inhibition efficiency is obtained at OCP and overpotential of 250 mV, compared with 100% inhibition efficiency of BTA under similar conditions. However, at 500 mV and 750 mV overpotentials, SHA has a better inhibition efficiency than BTA.

(a)

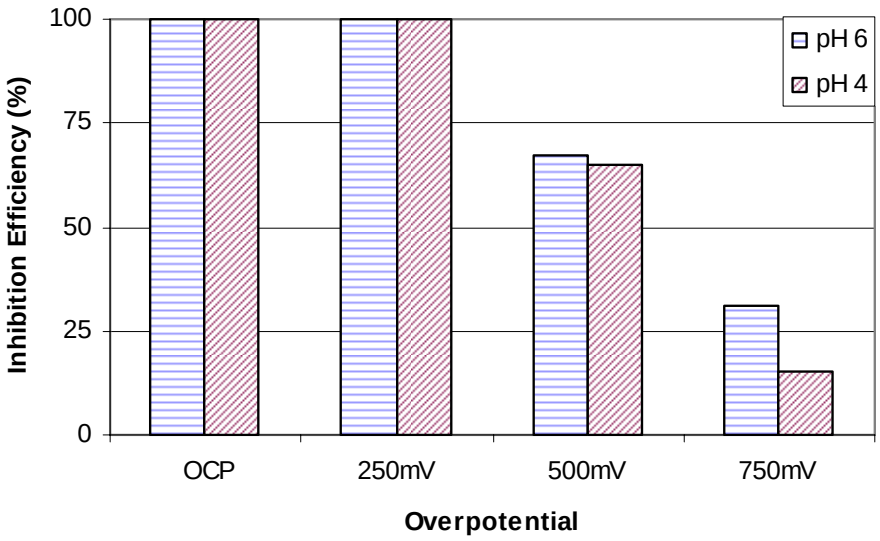

(b)

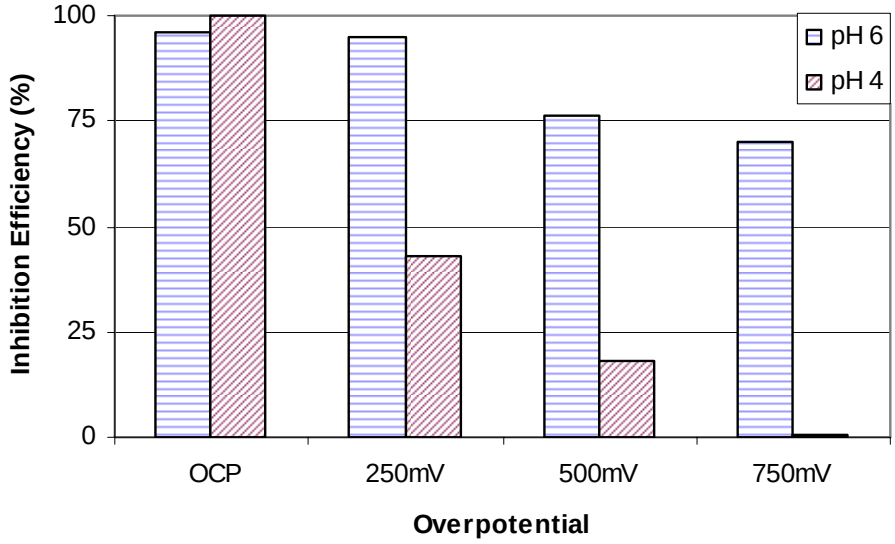

Figure 4.15: Inhibition efficiency of (a) 0.01M BTA and (b) 0.01M SHA as a function of overpotential in 0.5M hydroxylamine solution at pH 4 and 6.

4.2.7. Mechanism of Passivation by BTA

The mass change of copper film at OCP condition in 0.5M hydroxylamine solution containing 0.01M BTA at pH 4 and 6 has been re-plotted in Figure 4.16. It can be seen that the mass rapidly increases as soon as the copper sample is exposed to the chemistry. At pH 6, the mass increases up to one minute and then saturates after it reaches 0.14 $\mu g/cm^2$. At pH 4, the mass increases much more rapidly than that observed at pH 6 and in one minute, the mass increases by 0.26 $\mu g/cm^2$. The BTA molecules can adsorb on to the copper surface in two different orientations; the aromatic ring can either stand upright (perpendicular to the copper surface) or lie flat on the surface [4.3, 4.4]. If the BTA molecule stands upright, its cross sectional area is roughly 30 $Å^2$ and if it lies flat, its cross sectional area is 60 $Å^2$.

Based on these cross sectional areas, and using the actual surface area obtained from AFM measurements which is about 5 % larger than the geometrical area, the measured mass increase at pH 6 corresponds to either 2 or 4 layers, depending on orientation. At pH 4, the measured mass change corresponds to either 4 or 8 layers. Literature indicates the formation of BTA multilayers on the copper surface at acidic conditions [4.5, 4.6]. While it is not possible to conclude from the QCM results whether the first layer of BTA is chemisorbed or not, the literature contains many reports that the adsorbed BTA in the first layer forms a cuprous-BTA polymeric complex, while the subsequent BTA layers attach by physisorption [4.6]. This is shown schematically in Figure 4.17.

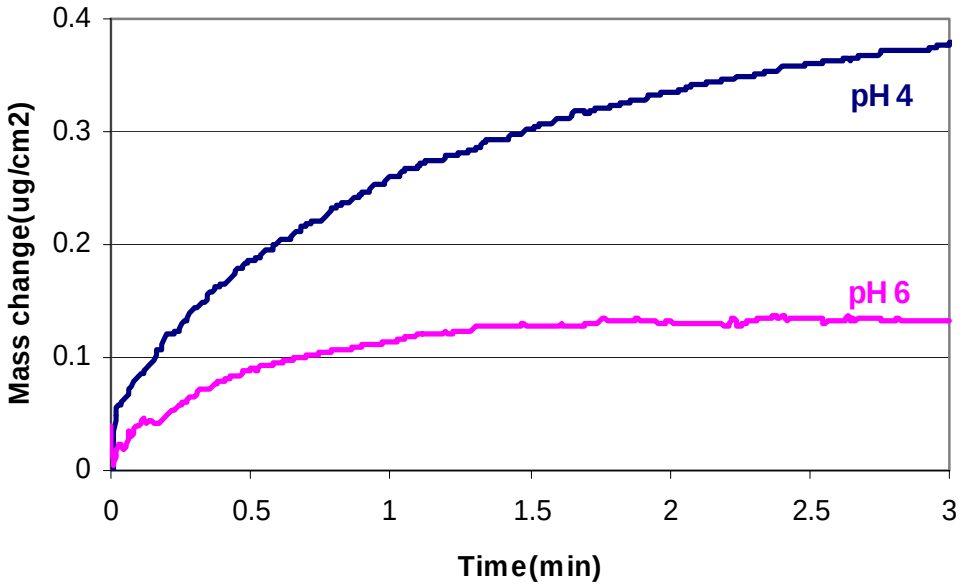

Figure 4.16: Mass change of copper film when exposed to 0.5M hydroxylamine containing 0.01M BTA at pH 4 and 6 under OCP conditions.

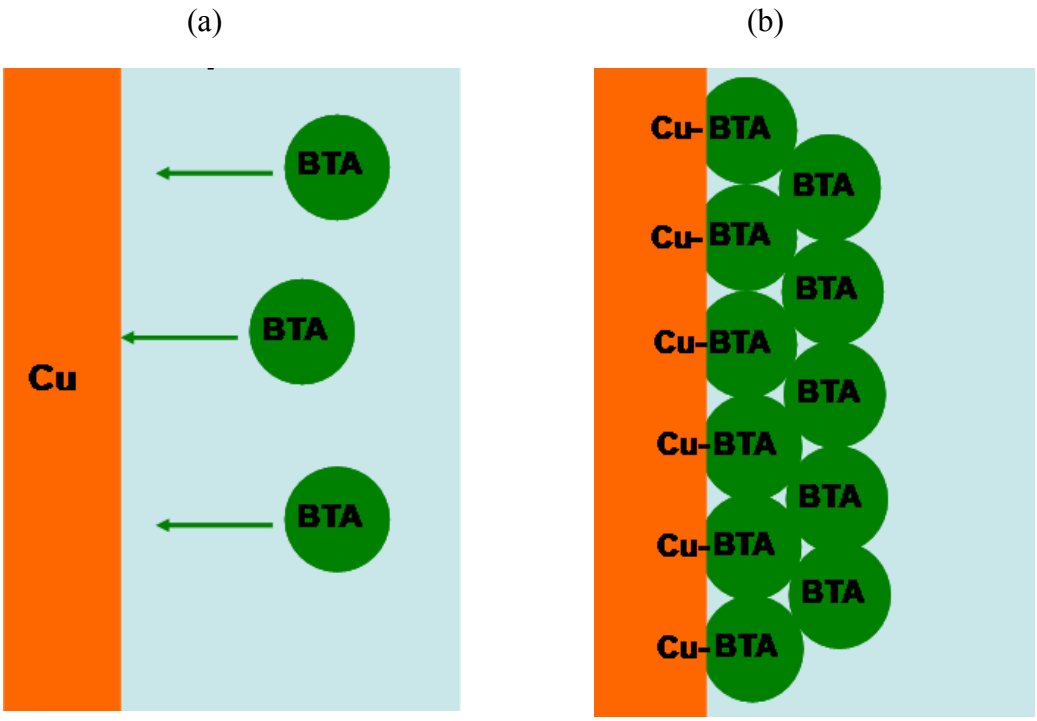

Figure 4.17: Schematic representation showing the mechanism of copper passivation by BTA in hydroxylamine solutions; a) adsorption of BTA on copper, b) formation of cuprous-BTA passive monolayer followed by physisorption.

4.2.8. Mechanism of Passivation by SHA

Figure 4.18 shows the mass change of the copper film when exposed to 0.5M hydroxylamine solution containing 0.01M SHA at pH 4 and 6 under OCP conditions. At pH 6, the mass decreases to -2 $\mu g/cm^2$ for one minute. This decrease corresponds to a copper removal rate of ~ 20 Å/min. As mentioned earlier, it should be noted that in the absence of SHA, the copper removal rate is ~ 500 Å/min. This clearly shows that the presence of SHA reduces the amount of copper dissolution. However, at pH 4, mass actually increases to ~ 0.7 $\mu g/cm^2$ for one minute, indicating adsorption/surface precipitation. It has been reported in the literature that the polar cross sectional area of SHA is ~ 65 $Å^2$. Based on the cross sectional area, the measured mass increase roughly corresponds to 20 layers.

The XPS study by Tamilmani indicates the formation of an insoluble Cu (+2)-SHA-OH compound on the surface of copper [2.36]. Additionally, at pH 6, SHA is unable to prevent copper dissolution even under OCP conditions. This suggests that copper is first dissolved by hydroxylamine and the copper (+2) - hydroxylamine complex then reacts with the hydroxide ion to form an insoluble Cu-SHA polymeric compound at the surface of the copper, providing some degree of protection. This is schematically shown in Figure 4.19.

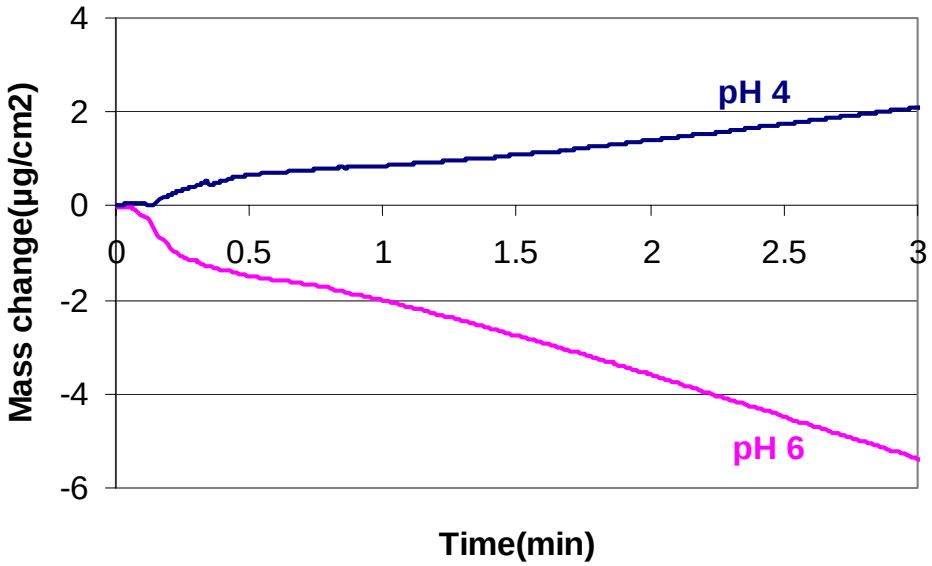

Figure 4.18: Mass change of copper film when exposed to 0.5M hydroxylamine solution containing 0.01M SHA at pH 4 and 6 under OCP conditions.

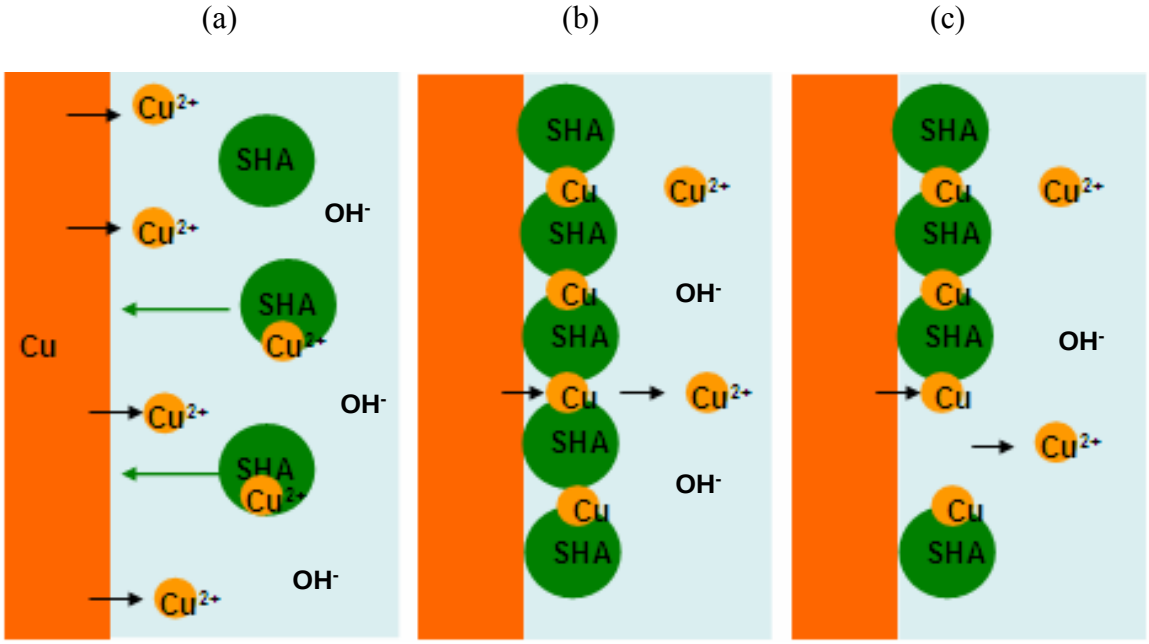

Figure 4.19: Schematic representation showing the mechanism of copper passivation by SHA in hydroxylamine solution; (a) copper dissolution and complexation of dissolved copper by SHA (b) formation of Cu-SHA polymeric film on copper surface and (c) breakdown of polymeric film.

4.3. Polishing Studies on Copper using EC-AC Tool

4.3.1 Hydroxylamine Based Solution (pH 4)

The removal rates of electroplated copper films under ECMP conditions in hydroxylamine based solutions with and without inhibitors were investigated using the EC-AC tool at a pressure of 0.5 psi. As a first step, the static rate of copper was studied as a function of applied overpotentials and the results are shown in Figure 4.20 (a). Under the OCP condition, the removal rate of copper in 0.5M hydroxylamine solution is of the order of 80 Å/min. At overpotential values of 250 mV and 500 mV, the removal rate increases to 2400 and 4140 Å/min, respectively. A higher removal rate of the order of 6370 Å/min was obtained at 750 mV overpotential. The addition of 0.01M SHA to the solution containing 0.5M hydroxylamine reduces the static rate to zero under the OCP condition. At higher overpotentials, SHA becomes less effective in preventing static removal rate. For example, the static rate of copper at overpotential of 500 mV and 750 mV is 3590 and 6180 Å/min, respectively. Similarly, the addition of 0.01M BTA reduces the static rate to zero at $\eta \leq 250$ mV. At overpotentials of 500 mV and 750 mV, the static rate is 1780 and 5040 Å/min. These results indicate that BTA is more effective than SHA at any given overpotential value at pH 4 under static conditions.

Figure 4.20 (b) shows the polishing rate of copper at pH 4. A pressure of 0.5 psi was used for these experiments. In 0.5M hydroxylamine solution, the removal rate of copper is 140 Å/min at OCP condition. At higher overpotentials ($\eta \geq 250$ mV), the removal rate increases by 500 - 600 Å/min, compared to the static rate under similar conditions. The addition of inhibitors only slightly reduces the removal rate of copper under all conditions.

From these results, it is clear that the best polishing condition at pH 4 is observed at an overpotential of 250 mV in 0.5M hydroxylamine solution containing 0.01M BTA. Under this condition, since the static rate is zero, the low lying regions are completely protected. At the same time, since the polishing rate of copper is 2100 Å/min, the higher regions of the film were selectively removed, thereby achieving planarity.

(a)

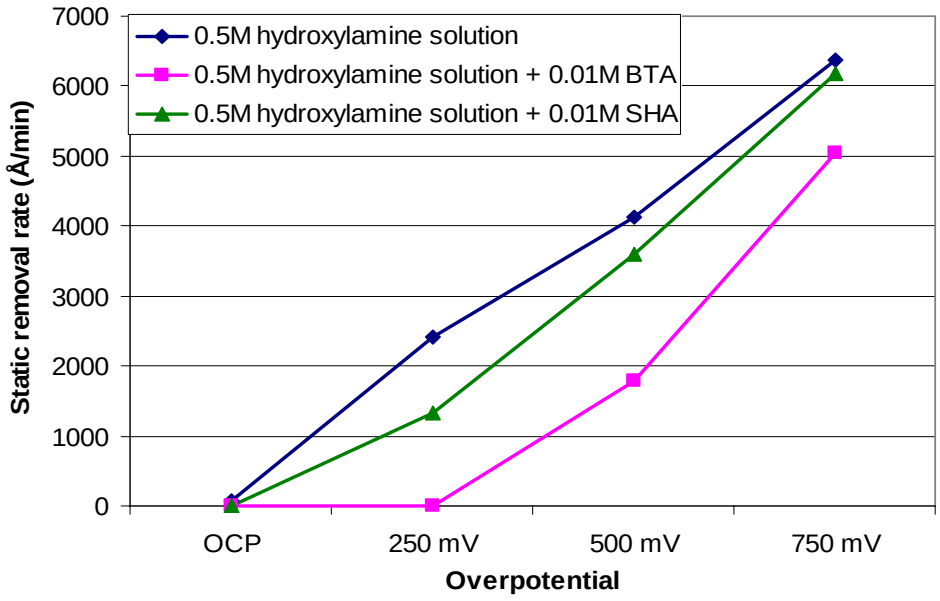

(b)

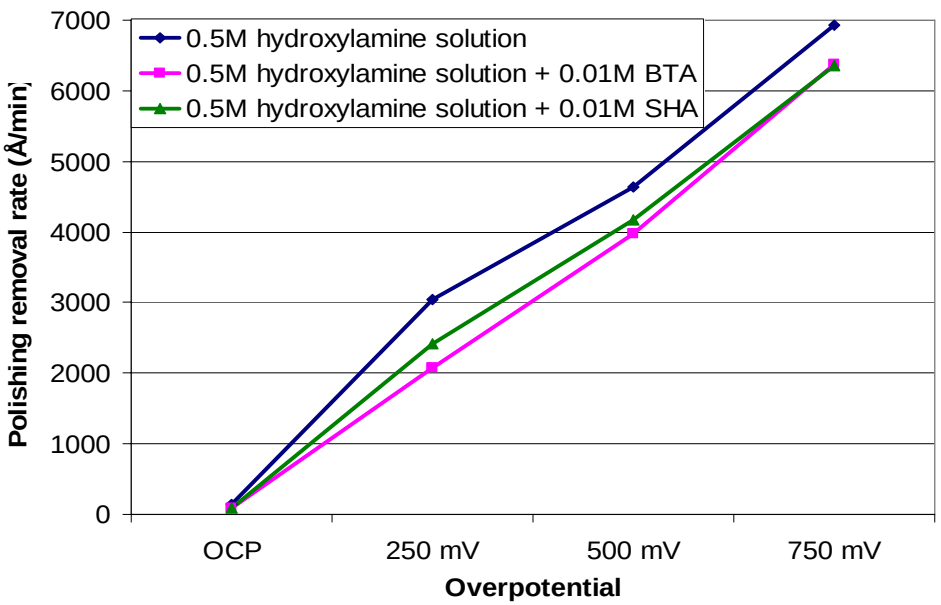

Figure 4.20: (a) Static and (b) polishing rate of copper as a function of applied overpotentials in 0.5M hydroxylamine based solution at pH 4.

4.3.2. Hydroxylamine Based Solution (pH 6)

Static and polishing studies of copper in 0.5M hydroxylamine based solutions at pH 6 were performed using EC-AC tool. Figure 4.21 (a) shows the static rate of copper in hydroxylamine based solutions with and without inhibitors as a function of applied overpotentials at pH 6. The removal rate of copper under the OCP condition is ~ 500 Å/min. At an overpotential of 250 mV, the removal rate increases to 2200 Å/min. At higher overpotentials of 500 and 750 mV, the removal rate have decreased to 1200 Å/min. Copper dissolution is observed in solutions containing 0.01M SHA at $\eta \leq 250$ mV, as compared with complete inhibition observed in 0.01M BTA. However, at overpotentials of 500 mV and 750 mV, SHA appears to be a much more effective inhibitor than BTA. It may be concluded from these results that the inhibitory properties of BTA and SHA decreases with increasing anodic overpotential.

Figure 4.21 (b) shows the polishing rate of copper in hydroxylamine based solutions as a function of applied overpotentials at pH 6. A pressure of 0.5 psi was used for these experiments. Under the OCP condition, the removal rate of copper is 760 Å/min in 0.5M hydroxylamine solution. At an overpotential of 250 mV, the removal rate increases to 2550 Å/min. At higher overpotentials of 500 mV and 750 mV, the removal rate increases to 2000 Å/min. It may be noted that the addition of 0.01M SHA reduces the removal rate by ~ 500 Å/min at an overpotential ≥ 250 mV. However, BTA reduces the removal rate only marginally under all applied overpotentials.

From these results, the best polishing condition at pH 6 was observed at an overpotential of 250 mV in 0.5M hydroxylamine solution containing 0.01M BTA, where the static rate is zero and the polishing rate is ~ 2000 Å/min.

(a)

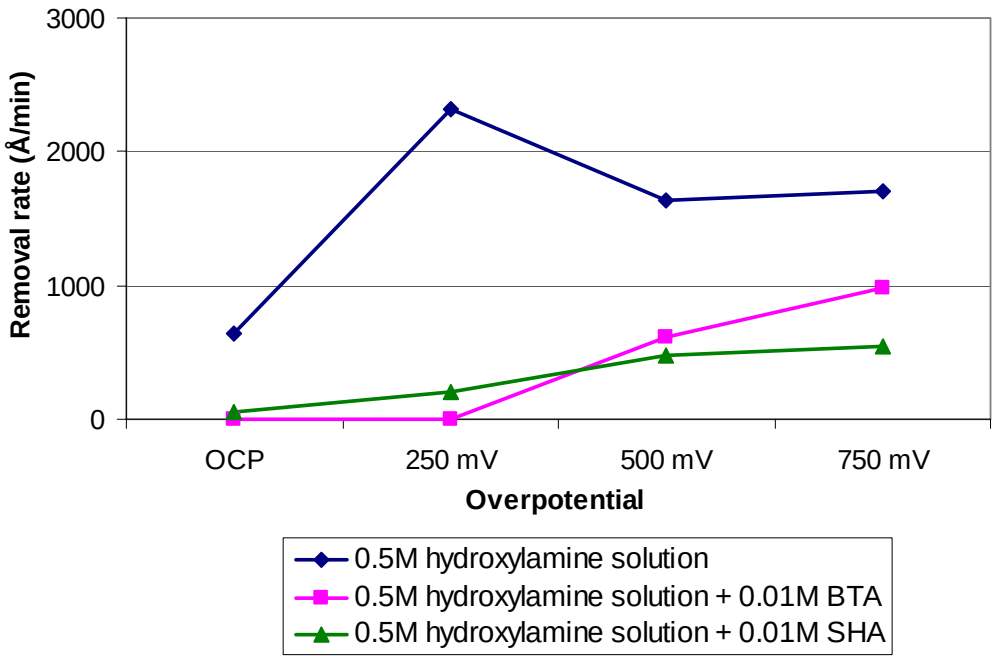

(b)

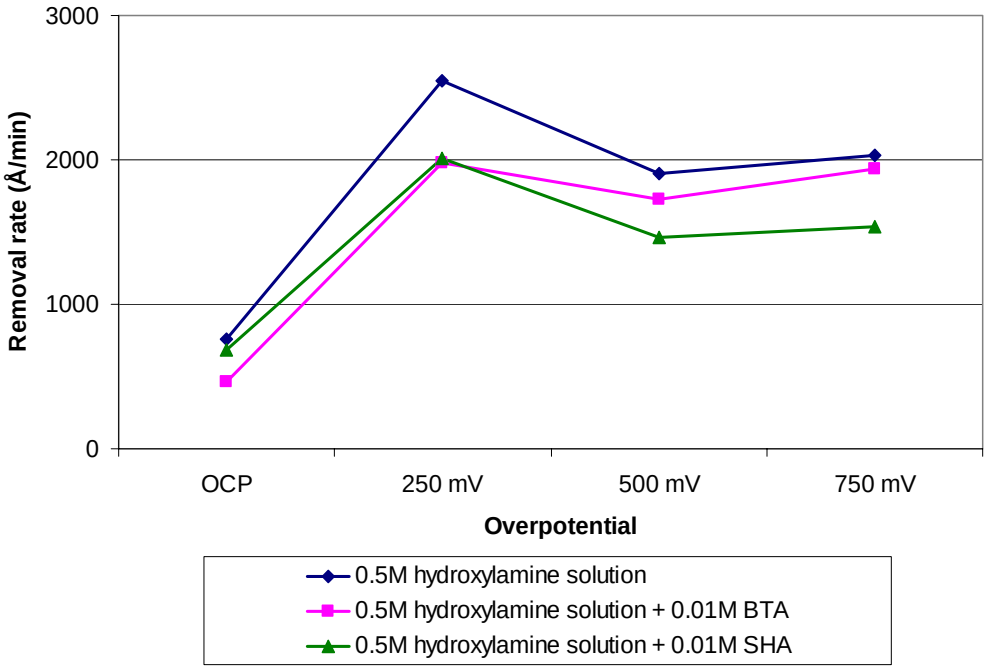

Figure 4.21: (a) Static and (b) polishing rate of copper as a function of applied overpotentials in 0.5M hydroxylamine based solution at pH 6.

4.3.3. Characterization of Polished Copper Surface by AFM

The topography of the copper surface before and after polishing in hydroxylamine based chemistries was examined using AFM. The surface of electroplated blanket copper film was used as a baseline. The samples used for the investigation were copper samples subjected to planarization in an industrial CMP tool using peroxide based slurry. Under ECMP condition, the film was removed to simulate bulk copper removal. The roughness of the copper sample before subjected to polishing under ECMP condition was found to be ~ 5 nm. The blanket copper film was polished in 0.5M hydroxylamine solution (pH 4) at an overpotential of 250 mV for 1 minute. Then the sample was rinsed with DI water and dried with nitrogen gas, and the surface was imaged (Figure 4.22). The topographic image shows that the copper surface has been severely etched with a surface roughness of 16 nm. It can be seen that copper grains are missing in some areas while the grain boundaries have been etched forming deep trenches. From the image it is clear that the grain boundaries are preferentially attacked causing the copper grains to fall off from the surface.

The effect of BTA and SHA on the topography of copper surface was also studied. Figure 4.23 shows the polished surface (1 μm x 1 μm) that was exposed to 0.5M hydroxylamine solution containing 0.01M BTA (pH 4) at an overpotential of 250 mV for 1 minute. It can be seen that the surface is uniformly covered by small granular structures. As mentioned before, the size of the granular structure is too large to be a single BTA or Cu-BTA molecule, but it indicates that the adsorbed BTA and Cu-BTA compounds group to form nodules. The surface roughness was found to be 1.5 nm,

slightly higher than the polished copper surface but an order of magnitude lower than the surface etched by hydroxylamine.

Figure 4.24 shows the copper surface (1 μm x 1 μm) exposed to 0.01M SHA containing 0.5M hydroxylamine solution (pH 4) at an overpotential of 250 mV for 1 minute. Similar to the BTA system, the copper surface is covered with Cu-SHA nodules. However, the surface roughness is about ~ 10 nm which is relatively higher compared to the BTA system. This could be attributed to the fact that SHA is not 100% effective in preventing copper dissolution in low lying areas at this overpotential.

Thus in hydroxylamine based system, BTA is a much better inhibitor than SHA, providing lower roughness.

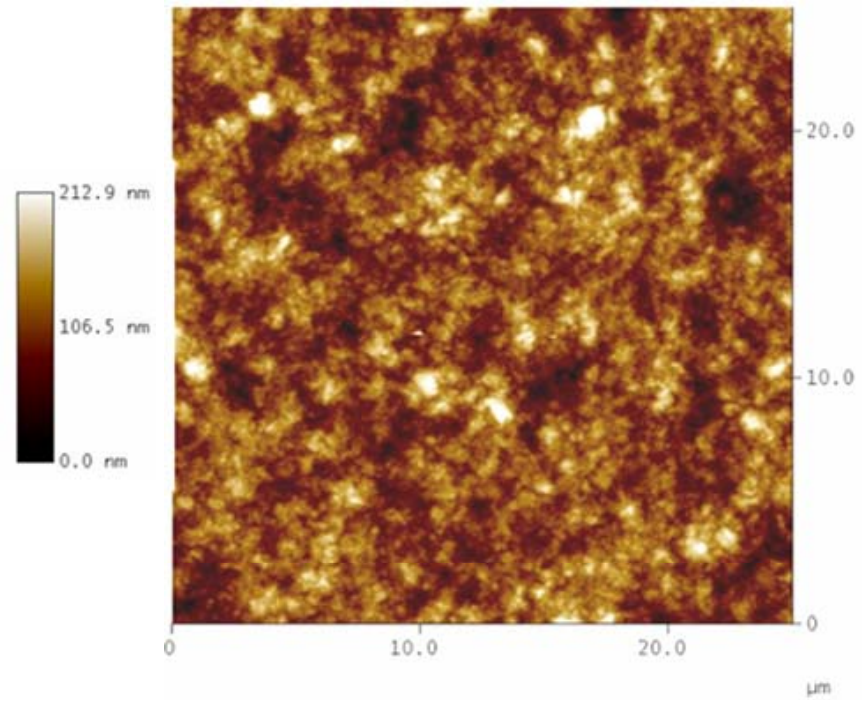

Figure 4.22: AFM topographic images of copper surface (25 µm x 25 µm) polished in 0.5M hydroxylamine solution (pH 4) at an overpotential of 250mV for 1 minute.

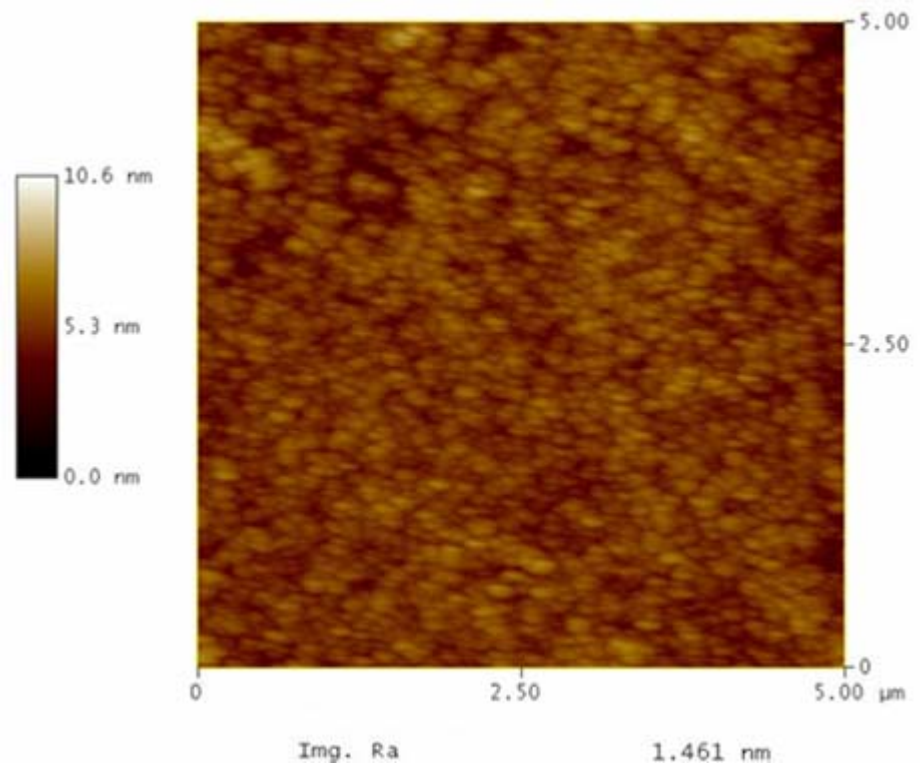

Figure 4.23: AFM topographic images of copper surface (5 µm x 5 µm) polished in 0.5M hydroxylamine solution containing 0.01M BTA (pH 4) at an overpotential of 250mV for 1 minute.

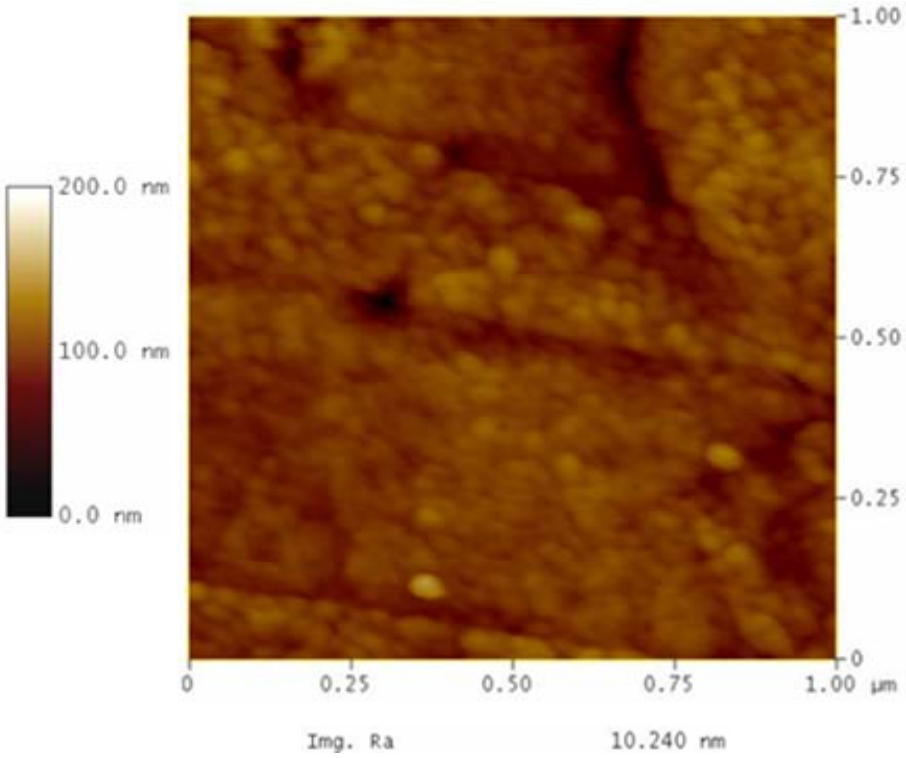

Figure 4.24: AFM topographic images of copper surface (1 µm x 1 µm) polished in 0.5M hydroxylamine solution containing 0.01M SHA (pH 4) at an overpotential of 250mV for 1 minute.

4.4. Evaluation of DBSA Solution for ECMP of Tantalum

4.4.1. Anodic Polarization of Tantalum under Abrasion

For preliminary experiments, a pH value of 10 was chosen since conventional CMP is typically carried out at this pH. Figure 4.25 displays the anodic polarization curves for tantalum and copper collected during abrasion at 0.5 psi in DBSA solutions at pH 10. The solid and the dashed lines represent the I-V curve for tantalum and copper respectively. The open circuit potential (OCP) of tantalum in 0.1M DBSA solution is -680mV vs. SCE. During anodic polarization, a current density of 0.08 mA/cm^2 is measured for overpotential (η) of 1 V. Upon the addition of 0.1% SiO_2 to 0.1M DBSA solution, the OCP becomes more negative (-840 mV vs. SCE), likely due to enhanced removal of tantalum oxide from the surface. The current density increases exponentially up to a potential of -400 mV vs. SCE and saturates at 0.15 mA/cm^2 thereafter. For a solution containing 0.3M DBSA and 0.1% SiO_2 particles, an increase in current density with potential is observed up to -600 mV vs SCE above which it saturates at 0.25 mA/cm^2. No significant change in OCP is observed with an increase in the concentration of DBSA. The addition of 1.2M H_2O_2 to 0.3M DBSA solution containing 0.1% SiO_2 increases the OCP by 100 mV and the current density is doubled to ~ 0.5 mA/cm^2 at 1V overpotential.

In the absence of peroxide, the OCP of copper in 0.3M DBSA solution containing 0.1% SiO_2 is -430 mV vs SCE, which is much more positive than the OCP of bare tantalum under the same conditions. A current density of ~ 20 mA/cm^2 is measured for overpotential of 1 V. The addition of 1.2M H_2O_2 increases the OCP by 300 mV and the current density is doubled to ~ 40 mA/cm^2 at an overpotential of 1 V. Since the

maximum solubility of DBSA is 0.3M, it was decided to use this concentration for further experiments.

4.4.2. Cyclic Voltammetry (CV) of Tantalum

Experiments were carried out to determine the oxidation potential of tantalum. A typical electrochemical set up was used where the tantalum film acts as the working electrode. Saturated Calomel (Hg/Hg_2Cl_2) and platinum were used as reference and counter electrodes, respectively. It may be noted that the tantalum film was dipped in dilute HF (1%) to remove native oxide, rinsed in DI water and dried in N_2 gas.

The potential was swept from open circuit potential (OCP) to 1.5 V vs. OCP and then was reversed back to OCP. Figure 4.26 (a) shows the cyclic voltammogram of tantalum in 0.3M DBSA solution containing 1.2M H_2O_2 at pH 10 at a scan rate of 100 mV/s. When the potential was increased from OCP (- 250 mV vs. SCE), a peak was observed at 350 mV vs. SCE. This peak formation could be attributed to the oxidation of tantalum or DBSA solution. Further, to determine the nature of peak, experiment was conducted on platinum electrode under same condition. Figure 4.26 (b) shows the cyclic voltammogram of platinum electrode in 0.3M DBSA solutions containing 1.2M H_2O_2 at pH 10. No peak formation was observed during the scan. This indicates that the peak formed in Figure 4.26 (a) could be attributed to the oxidation of tantalum. Also, no distinguishable peak was observed during the reversal of the scan back to OCP. This indicates that the oxidation reaction is not reversible.

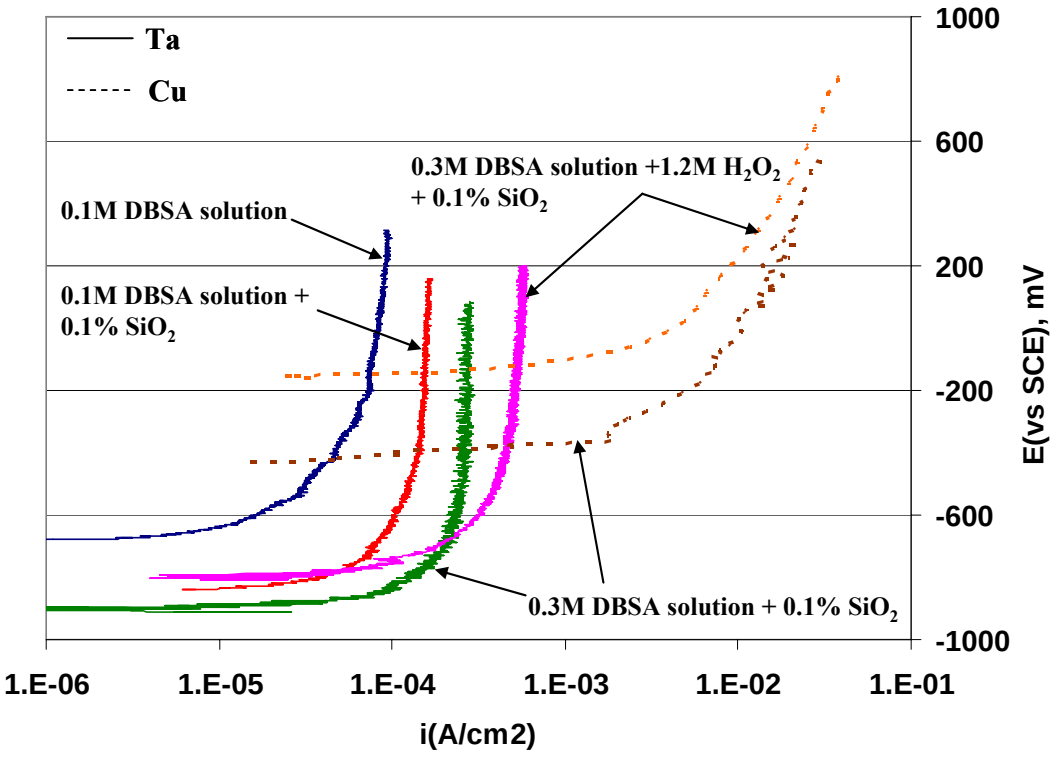

Figure 4.25: Anodic polarization of tantalum and copper while being abraded with a polyurethane pad in DBSA solution at pH 10.

(a)

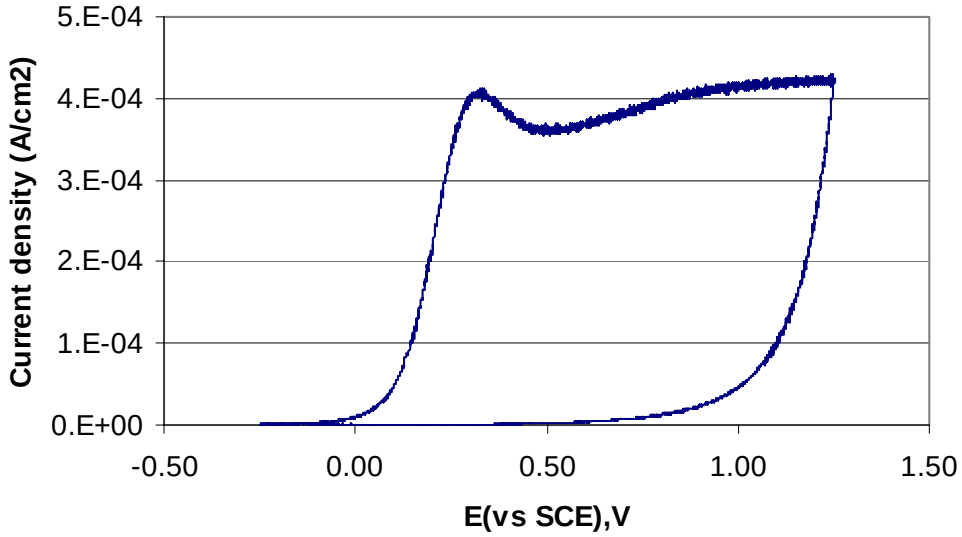

(b)

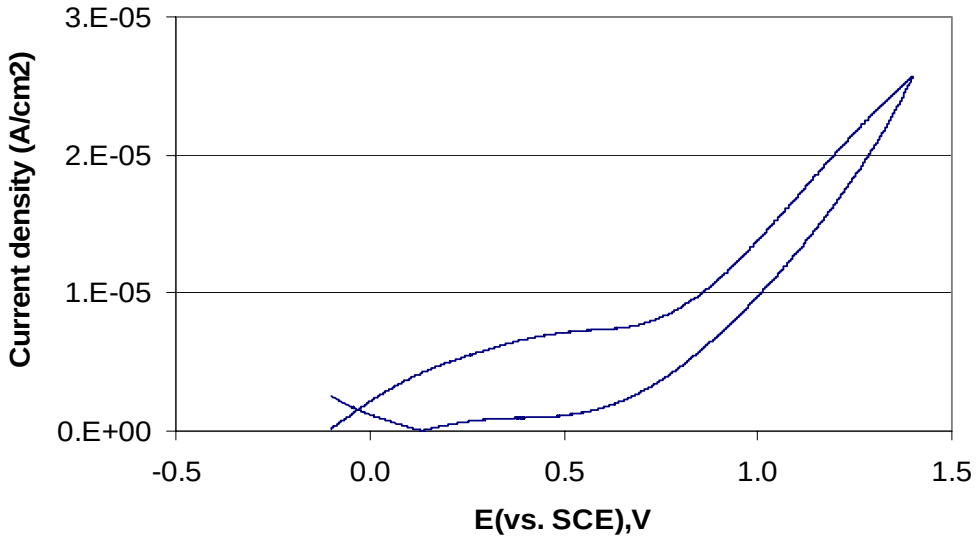

Figure 4.26: Cyclic voltammogram of (a) tantalum and (b) platinum in 0.3M DBSA solutions containing 1.2M H_2O_2 at pH 10.

4.4.3. Effect of Silica and Peroxide Concentration on Removal Rate

The effect of silica and peroxide concentration on the removal rate of tantalum in sulfonic acid solutions was then investigated. The removal rate of tantalum as a function of silica concentration in 0.3M DBSA solution (pH 10) at an applied current density of 0.25mA/cm^2 is shown in Figure 4.27. In the absence of silica particles, the removal rate of tantalum is very low ~ 20 Å/min. The addition of 0.05% SiO_2 slightly increases the removal rate to 35 Å/min. Increase in the silica particle concentration to 0.1% nearly triples the removal rate to 90 Å/min. At 4% SiO_2 concentration, the removal rate is found to be 130 Å/min. These results indicate that the presence of a small amount (~ 0.1%) of colloidal silica particles is needed to provide reasonable tantalum removal rates in DBSA solutions.

The effect of peroxide on the removal rate of tantalum in 0.3M DBSA solution containing 0.1% SiO_2 (pH 10) at an applied current density of 0.25mA/cm^2 is shown in Figure 4.28. The removal rate of tantalum is 90 Å/min in the absence of peroxide and the addition of 0.6M H_2O_2 increases the removal rate to 120 Å/min. Increase in peroxide concentration to 1.2M further increases the removal rate to 160 Å/min. Peroxide concentration greater than 1.2M increases the removal rate only marginally.

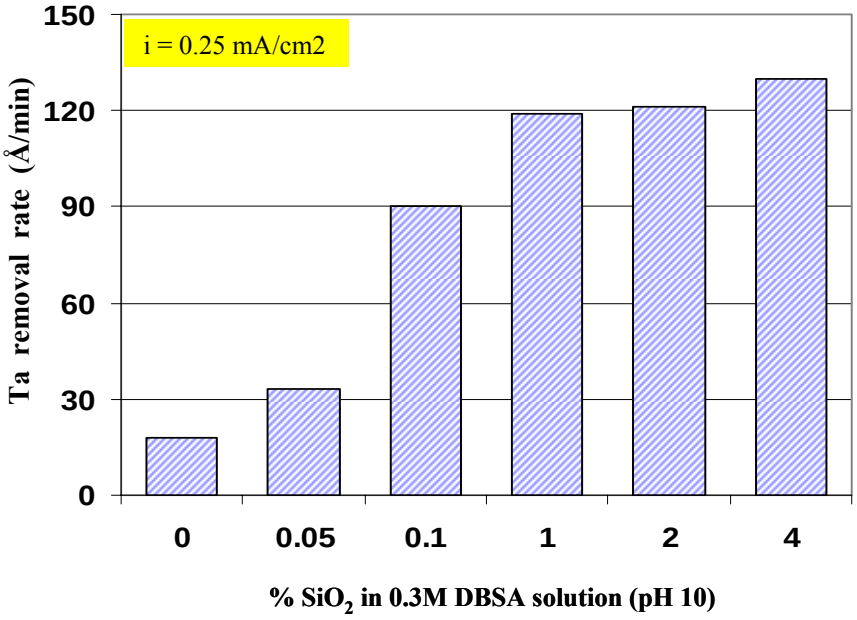

Figure 4.27: Effect of silica concentration on the removal rate of tantalum in 0.3M DBSA solution (pH 10) at a current density of 0.25mA/cm^2

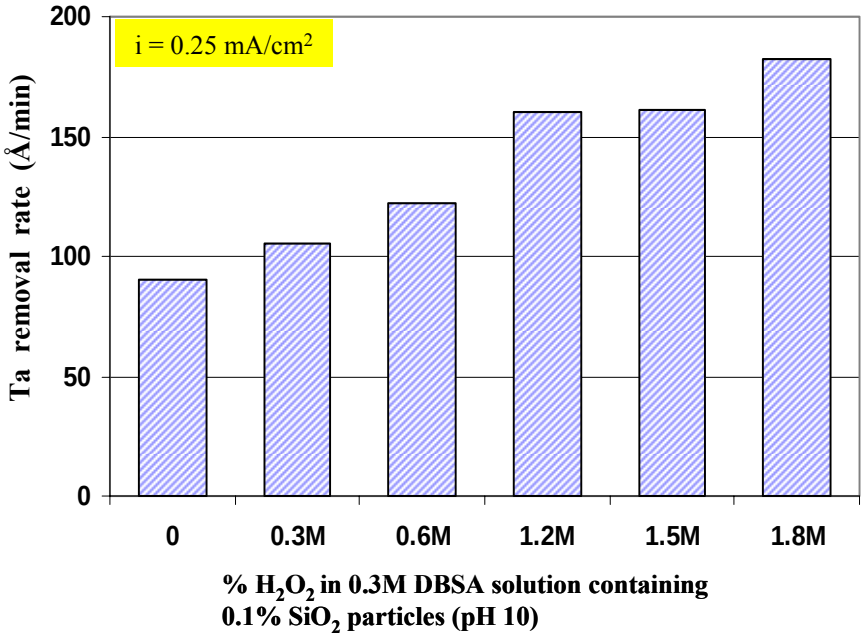

Figure 4.28: Effect of peroxide concentration on the removal rate of tantalum in 0.3M DBSA solution (pH 10) at a current density of 0.25mA/cm^2

4.4.4. Removal Rate vs. pH

Figure 4.29 (a) shows the removal rate of tantalum in 0.3M DBSA solution containing 0.1% SiO_2 as a function of pH in the presence and absence of peroxide at a current density of 0.25 mA/cm^2. At pH 4, the removal rate of tantalum is 70 Å/min in the absence of peroxide, while the removal rate in the presence of 1.2M peroxide is 95 Å/min. Increasing the pH to 7 results in a decrease in the tantalum removal rate both in the presence and absence of peroxide. At pH 10, as mentioned previously, higher removal rates of tantalum, of the order of 90 and 160 Å/min, are obtained in the absence and presence of peroxide, respectively.

The removal rate of copper in 0.3M DBSA solution containing 0.1% SiO_2 as a function of pH in the presence and absence of peroxide at a current density of 0.25 mA/cm^2 is shown in Figure 4.29 (b). The highest removal rate is obtained at pH 4, of the order of 120 and 175 Å/min in the absence and presence of peroxide, respectively. It may be noted that the removal rate decreases with pH. At pH 10, the removal rates of 80 and 140 Å/min are obtained in the absence and presence of peroxide, respectively.

(a)

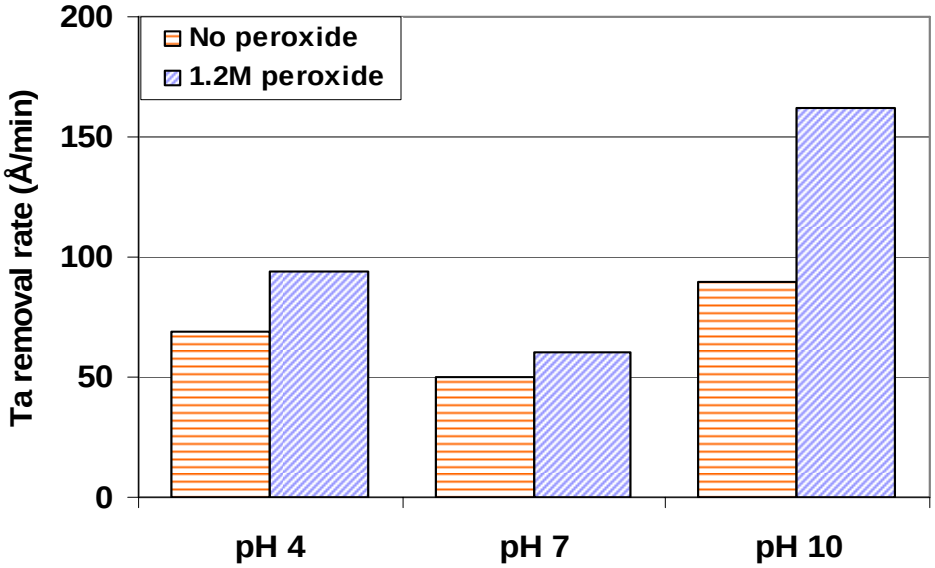

(b)

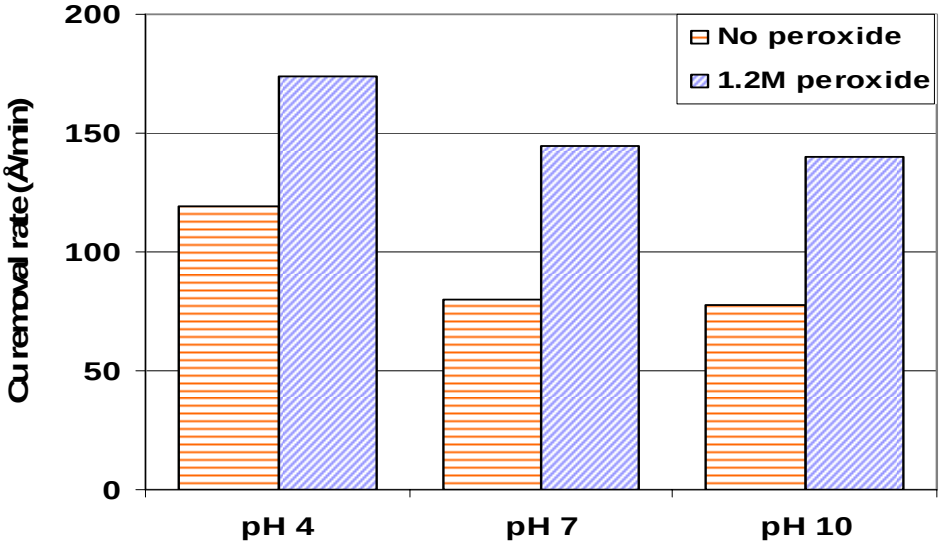

Figure 4.29: Removal rate of (a) tantalum and (b) copper in 0.3M DBSA solution containing 0.1% SiO_2 in the presence and absence of peroxide as a function of pH at a current density of 0.25 mA/cm^2.

4.4.5. Effect of Current Density

Since higher removal rates of tantalum were obtained at pH 10, it was decided to investigate this pH in more detail. Figure 4.30 shows the removal rate of tantalum as a function of applied current density at pH 10. In a solution containing 0.1% SiO_2 particles, the removal rate is very low ~ 15 Å/min under OCP condition. When a current density of 0.1 mA/cm^2 is applied, the removal rate doubles to ~ 30 Å/min. However, the removal rate plateaus above 0.25 mA/cm^2.

When 1.2M H_2O_2 is added to the solution containing 0.1% SiO_2 particles, the removal rate increases by 10-20 Å/min for all applied current densities. In order to examine the role of DBSA, the removal rate of tantalum in a solution containing 0.3M DBSA and 0.1% SiO_2 particles was studied. Under OCP condition, the removal rate was 30 Å/min whereas at 0.1 mA/cm^2, the removal rate was found to be 65 Å/min. This removal rate was nearly twice the value observed in the absence of sulfonic acid. Increasing the current density to 0.25 and 0.5 mA/cm^2, the removal rate increased to 90 and 120 Å/min, respectively.

The addition of 1.2M H_2O_2 to 0.3M DBSA solution containing 0.1% SiO_2 particles was then examined. Under OCP condition, the removal rate of ~ 60 Å/min was obtained. When a current density of 0.1 mA/cm^2 was applied, the removal rate increased to 85 Å/min. At higher current densities, the removal rate increased, yielding a higher rate of 195 Å/min at 0.5 mA/cm^2.

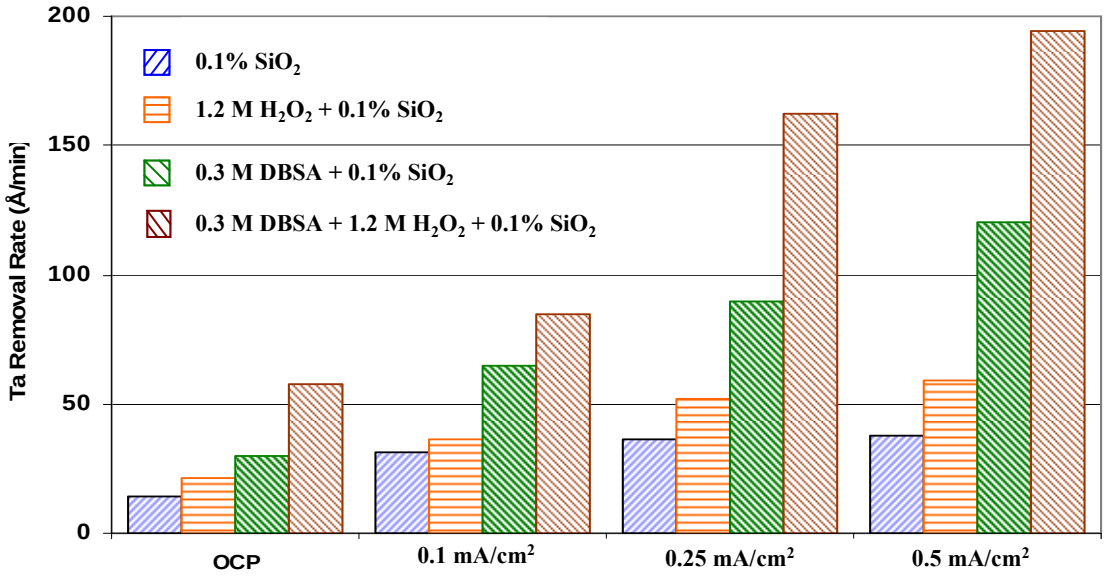

Figure 4.30: Effect of current density on the removal rate of tantalum at pH 10.

4.4.6. Selectivity

Selectivity is defined as the ratio of the removal rate of tantalum to the removal rate of copper. Selectivity between tantalum and copper as a function of applied current density in 0.3M DBSA solution containing 1.2M H_2O_2 and 0.1% SiO_2 at pH 10 is shown in Figure 4.31. Under OCP conditions, the selectivity (Ta/Cu) is 0.5. At a current density of 0.25 mA/cm^2, the selectivity increases to ~ 1.2. Upon further increase of the applied current density 0.5 mA/cm^2, the selectivity decreases to ~0.85.

4.4.7. Characterization of Tantalum Surface by AFM

The topography of the tantalum surface before and after polishing in DBSA solution was examined using an atomic force microscope. Figure 4.32 shows the AFM topographic image of the bare tantalum surface (2 μm x 2 μm) before polishing. It may be noted that the tantalum sample was cleaned in dilute hydrofluoric acid (1%) for 10 seconds to remove any native oxide before imaging. The average roughness (R_a) of the tantalum surface was 4 nm.

The tantalum film was then polished in 0.3M DBSA solution containing 1.2M H_2O_2 and 0.1% SiO_2 at pH 10 for a current density of 0.5 mA/cm^2 for one minute. Figure 4.33 shows the AFM image of the polished tantalum surface (1 μm x 1 μm). The average roughness was reduced to 1 nm. Then the polishing was carried out to ensure complete removal of tantalum film, thereby exposing the underneath carbon doped oxide (CDO). Figure 4.34 shows the CDO surface (1 μm x 1 μm) after polishing under the same conditions. It may be noted that the surface roughness is even reduced to 0.5 nm. These results show that polishing reduces the topographical variation and planarizes the surface.

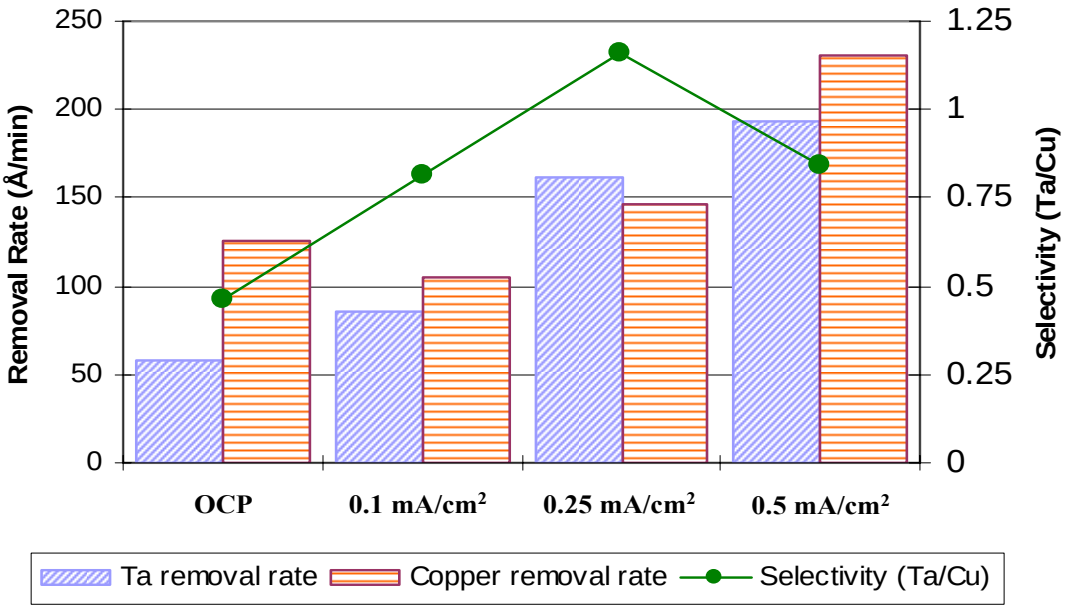

Figure 4.31: Selectivity between tantalum and copper at different applied current densities in 0.3M DBSA solution containing 1.2M H_2O_2 and 0.1% SiO_2 at pH 10.

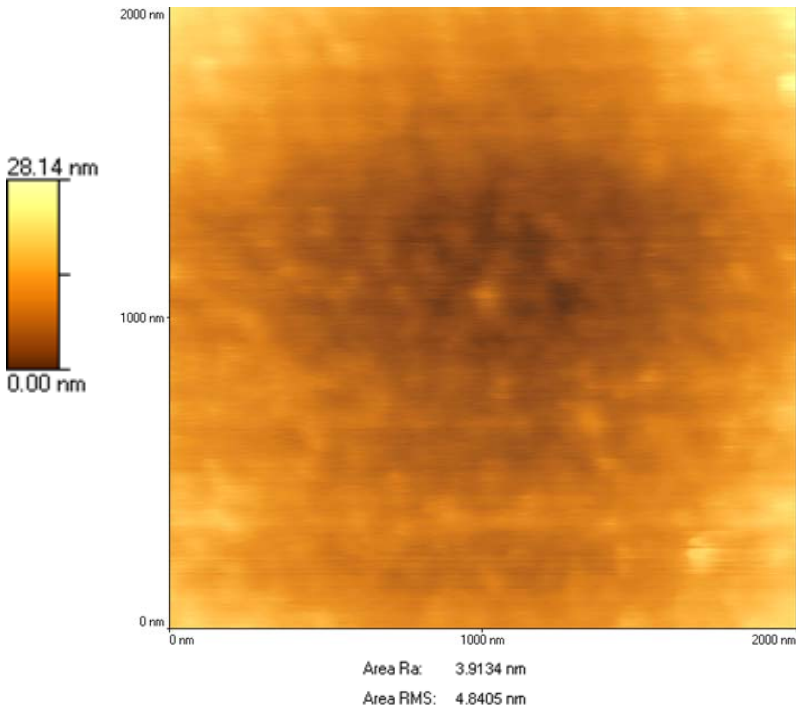

Figure 4.32: AFM topographic image of the bare tantalum surface (2 μm x 2 μm) after exposing to dilute HF (1%) for 10 seconds to remove any native oxide.

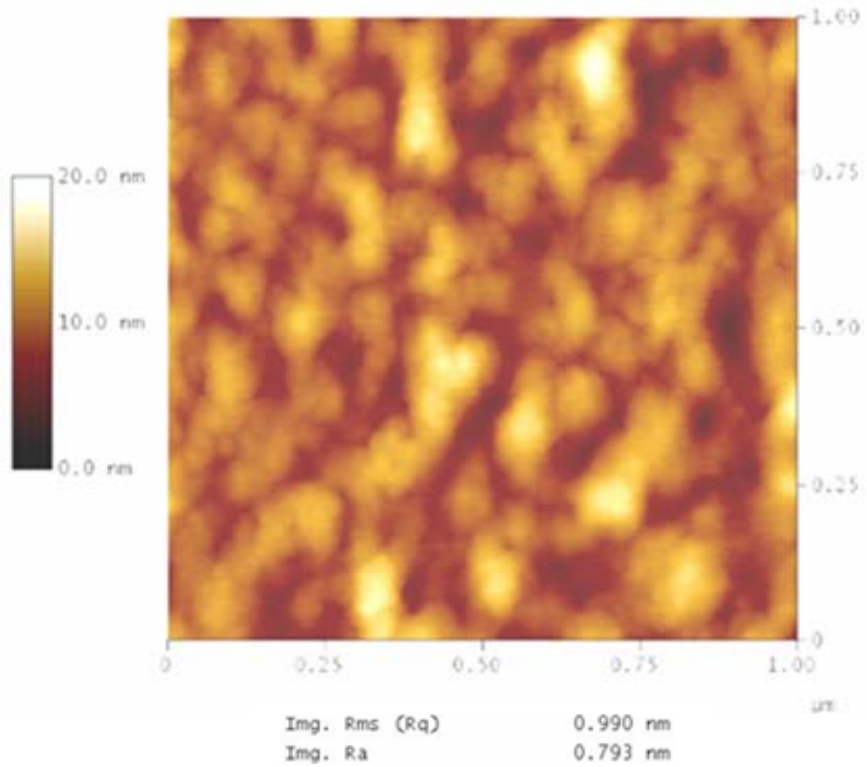

Figure 4.33: AFM image of the tantalum surface (1 µm x 1 µm) after polishing in 0.3M DBSA solution containing 1.2M H_2O_2 and 0.1% SiO_2(pH 10) at a current density of 0.5 mA/cm^2.

.

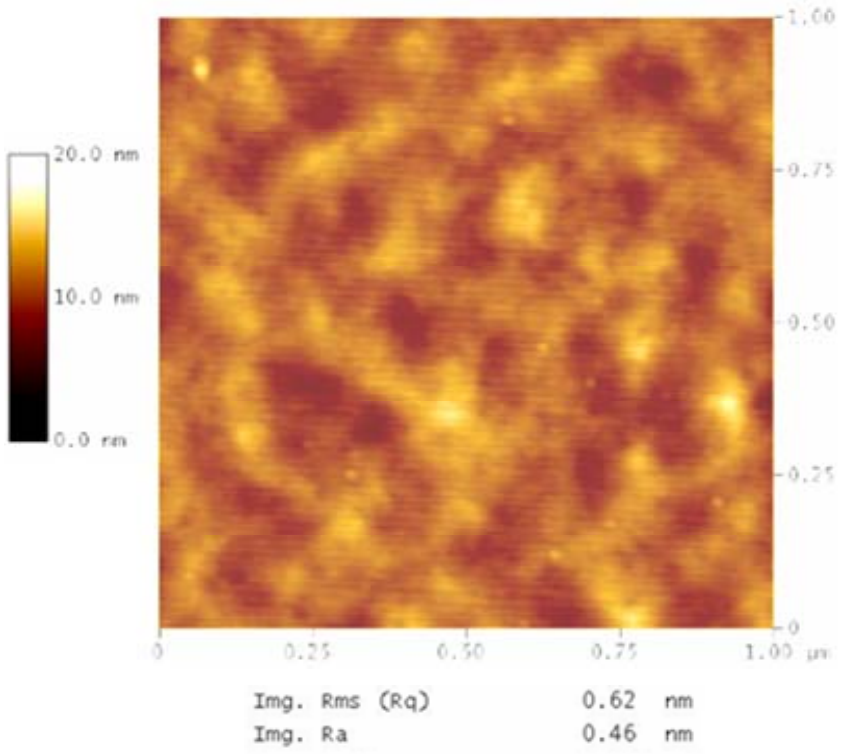

Figure 4.34: AFM image of the carbon doped oxide surface (1 µm x 1 µm) after complete removal of tantalum film by polishing in 0.3M DBSA solution containing 1.2M H_2O_2 and 0.1% SiO_2 (pH 10) at a current density of 0.5 mA/cm^2.

4.4.8. Proposed Mechanism and Current Efficiency

The results have shown that both peroxide and DBSA significantly improve the removal rate of Ta under simultaneous application of pressure and current. Under mildly alkaline conditions [4.7], the most stable form of Ta is Ta_2O_5 (s). However, it is well known that Ta can form metastable oxides such as TaO, Ta_2O_3 and TaO_2 during thermal oxidation [4.8]. Kerrec et al. [4.9] and Kerrec [4.10] have shown by means of XPS and EIS studies that the tantalum oxide film formed under anodic conditions consists of a mixture of TaO and Ta_2O_5. These studies have also shown that TaO forms a significant portion of the surface oxide in the case of thin films ($t < 20$ nm), while in the case of relatively thick tantalum oxide films ($t > 20$ nm), Ta_2O_5 is the dominant oxide formed. Further, it has been shown that mechanical polishing using alumina slurries followed by air exposure induces the formation of a mixed oxide film composed of a mixture of TaO and Ta_2O_5. In this study, since the removal rate of tantalum is of the order of ~ 20 nm/min, it is reasonable to expect that TaO would form a significant portion of the surface tantalum oxide during the ECMP process.

As discussed in the background section, DBSA molecule contains complexing groups. In conjunction with H_2O_2, DBSA may aid the oxidative dissolution of TaO in the form of peroxotantalate complexes such as $[Ta\ (O_2)\ L_6]^{3-}$, $[Ta\ (O_2)_2\ L_4]^{3-}$or $[Ta\ (O_2)_3\ L_2]^{3-}$, where L_2^{2-} represents one ionized DBSA molecule. Such peroxo complexes have been reported by Bayot et al. [4.11]. As an example, the formation of triperoxotantalate complex, $[Ta\ (O_2)_3\ L_2]^{3-}$ can be represented by the following reaction.

$$TaO\ (surface) + (9/2)H_2O_2\ (bulk) + 3OH^- + H_2L_2 \rightarrow [Ta\ (O_2)_3\ L_2]^{3-} + 7\ H_2O$$

Obviously, detailed spectroscopic analysis is required to determine the exact nature of the complex formed.

In summary, it is proposed that the tantalum ECMP process in DBSA based chemical systems occurs by the following mechanism.

1. Tantalum is oxidized to TaO by an interfacial two electron transfer reaction.
2. TaO is oxidized and dissolved by H_2O_2 and DBSA in the bulk solution in the form of complexes of the type $[Ta\ (O_2)_x\ L_y]^{3-}$, where x = {1,2,3} with corresponding y ={6,4,2}.

Based on two electron transfer reaction, the current efficiency values calculated from results obtained in 0.3 M DBSA solution containing 1.2 M H_2O_2 and 0.1% SiO_2 at pH 10 are shown in Table 4.5. It is pertinent to mention the removal rates at different applied current densities were corrected by subtracting rates at OCP conditions. The current efficiency in excess of 100% might be attributed to the analytical errors.

Applied current density (mA/cm^2)	Estimated removal rate (Å/min) of tantalum based on 2 e^- transfer	Actual removal rate of tantalum (Å/min) in 0.3M DBSA + 1.2M H_2O_2 + 0.1% SiO_2 (pH 10)	Calculated current efficiency (%) after correcting for OCP removal rate
OCP	-	60	-
0.1	34	85	80
0.25	85	160	109*
0.5	169	195	81

Table 4.5: Current efficiency (%) as a function of pH under different conditions

(*: Please see text for explanation of current efficiencies higher than 100%)

4.4.9. Comparison of DBSA and MSA Based Chemical System for Tantalum Removal

Figure 4.35 shows the comparison of DBSA and methane sulfonic acid (MSA) for the removal rate of tantalum as a function of applied current density. Under OCP condition, the removal rate of tantalum in 0.3M MSA solution containing 1.2M H_2O_2 and 0.1% SiO_2 at pH 10 is 40 Å/min. At an applied current density of 0.1 mA/cm^2, the removal rate is almost the same ~ 45 Å/min. The removal rate increases to 70 Å/min for a current density of 0.25 mA/cm^2. The highest removal rate of 80 Å/min was obtained at an applied current density of 0.5 mA/cm^2. This is roughly one half of that obtained with DBSA solution. Thus DBSA gives better removal rates of tantalum than MSA under the same ECMP conditions.

4.4.10. Evaluation of DBSA Based Chemical System for ECMP of Tantalum Nitride

Since 0.3M DBSA solution containing 1.2M H_2O_2 and 0.1 % silica particles at pH 10 yielded a high removal rate of tantalum, it was decided to evaluate the same chemical system for the removal of tantalum nitride under ECMP conditions. Figure 4.36 shows the removal rate of tantalum nitride as a function of applied current densities in 0.3M DBSA solution containing 1.2M H_2O_2 and 0.1 % SiO_2 (pH 10). Under OCP condition, the removal rate of tantalum nitride is 40 Å/min. At a current density of 0.1 and 0.25 mA/cm^2, the removal rate increases to 55 and 85 Å/min, respectively. At a higher current density of 0.5 mA/cm^2, the removal rate increases to 95 Å/min. This is roughly one half the removal rate of tantalum. These preliminary results indicate that DBSA is not effective for the removal of tantalum nitride as it is for tantalum under ECMP conditions.

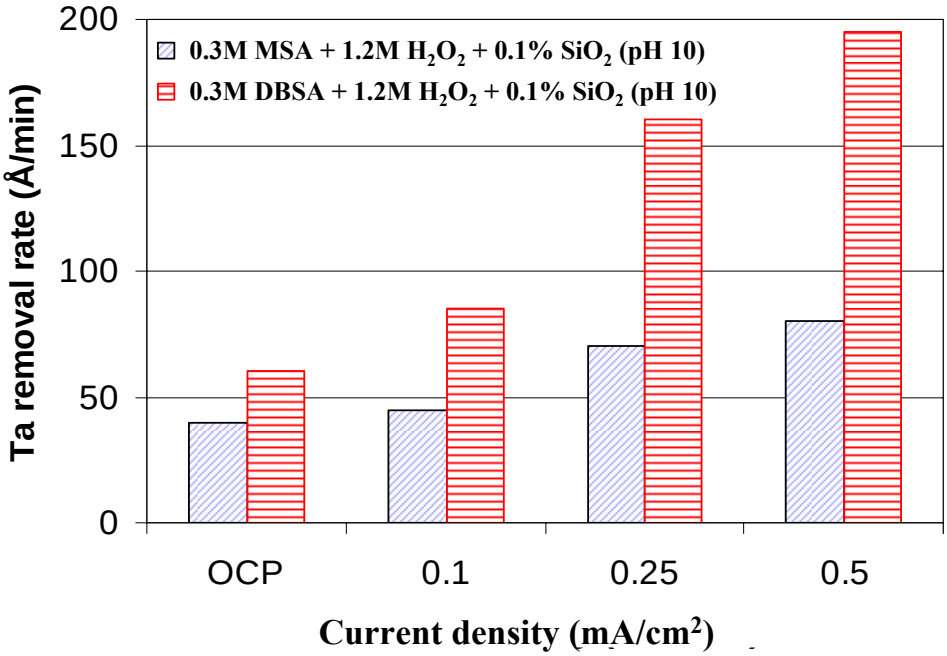

Figure 4.35: Comparison of DBSA and MSA Based Chemical System for Ta Removal under ECMP conditions.

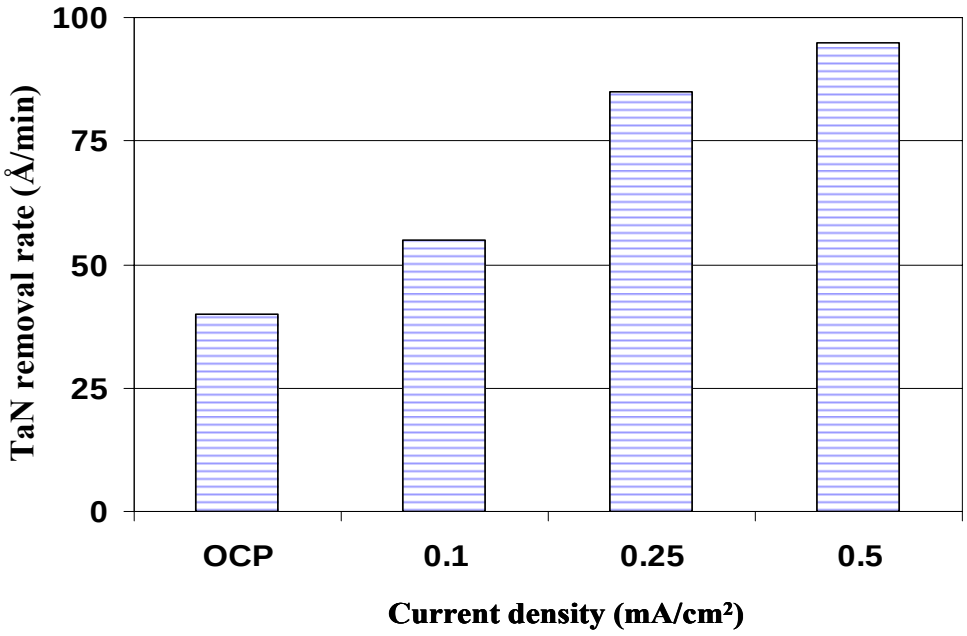

Figure 4.36: Removal rate of tantalum nitride as a function of applied current densities in 0.3M DBSA solution containing 1.2M H_2O_2 and 0.1 % SiO_2 (pH 10).

4.4.11. Patterned Test Structure for ECMP

Figure 4.37 shows the cross section of the as-received test structure studied using focused ion beam (FIB) - scanning electron microscope (SEM) technique. The interface between the dielectric and barrier film is clearly seen. The thickness of barrier film is ~ 30 nm. It may be noted that a step height of ~ 33 nm is seen between the barrier layer and copper, which could be due to copper recess from the previous CMP processing steps carried on platen 1 and 2.

Polishing of the test structure in optimized formulation (0.3M DBSA solution containing 1.2M H_2O_2 and 0.1% SiO_2 at pH 10) at a current density of 0.5 mA.cm^2 for 3 minutes results in the removal of barrier layer. However, surface planarity was not achieved as the step height is almost the same. This is shown in Figure 4.37(b). This is due to the fact that the optimized solution has 1:1 selectivity with respect to copper. So, the optimized solution is removing the barrier layer at the same rate as copper. It may be noted that the pad may not be in contact with the low lying copper region. However, the removal rate of copper even in the absence of abrasion is ~ 100 Å/min. Thus polishing the sample under these conditions would result in a non-planar surface. In order to achieve surface planarity, it is necessary to protect the low lying copper region and selectively remove the barrier layer. For this reason, it was decided to add BTA to the DBSA based solution as a corrosion inhibitor for copper.

Samples were polished in the optimized formulation containing 0.01M BTA (pH 10) at a current density of 0.5 mA/cm^2 for 1.5 and 3 minutes. Figure 4.38 (a) shows the FIB-SEM image of the sample polished for 1.5 minutes. It can be seen that the barrier film thickness as well as step height is reduced to ~13 nm. Figure 4.38 (b) shows the FIB-

SEM image of the sample polished for 3 minutes. It is clear that the barrier film is completely removed and the surface appears to be planar.

From these results, it may be concluded that BTA effectively inhibits the removal of copper from low lying regions while the barrier layer is completely removed, resulting in a planar surface.

(a)

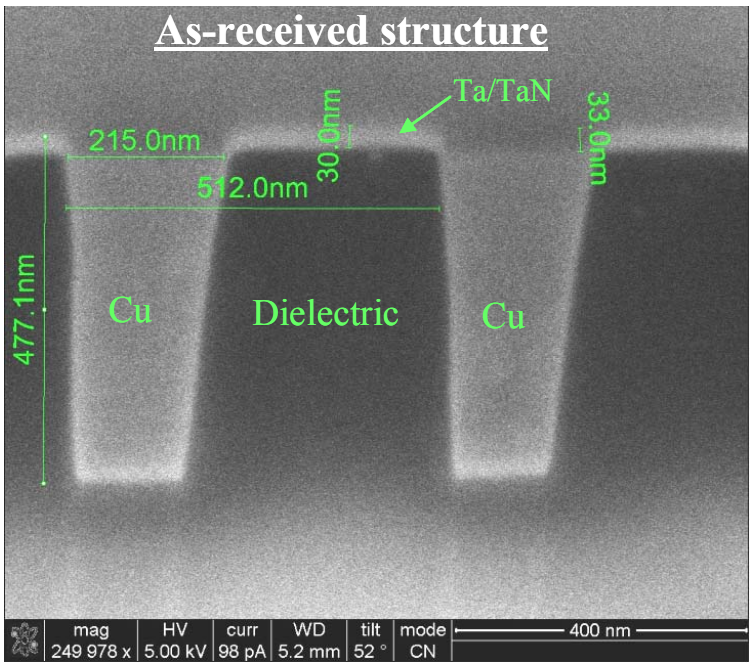

(b)

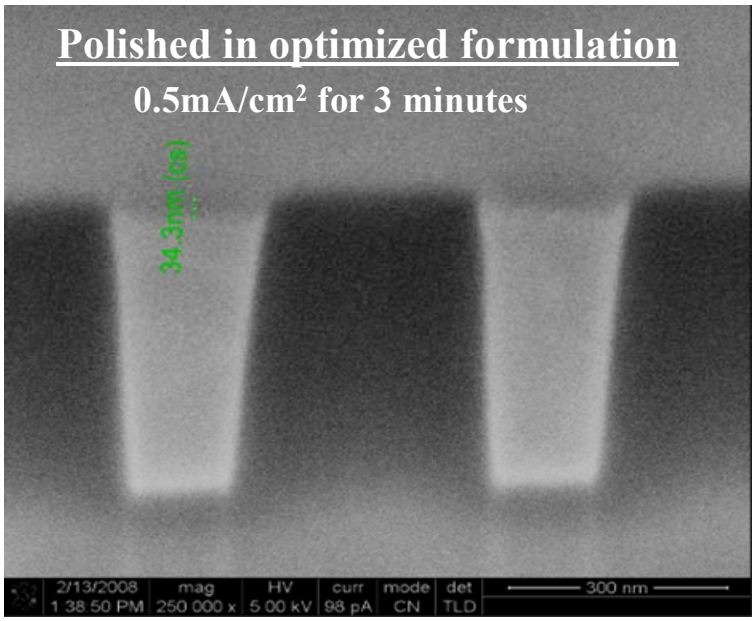

Figure 4.37: FIB-SEM image showing the cross section of (a) as-received test structure and (b) polished in optimized formulation for 3 minutes.

(a)

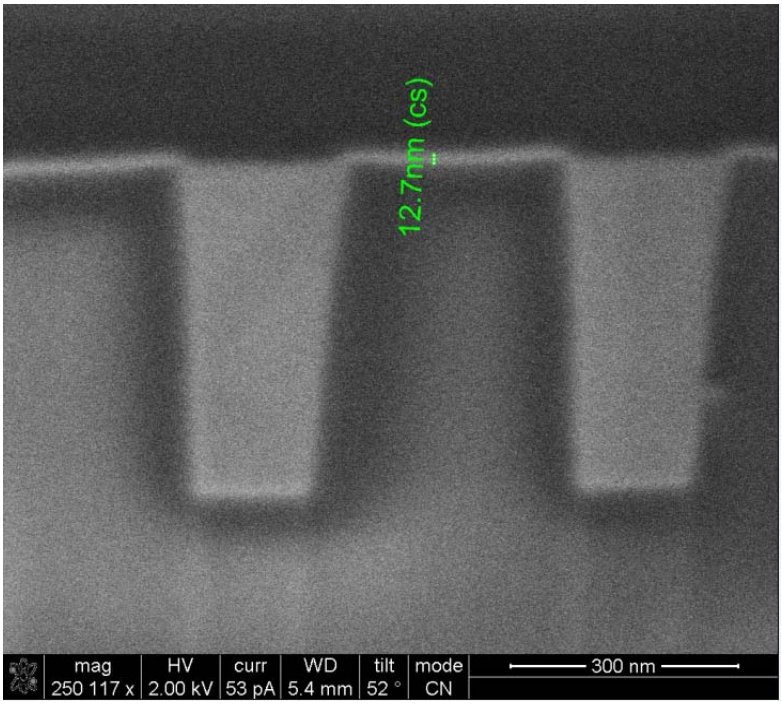

(b)

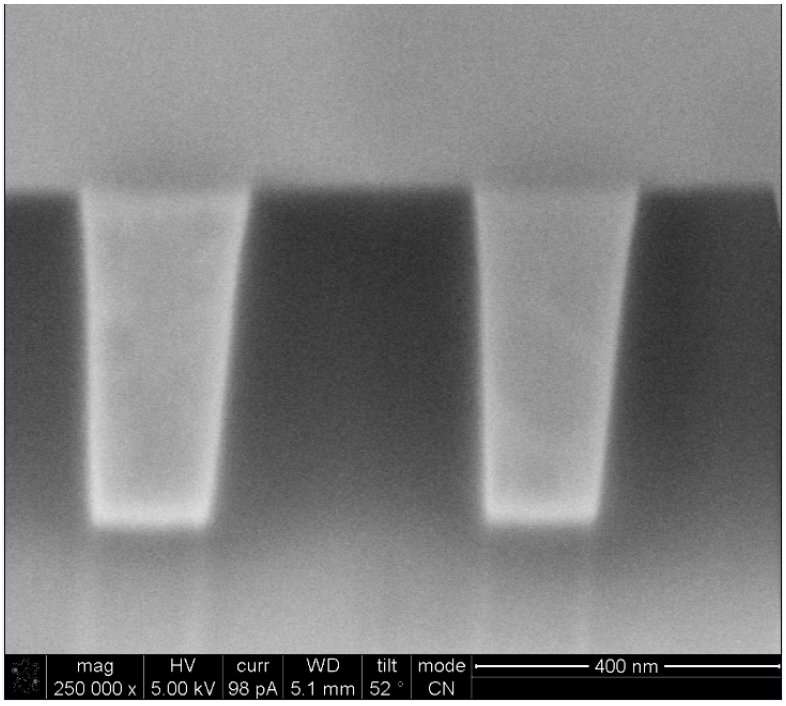

Figure 4.38: FIB-SEM image of the patterned test structure polished for (a) 1.5 minutes and (b) 3 minutes in optimized formulation containing 0.01M BTA at 0.5 mA/cm^2.

CHAPTER 5: CONCLUSIONS AND FUTURE WORK

5.1. Conclusions

The following conclusions can be made from this study:

1 (a). Evaluation of Copper Dissolution in Hydroxylamine Based Solutions using QCM

1. Copper dissolution increases with respect to overpotential, and dissolution rates as high as 6000 Å/min have been obtained at pH 4 for an overpotential of 750mV.
2. High current efficiencies greater than 70% at pH 4 up to an overpotential of 500 mV make hydroxylamine chemistry suitable for ECMP application.
3. Benzotriazole and salicylhydroxamic acid inhibit copper dissolution in hydroxylamine solution. However, both inhibitors are effective only at low anodic overpotential values ($\leq$ 250mV).
4. The mechanism of passivation by BTA indicates that the adsorbed BTA in the first layer forms a cuprous-BTA polymeric complex, while the subsequent BTA layers attach by physisorption. Based on these cross sectional areas, the measured mass increase at pH 6 corresponds to either 2 or 4 layers, depending on orientation. At pH 4, the measured mass change corresponds to either 4 or 8 layers.
5. Passivation mechanism by SHA indicates that copper is first dissolved by hydroxylamine and the copper (+2) - hydroxylamine complex reacts with the hydroxide ion to form an insoluble Cu-SHA polymeric compound at the surface of copper, providing some degree of protection. Based on the cross

sectional area, the measured mass increase at pH 4 roughly corresponds to 20 layers.

1 (b). Polishing Studies on Copper using EC-AC Tool

(i) 0.5M Hydroxylamine Based Solution at pH 4

1. Highest copper polishing rate of ~ 6930 Å/min was obtained in 0.5 M hydroxylamine solution at an overpotential of 750 mV. Under the same condition, the static dissolution rate was found to be 6030 Å/min. This indicates inhibitors are required to protect low-lying areas from dissolving rapidly due to static dissolution rate.
2. BTA is effective at an overpotential ≤ 250 mV. The addition of 0.01 M BTA to 0.5M hydroxylamine solution at an overpotential of 250 mV reduces the static rate to zero and the polishing rate to 2100 Å/min.
3. The addition of 0.01 M SHA to 0.5M hydroxylamine solution at an overpotential of 250 mV, a static rate of 1330 Å/min and a polishing rate of 2415 Å/min was observed. Thus, SHA is not effective in inhibiting static copper dissolution.

(ii) 0.5M Hydroxylamine Based Solution at pH 6

1. Polishing of electroplated copper film in 0.5 M hydroxylamine solution at an overpotential of 250 mV results in a static rate of 2200 Å/min and polishing rate of 2550 Å/min.

2. The addition of 0.01 M SHA to 0.5M hydroxylamine solution at an overpotential of 250 mV reduces the static rate to 110 Å/min and a polishing rate of 2015 Å/min was achieved.
3. The addition of 0.01 M BTA to 0.5M hydroxylamine solution at an overpotential of 250 mV reduces the static rate to zero and the polishing rate to 1980 Å/min. This indicates that BTA is a better inhibitor than SHA.

2 (a). Evaluation of DBSA Solution for ECMP of Tantalum

1. The presence of a small amount (~ 0.1%) of colloidal silica particles is needed to provide good tantalum removal rates in DBSA solutions.
2. The higher removal rate of tantalum was obtained at pH 10. In the absence of peroxide, the removal rate of tantalum in 0.3M DBSA solution containing 0.1% SiO_2 at a current density of 0.5 mA/cm^2 is 120 Å/min. The addition of 1.2M H_2O_2 increases the removal rate to ~ 200 Å/min.
3. Selectivity (Ta/Cu) of 1:1 is observed at pH 10 at a current density of 0.5 mA/cm^2 (oxide removal rate in the formulation is 30 Å/min).
4. AFM study on the tantalum surface after polishing for 1 minute in optimized solution at a current density of 0.5 mA/cm^2 shows a reduction in surface roughness from 4 nm to 1 nm.
5. Tantalum ECMP process in DBSA based chemical systems is proposed as follows
    a. Tantalum is oxidized to TaO by an interfacial two electron transfer reaction

b. TaO is oxidized and dissolved by H_2O_2 and DBSA in the bulk solution in the form of complexes of the type $[Ta\ (O_2)_x\ L_y]^{3-}$, where x = {1,2,3} with corresponding y = {6,4,2}.

6. The current efficiency is above 80% under all applied current density.

2 (b). Comparison of DBSA and MSA Based Chemical System for Tantanlum Removal

1. The highest removal rate of 80 Å/min was obtained in 0.3M MSA solution containing 1.2M H_2O_2 and 0.1% SiO particles (pH 10) at a current density of 0.5 mA/cm^2. This removal rate is roughly one half of that obtained with DBSA solution. Thus DBSA gives better removal rates of tantalum than MSA under the same ECMP conditions.

2 (c). Evaluation of DBSA Based Chemical System for ECMP of Tantalum Nitride

1. The higher removal rate of 95 Å/min was obtained at a current density of 0.5 mA/cm^2 in 0.3M DBSA solution containing 1.2M H_2O_2 and 0.1% SiO_2 (pH 10). This is roughly one half the removal rate of tantalum. These preliminary results indicate that DBSA is not as effective for the removal of tantalum nitride as it is for tantalum under ECMP conditions.

2 (d). Patterned Test Structure for ECMP

1. Cross sectional FIB-SEM images of as received test structure indicates copper recess from the previous CMP steps. Polishing of the test structure in optimized solution containing 0.01M BTA for 3 minutes at a current density of 0.5 mA/cm^2

results in complete removal of barrier film, while the low lying copper region are effectively protected by BTA thereby achieving surface planarity.

5.2. Future Work

1. Possibility of increasing the TaN removal rate using different oxidants such as KIO_3
2. Develop chemical systems for the removal of other barrier layers (WN, Ru).
3. Design of pads for ECMP.
4. Near neutral chemical system for one step removal of copper and barrier layer.

REFERENCES

1.1. T. McMannus, "Environmental Technology in Semiconductor Manufacturing-Challenges & Opportunities," NSF-SRC center for Environmentally Benign Semiconductor Manufacturing Review meeting, Aug. (2004).

1.2. G. Moore, "Cramming More Components Onto Integrated Circuits," Electronics, 38 (8) (1965).

1.3. J.P. Colinge and C.A. Colinge, Physics of Semiconductor devices, Kluwer Academic publisher, Boston (2002).

1.4. R. Rosenberg, MRS Symposium Proceedings., 337, 33 (1994).

1.5. W. W. Lee, S. Russell, "Integration Challenges of Low k Materials," Future Fab Intl. Vol. 8 (2002).

1.6. International Technology Roadmap for Semiconductors (Interconnects), (2007).

1.7. V. Lowalekar, "Oxalic Acid Based Chemical System for Electrochemical Mechanical Planarization of Copper," Ph. D. Dissertation, University of Arizona (2006).

1.8. Bohr, "Interconnect Scaling -The Real Limiter to High Performance ULSI", IEEE Proceedings, 241-242 (1995).

1.9. S. Kondo, S. Tominaga, A. Namiki, K.Yamada, D. Abe, K. Fukaya, M. Shimada and N. Kobayashi, IEEE International Interconnect Technology Conference, June (2005).

1.10. I. Suni and B. Du, IEEE Trans. Semicond. Manuf. 18 (3), pp.341-49 (2005).

1.11. P. Leduc, M. Savoye, S. Maitrejean, D. Scevola, V. Jousseaume, G. Passemard, Proc. of the IITC (2005).

1.12. M. Cao, V.V. Paul, C. Mike, G. Wayne, IEEE Electron Device Lett., 19(8), 291-93 (1998).

1.13. Robert Chau, Justin Brask, Suman Datta, Gilbert Dewey, Mark Doczy, Brian Doyle, Jack Kavalieros, Ben Jin, Matthew Metz, Amlan Majumdar, and Marko Radosavljevic, Journal of Microelectronic Engineering, Vol.80, June pp. 1-6 (2005).

1.14. J. M. Steirgelwald, S. P. Murarka, R. J. Gutmann, Chemical Mechanical Planarization of Microelectronic Materials, John Wiley & Sons, NY (1997).

1.15. S. Tamilmani, "Dissolution, Corrosion and Environmental Issues in Chemical Mechanical Planarization of Copper," Ph. D. Dissertation, University of Arizona (2005).

1.16. L. Chen, Semiconductor Fabtech, 24th edition, pp. 37- 141 (2004).

1.17. Y. Hong, D. Roy and S. V. Babu, Electrochem. Solid - State Lett., 8(11), G297-G300 (2005).

1.18. L. Chen, W. Hsu, A. Duboust, R. Morad, D.A. Carl, United States Patent Application 038066, Applied Materials Inc. (2004).

1.19. L. Economikos, X.Wang, A. Sakamoto, P. Ong, M. Naujod, R. Knarr, L. Chen, Y. Moon, S. Neo, J.Salfelder, A. Duboud, A. Maned, W. Lu, S. Shraud, F. Lid, S. Tsai and W. Swart, IEEE International Interconnect Technology Conference, pp. 233-235, June (2004).

1.20. A. Brown, IEEE Spectrum, Jan (2005).

1.21. Y. Hong, D. Roy and S. V. Babu, Electrochem. Solid - State Lett., 8(11), G297-G300 (2005).

1.22. A.Muthukumaran, N. Venkataraman, S. Tamilmani and S. Raghavan, Proceedings of The Corrosion Control 007 Conference, Australia, Paper 105, 8 pp (2007).

1.23. P. C. Andricacos et al, United States Patent Application 20060163083, IBM (2006).

1.24. A.Muthukumaran, V.Lowalekar and S.Raghavan, Mater. Res. Soc. Symp. Proc., 914, 213-16 (2006).

1.25. A. Jindal and S. V. Babu, J. Electrochem. Soc., 151(10), G709-G716 (2004).

2.1. J. M. Steigerwald, A fundamental Study of Chemical Mechanical Polishing of Copper Thin Films, PhD Thesis, Rensseler Polytechnic Institute, Troy, NY (1995).

2.2. P. Singer, "Copper CMP: Taking Aim at Dishing," Semiconductor International, October (2004).

2.3. W. H. Huang, "Fundamental Studies on the Removal of Copper in Hydroxylamine Based Chemistries of Interest to Chemical Mechanical Planarization", Ph.D dissertation, University of Arizona (2003).

2.4. J. M. Steigerwald, R. Zirpali, S. P. Murarka, D. Price, and R. J. Gutmann, J. Electrochem. Soc., 141 (10), 2842-48 (1994).

2.5. L. Chen, Semiconductor Fabtech, 24th Edition, pp. 37- 141 (2005).

2.6. M.R. Oliver, ed., Chemical Mechanical Planarization of Semiconductor Materials, Springer, New York, (2004).

2.7. Suba™ Products, Rodel Corporation, 451 Bellevue Rd, Newark, DE 19713 (2001).

2.8. IC1000 CMP Pad, Rodel Corporation, 451 Bellevue Rd, Newark, DE 19713 (2001).

2.9. R. Jairath, J. Farkas, C.K. Huang, M. Stell and S.M. Tzeng, Solid State Technol., 37, 71 (1994).

2.10. P. B. Zantye, A. Kumar and A. K. Sikhder, "Chemical mechanical planarization for microelectronics application," Materials Science and Engineering, 45, 89-220, (2004).

2.11. 3M SlurryFree™ CMP, Rodel Corporation, 451 Bellevue Rd, Newark, DE 19713 (2001).

2.12. T. Katoh, H. G. Kang, U. Paik and J.G. Park, Jpn. J. Appl. Phys. Vol. 42, pp. 1150–1153 (2003).

2.13. T. Katoh, M. Kim, U. Paik and J.G. Park, Jpn. J. Appl. Phys. Vol. 43, No. 2A, pp. L 217–L 220 (2004).

2.14. N. Kim, P. Ko, G. Choi, Y. Seo, W. Lee, Thin Solid Films, 504, 166–169 (2006).

2.15. G.B.Basim, et al., Proceedings of the Eletrochemical Society, Vol. 20 (2000).

2.16. W. Huang, S. Tamilmani, S. Raghavan and R. Small, Int. J. Miner. Process, 72, 365-372 (2003).

2.17. S. Tamilmani, W. Huang, S. Raghavan and R. Small, Solid State Phenomena, Vol. 92, pp. 271-274 (2003).

2.18. D. Eom, J.G. Park and E.S.Lee, Jpn. J. Appl. Phys. Vol. 41, pp. 1305–1310 (2002).

2.19. D. Tromans, J. Electrochem. Soc., Vol. 145 (3), L42-45 (1998).

2.20. M. K. Carter and R. Small, J. Electrochem. Soc., Vol. 151 (10), B563-71 (2004).

2.21. J. Telegdi, A. Shaban, E. Kalman, Electrochimica Acta, Vol. 45, 3639–3647 (2000).

2.22. K. Mansikkamaeki, P. Ahonen, G. Fabricius, L. Murtomaki and K. Kontturi, J. Electrochem. Soc., 152(1), B12-B16 (2005).

2.23. V. Brusic, M.A. Frisch, B.N. Eldridge, F.P. Novak, F.B. Kaufman, B.M. Rush, and G.S. Frankel, J. Electrochem. Soc., 138(8), 2253-2259 (1991).

2.24. V. Lowalekar, Ph. D. Dissertation, University of Arizona, (2006).

2.25. A.Muthukumaran, N. Venkataraman, S. Tamilmani and S. Raghavan, Proceedings of The Corrosion Control 007 Conference, Australia, Paper 105, 8 pp (2007).

2.26. F. W. Preston, "The theory and design of plate-glass polishing machines," J. Soc. Glass Tech., 11, p. 214-56 (1927).

2.27. J. E. J. Schmitz, Chemical Vapor Deposition of Tungsten and Tungsten Silicides for VLSI\ULSI Applications, Noyes Publications, Park Ridge (1992).

2.28. S. R. Runnels, J. Electrochem. Soc., 141, 1900 (1994).

2.29. W. T. Tseng and Y. L. Wang, J. Electrochem. Soc., 144, L15 (1997).

2.30. N. J. Brown, "Preparation of Ultrasmooth Surfaces," Annual Review of Materials Science, 16, pp. 371-388 (1986).

2.31. N. J. Brown, P. C. Baker and R. T. Maney, Proceedings of SPIE-The International Society for Optical Engineering, pp. 42-57 (1981).

2.32. N. J. Brown and L. Cook, "Paper TuB-A4, Tech Digest," in Topical Meeting on the Science of Polishing, Optical Soc. of America, (1984).

2.33. G. Nanz and L. E. Camelletti, IEEE Trans. Semi. Manuf., 8, 382 (1995).

2.34. S. R. Runnels, J. Electrochem. Soc., 25, 1574 (1996).

2.35. A. J. Bard, R. Parsons and J. Jordan, Standard Potentials in Aqueous Solution, Marcel Dekker, Inc., New York, (1985).

2.36. S. Tamilmani, Ph. D. Dissertation, University of Arizona (2005).

2.37. M. Hariharaputhiran, J. Zhang, S. Ramarajan, J. J. Keleher, Yuzhuo Li and S. V. Babu, Journal of The Electrochemical Society, 147 (10) 3820-3826 (2000).

2.38. J.M. Steigerwald, S.P. Murarka, R.J. Gutmann, D.J. Duquette, Materials Chemistry and Physics, 41, 217-228 (1995).

2.39. Wayne H. Huang, Subramanian Tamilmani, Creighton Anderson, and Srini Raghavan, IEEE Transactions on Semiconductor Manufacturing, 17 (4), Nov (2004).

2.40. R. J. Small, L. McGhee, D. J. Maloney and M. L. Peterson, "Redox slurries for chemical-mechanical polishing of semiconductor wafers and related circuit boards," Wo Patent 9804646, EKC Technology, Inc., 47 pp., (1998).

2.41. R. J. Small, L. McGhee, D. J. Maloney and M. L. Peterson, "Chemical Mechanical Polishing Composition and Process," US Patent 6313039, EKC Technology, Inc, (2001).

2.42. R. J. Small, L. McGhee, D. J. Maloney and M. L. Peterson, "Chemical Mechanical Polishing Composition and Process," US Patent 6117783, EKC Technology, Inc, (2000).

2.43. M. L. Peterson, R. J. Small, G. A. S. III, Z. J. Chen and T. Truong, "Investigating CMP and post-CMP cleaning issues for dual-damascene copper technology," MICRO, 17(1), p. 27-34 (1999).

2.44. M. L. Peterson, R. J. Small, T. Truong and J.-Y. Lee, "Challenges of Electroplated Copper Film and Device Characteristics for Copper Slurry Design," Semiconductor Fabtech, 11, p. 283-287 (2000).

2.45. M. van der Puy and J. H. Dimmit, Hydroxylamine: Redox Properties of Hydroxylamines, Part 1, Inorganic Reactions, AlliedSignal Inc., (1985).

2.46. A.Muthukumaran, N. Venkataraman, S.Tamilmani and S. Raghavan, in communication with Corrosion Engineering Science and Technology.

2.47. W. Huang, Ph. D. Dissertation, University of Arizona (2004).

2.48. M. K. Carter and R. J. Small, J. Electrochem. Soc., 150(2), G107-G111 (2003).

2.49. A. Jindal, Y. Li and S.V. Babu, Mat. Res. Soc. Symp Proc., Vol. 671, 6pp (2001).

2.50. R.K. Iler, The Colloid Chemistry of Silica and Silicates (Cornell University, Ithaca, NY, 1995).

2.51. Y. Li, M. Hariharaputhiran and S.V. Babu, J. Mater. Res., Vol.16, 1066-1073 (2001).

2.52. M. Hariharaputhiran, Y. Li, S. Ramarajan, and S. V. Babu, Electrochemical and Solid-State Letters, 3 (2), 95-98 (2000).

2.53. J. Zhang, S. Li, and P. W. Carter, J. Electrochem. Soc., 154 (2), H109-H114 (2007).

2.54. A.Muthukumaran, N. Venkataraman and S. Raghavan, J. Electrochem. Soc., 155 (3), H184-87 (2008).

2.55. Y. Chen, United States Patent 7244168, Applied Materials Inc. (2007).

2.56. C. Yu, Future Fab Intl. Vol. 10 (2001).

2.57. F. Q. Liu, L. Chen, A. Duboust, S. Tsai, A. Manens, Y. Wang and W. Y. Hsu, Mater. Res. Soc. Symp. Proc, 869, 87-96 (2005).

2.58. Feng Q Liu,z Tianbao Du, Alain Duboust, Stan Tsai, and Wei-Yung Hsu, J. Electrochem. Soc., 153 (6), C377-C381 (2006).

2.59. L. Economikos, et al. IEEE International Interconnect Technology Conference, pp. 233-235, June (2004).

2.60. I. I. Suni and B. Du, IEEE Trans. Semicond. Manuf. 18 (3), 341-49 (2005).

2.61. Y. Hong, D. Roy and S.V. Babu, Electrochemical and Solid State Letters, 8(11), G297-300 (2005).

2.62. L. Economikos, 2nd PacRim CMP Conference, November (2005).

2.63. Source: http://www.appliedmaterials.com/products/ecmp_4.html

2.64. S. Kondo, S. Tominaga, A. Namiki, K.Yamada, D. Abe, K. Fukaya, M. Shimada and N. Kobayashi, IEEE International Interconnect Technology Conference, June (2005).

2.65. Y. Wada, I. Noji, I. Kobata, T. Kohama, A. Fukunaga, and M. Tsujimura, Proceedings of IITC, June (2005).

2.66. T. Kwon, I. Kim, and J. Park, Mater. Res. Soc. Symp. Proc. Vol. 991, 6 pp (2007).

2.67. S. Tamilmani, W. Huang, S. Raghavan, J. Electrochem. Soc., 149 (12), G638-G642 (2002).

2.68. S. Tamilmani, J. Shan, W. Huang and S. Raghavan, Mat. Res. Soc. Symp. Proc. Vol. 767, 6 pp (2003).

2.69. Y. Hong, D. Roy and S. V. Babu, Electrochem. Solid - State Lett., 8(11), G297-G300 (2005).

2.70. J. Huo, R. Solanki, and J. McAndrew, "Electrochemical Planarization of Patterned Copper Films for Microelectronic Applications," J. Mater. Eng. Perform., 13(4), 413-420 (2004).

2.71. J. Huo, R. Solanki, and J. McAndrew, "Study of Anodic Layers and Their Effects on Electropolishing of Bulk and Electroplated Films of Copper," J. Appl. Electrochem., 34, 305-314 (2004).

2.72. V. Lowalekar, Ph. D. Dissertation, University of Arizona (2006).

2.73. P. W. Carter, J. Zhang, S. K. Grumbine, T. Rege, F. De, United States Patent Application 20060030158, Cabot Microelectronics (2006).

2.74. M. K. Carter, R. J. Small, X. C. Shang, D. W. Frey, United States Patent Application 2005090109, (2005).

2.75. H. Sasayama, United States Patent Application 740400, (2006).

2.76. Leonard Johannes Joseph Janssen, Richard Johannes Van Der Net, European Patent WO0171068, (2001).

2.77. S. Tsuchiya, T. Kojima, Japanese Patent 03053099, Matsushita Electric Ind Co Ltd., (1991).

2.78. A. E. Martell and R. M. Smith, Critical stability constants, Plenum, New York (1974).

2.79. S. Wang, et al. United States Patent Application 20060219663, Applied Materials Inc. (2006).

2.80. F. Q. Liu, et al. United States Patent Application 20060219663, Applied Materials Inc. (2006).

2.81. J. A. V. Butler, "Studies in heterogeneous equilibria. II. The kinetic interpretation of the Nernst theory of electromotive force," Trans. Faraday Soc. (1924).

2.82. J. A. V. Butler, "Studies in heterogeneous equilibria. III. A kinetic theory of reversible oxidation potential at inert electrodes," Trans. Faraday Soc. (1924).

2.83. T. Erdey-Gruz and M. Volmer, "The theory of hydrogen overvoltage," Z. physik. Chem., 150(Abt. A), p. 203-13 (1930).

2.84. C. M. A. Brett and A. M. O. Brett, Electrochemistry: principles, methods, and applications, Oxford science publications, Oxford University Press, Oxford ; New York, xxviii, 427 (1993).

2.85. W. H. Huang, "Fundamental Studies on the Removal of Copper in Hydroxylamine Based Chemistries of Interest to Chemical Mechanical Planarization", Ph.D dissertation, University of Arizona, (2003).

2.86. J. Tafel, Z. Phys. Chem. (Leipzig), 50, p. 641, (1904).

2.87. M. G. Fontana, Corrosion Engineering, 3rd ed, McGraw-Hill, New York, (1986).

2.88. J. O'M. Bockris, A. K. N. Reddy, and M. Gamboa-Aldeco, "Modern Electrochemistry," 2nd Edition, Kluwer Academic Publisher, New York, (2003).

2.89. H. G. Seiler, A. Sigel, H. Sigel, "Handbook on Metals in Clinical and Analytical Chemistry," 1st Edition, Published by CRC press (1994).

2.90. R. Thomas, "Practical Guide to ICP-MS," 1st edition published by Marcel Dekker (2003).

3.1 Operation manual, Research Quartz Crystal Microbalance, MAXTEK Inc., CA. (2004).

3.2 Operation Manual, LORESTA AP Super-Intelligent Resistivity Meter, Mitsubishi, Japan (2003).

4.1 E.C. O'Brien, S. Le Roy, J. Levaillain, D.J. Fitzgerald, K.B. Nolan, Inorg. Chim. Acta, 266, 117 (1997).

4.2 E.C. O'Brien, E. Farkas, M. J. Gil, D. Fitzgerald, A. Castineras, K. B. Nolan, Journal of Inorganic Biochemistry, 79, 47 (2000).

4.3 J. M. Bastidas, P. Pinilla, J. L. Polo and E. Cano, Corrosion, 58(11), 922-931 (2002).

4.4 D. A. Johnson and F. Y. Flu, Proceedings of the 8th European Symposiums on Corrosion Inhibitors, 10, 989-998 (1995).

4.5 V. Brusic, M.A. Frisch, B.N. Eldridge, F.P. Novak, F.B. Kaufman, B.M. Rush, and G.S. Frankel, J. Electrochem. Soc., 138(8), 2253-2259 (1991).

4.6 K. Mansikkamaeki, P. Ahonen, G. Fabricius, L. Murtomaki and K. Kontturi, J. Electrochem. Soc., 152(1), B12-B16 (2005).

4.7 S. Sapra, H. Li, Z. Wang and I. I. Suni, J. Electrochem. Soc, 152, B193-B197 (2005).

4.8 S. P. Garg, N. Krishnamurthy and A. Awasthi, Journal of Phase Equilibria and Diffusion, 17, 63-77 (1996).

4.9 O. Kerrec, D. Devilliers, H. Groult and M. Chemla, Electrochimica Acta., 40(6), 719-724 (1995).

4.10 O. Kerrec, Thesis, Paris (1992).

4.11 D. Bayot, M. Devillers and D. Peeters, European Journal of Inorganic Chemistry, 4118 – 23 (2005).